RESONANCE RAMAN STUDIES OF HEMOCYANIN AND RIBONUCLEOTIDE REDUCTASE: METAL CENTERS DESIGNED TO REACT WITH O_2

Jinshu Ling
B.S., Nankai University, China, 1983

A dissertation submitted to the faculty of the
Oregon Graduate Institute of Science & Technology
in partial fulfillment of the
requirements for the degree
Doctor of Philosophy
in
Biochemistry

October, 1993

The dissertation "Resonance Raman Studies of Hemocyanin and Ribonucleotide Reductase: Metal Centers Designed to React with O_2" by Jinshu Ling has been examined and proved by the following Examination Committee:

Joann Sanders-Loehr, Thesis Research Advisor
Professor

Thomas M. Loehr, Thesis Research Advisor
Professor

V. Renganathan
Associate Professor

Paul G. Tratnyek
Assistant Professor

This Dissertation Is Dedicated

To

My Parents

LING Guiying, YE Yongqing

And My wife

JIAO Nianxin

ACKNOWLEDGMENTS

I am indebted to my research advisors Professor Joann Sanders-Loehr and Professor Thomas M. Loehr, for their providing me the opportunity to pursue my Ph.D. studies at the OGI at the first place, for their extraordinary efforts in training me to a scientist, and for their great kindness to me.

I am very grateful to Dr. Gabriele Backes and Dr. Kamala D. Sharma for their help in the early stage of this research. I also wish to thank Nancy Cristie for her assistance during last five years.

TABLE OF CONTENTS

LIST OF TABLES

LIST OF FIGURES

CHAPTER II

CHAPTER III

CHAPTER IV

CHAPTER V

CHAPTER VI

ABSTRACT

RESONANCE RAMAN STUDIES OF HEMOCYANIN AND RIBONUCLEOTIDE REDUCTASE: METAL CENTERS DESIGNED TO REACT WITH O_2

Jinshu Ling, Ph.D.

Oregon Graduate Institute of Science & Technology
Supervising Professors: Joann Sanders-Loehr and Thomas M. Loehr

Resonance Raman (RR) spectroscopy has been used to study three dinuclear metal systems that are involved in the binding and activation of O_2. The enzyme ribonucleotide reductase (RnR) contains a dinuclear iron center which functions as a tyrosine oxidase, using O_2 to oxidize Tyr 122 to a stable radical inside the protein. The Phe 122 mutant, having an identical dinuclear iron center, was studied as a simplified model for O_2 activation. Oxidation with $^{18}O_2$ results in quantitative incorporation of ^{18}O into the dinuclear iron center as detected by a shift in the frequency of the Fe^{III}-O-Fe^{III} stretching vibration. This reaction most likely occurs via heterolytic cleavage of O_2 and the production of an oxo-bridged ferryl intermediate. The Tyr 208 mutant of the Phe adjacent to the dinuclear iron center is, instead, oxidized to dihydroxyphenylalanine (DOPA). When this product is formed in the presence of $H_2{}^{18}O$, its vibrational spectrum indicates that the second O atom in DOPA originates from H_2O rather than O_2. This reaction may utilize a similar ferryl intermediate with a terminal oxo group.

The oxygen-transport protein hemocyanin (Hc) contains a dinuclear copper center whose CuO_2Cu form has been identified as side-on (μ-η^2:η^2) peroxide by X-ray crystallography of arthropod Hc. Using RR spectroscopy, we have identified a $\nu_{as}(Cu_2O_2)$ mode at $\sim$545 cm^{-1} and a $2\nu_{as}(Cu_2O_2)$ at $\sim$1090 cm^{-1} for Hc from both arthropods and molluscs. Only a single $\nu_{as}(Cu_2O_2)$ is observed with $^{16}O^{18}O$, proving that the peroxo group is symmetrically bound between the Cu(II)'s in molluscan Hc. These results suggest that oxyHcs from molluscs and arthropods have the same μ-η^2:η^2 Cu-peroxide structure, despite probable differences in the number of histidine ligands.

The copper complex $[Cu_2(XYL\text{-}O\text{-})(OH)]^{2+}$ exhibits a ν_s(Cu-OH-Cu) mode at 465 cm^{-1} and a ν_{as}(Cu-OR-Cu) mode at 603 cm^{-1}. Analysis of the RR enhancement suggests that coupling to a chromophoric ligand such as phenolate is required for the observation of such M-OH(R) vibrations.

CHAPTER I

OXYGEN ACTIVATION BY METALLOPROTEINS

Since oxygen appeared more than 2.7 billions years ago, living things have evolved to utilize it as an oxidant in combustion of foodstuff and in other specialized metabolic reactions.[1] Since oxygen is inactive to most organic substrates under physiological conditions, organism has also evolved to utilize metal ions (mostly iron and copper) or organic cofactors (e.g., FAD) to activate oxygen. Free metal ions (e.g., Fe^{2+}) in solution are usually fatal to cells because when they react with oxygen, they may produce highly toxic hydroxyl radicals via Fenton chemistry.[2] However, biology has tamed metal ions (and oxygen) in a way that metal ions in metalloproteins activate oxygen to do specific oxidations and yet avoid damaging reactions.

This dissertation presents resonance Raman (RR) spectroscopic studies of three dinuclear metal clusters that are closely linked with oxygen. Ribonucleotide reductase (RnR), the focus of Chapter 3, is an important enzyme in DNA biosynthesis. Its small subunit (R2) contains a dinuclear iron center and functions as a tyrosine oxidase, using oxygen to oxidize a tyrosine residue to a stable radical inside the protein. Hemocyanin, the subject of Chapter 4, is a copper-containing oxygen-transport protein in invertebrates. Chapter 5 presents RR studies of a dinuclear copper complex, a structural model for multicopper oxidases, which catalyze the four-electron reduction of dioxygen to water with concomitant one-electron oxidations of

the reducing organic substrate.

The purpose of this Chapter is to review the current knowledge of chemical reaction mechanisms between molecular oxygen and some metalloproteins that are related to the studies in the following Chapters (Chapter 3, 4, and 5). This Chapter is divided into five sections. Because this dissertation focuses on results obtained from RR spectroscopy, the general methodology of studying oxygen activation by this technique is discussed first. Throughout these sections, the information obtained from resonance Raman spectroscopic studies is emphasized. The second section reviews the current understanding of hemerythrin, a non-heme oxygen carrier, for which resonance Raman studies laid the foundations for the investigations described in Chapter 4. Furthermore, its unique active site structure and spectral properties have been prototypes for so-called dinuclear iron-oxo proteins including ribonucleotide reductase, the subject of Chapter 3. Section 3 reviews the reaction mechanism of cytochrome P-450 monooxygenases, probably the most extensively studied oxygen activating system. It has been employed as a model in studying oxygen activation in many heme and non-heme systems including ribonucleotide reductase R2. Our knowledge of the oxygen activation mechanism of some dinuclear iron-oxo enzymes, particularly methane monooxygenase (MMO), an enzyme that is closely related to ribonucleotide reductase R2, is described in the fourth section. The last section of the Chapter covers blue copper oxidases, for which the hydroxyl-bridged copper complex of Chapter 5 serves as a model system.

1. The Study of Oxygen Activation Using Resonance Raman Spectroscopy

Raman spectroscopy, like infrared (IR) spectroscopy, is the study of vibrational properties of molecules, and provides information about the molecular structure of samples. Unlike IR, in which H_2O has very strong absorption, Raman spectroscopy is not obscured by the presence of an aqueous solvent. Because water has a weak Raman spectrum, biological samples are especially suited to investigation by this technique. Raman spectroscopy is a scattering phenomenon that requires input

of laser excitation at an incident energy of $h\nu_i$. The scattered photons measured in Raman spectroscopy are generally at lower energies, $h\nu_o$, and occur at Raman-active vibrational energies where $E_{vib.} = h\nu_i - h\nu_o$. The Raman spectrum is presented as the frequency shift in wavenumbers (cm^{-1}), $\Delta\nu = (\nu_i - \nu_o)$.

Resonance Raman (RR) effects are observed when using exciting radiation whose energy is within or lies close to an electronic absorption of the molecule. In this case, Raman intensity of the vibrations involving in the chromophore may be resonance enhanced by several orders of magnitude.[3,4] Proteins containing transition metal ions such as Fe^{3+} and Cu^{2+} usually exhibit ligand-to-metal charge transfer (CT) transitions. Resonance Raman spectroscopy can provide selective information about the metal binding site, where most chemistry in metalloenzymes occurs, by choosing excitation wavelengths in appropriate absorption bands.

RR spectroscopy is exceedingly useful in studying oxygen activation by metalloproteins. It can be helpful in probing the chemical mechanism of oxygen activation in several ways: a) It can be used to identify catalytic intermediates in the activation; b) it can provide information about metal ligation of active sites of metalloproteins; c) it can be used to identify products of oxygenation or oxidation reactions.

In biological reactions involving oxygen and metalloproteins, metal-bound superoxide and peroxide species are common intermediates, resulting from partial reduction of molecular oxygen.[5] RR spectroscopy is useful in identifying these species. Vibrational modes corresponding to an oxygen species can readily be recognized in Raman spectra by observing isotopic shifts using $^{18}O_2$ vs. $^{16}O_2$ in the activation process. The nature of the species can be revealed by its Raman frequency.[5] As Table 1 shows, a strong correlation exists between the O-O stretching frequency and the oxidation states of dioxygen species, e.g., $\sim 1550\ cm^{-1}$ for molecular oxygen (O_2), $\sim 1150\ cm^{-1}$ for superoxide (O_2^-), and $\sim 850\ cm^{-1}$ for peroxide (O_2^{2-}). A metal bound dioxygen species should also show an M-O_2 stretching vibration at $\sim 500\ cm^{-1}$ (Table 1). RR studies of the O-O and M-O_2 vibrations can also provide information about the symmetry of the metal-dioxygen species (superoxide and

peroxide) by use of mixed label O_2 ($^{16}O^{18}O$). For example, there should be only a single $\nu(^{16}O\text{-}^{18}O)$ as well as a single $\nu(M\text{-}^{16}O^{18}O)$ mode in a symmetrically coordinated (Figure 1a, b, and c) dioxygen moiety whereas two of each are expected in asymmetric moieties (Figure 1d and e; Table 1).

Ferryl-oxo [$Fe^{IV}=O$] and hydroxyl (Fe^{III}-OH) species, products of O-O bond cleavage and further reduction, respectively, are often involved as key intermediates in proposed mechanisms for many heme and non-heme systems. The existence of these species may also be verified by RR spectroscopy. The ferryl frequency [ν(Fe=O)] has been documented in many peroxidases and terminal oxidases in respiratory chains.[6-11] It usually appears at $\sim$800 cm^{-1} and is sensitive to $^{18}O_2$ oxygenation. There may be ambiguity in distinguishing ferryl vibrations from ν(O-O) of a peroxide, because both appear near 800 cm^{-1} and both show similar $^{18}O_2$ isotopic shifts (Table 1). However, there are two ways that can distinguish these: 1) search of the $^{18}O_2$-sensitive metal-peroxide stretching frequency, $\nu(M\text{-}O_2)$, at $\sim$500 cm^{-1}; 2) use mixed-isotope dioxygen. If the species is a ferryl, two peaks corresponding to $Fe=^{16}O$ and $Fe=^{18}O$ should be observed. On the other hand, if the species is a peroxide, three or four peaks (depending on the symmetry, see above), corresponding to $\nu(^{16}O\text{-}^{16}O)$, $\nu(^{16}O\text{-}^{18}O)$ (one or two modes with greater intensity) and $\nu(^{18}O\text{-}^{18}O)$ should be observed (Table 1). By a similar token, an Fe-OH mode can also be discriminated from an $Fe\text{-}O_2$ mode, for the latter often coexists with a ν(O-O) mode. Additionally, an Fe-OH species usually exchanges readily with $H_2{}^{18}O$ and D_2O solvent and may, therefore, show marked O and D isotopic shifts in the Raman spectrum.[12,13]

Further, Raman spectra of oxygen species in D_2O can provide information about hydrogen-bonding or the protonation state of the species. For example, RR studies on oxyhemerythrin exchanged with D_2O indicated that the peroxide in the protein is protonated (*vide infra*).[14] RR studies of horseradish peroxidase compound II reveal that the ferryl [Fe(IV)=O] species is hydrogen-bonded to an amino acid residue in neutral solution, by observation that ν(Fe=O) downshifts 2 cm^{-1} in D_2O.[7]

RR spectroscopy can also be used to investigate active site structures of

metalloproteins by studying metal-ligand vibrations. The μ-oxo bridge in dinuclear iron-oxo proteins such as hemerythrin and ribonucleotide reductase is a good example. RR studies revealed Fe-O-Fe moieties in these proteins by observing characteristic ν_s(Fe-O-Fe) and ν_{as}(Fe-O-Fe) at about 500 and 750 cm^{-1}, respectively, with the assignments verified by isotopic shifts with μ-^{18}O substitution.[14-17] In Chapter 4, studies of Cu-His vibrations of hemocyanins from arthropodan and molluscan phyla lead us to believe that the two have different patterns of copper-histidine ligation. RR studies of cytochrome P-450 monooxygenase and chloroperoxidase directly proved that cysteinate is the axial ligand in these heme enzymes by observations of ν(Fe-S) at $\sim$350 cm^{-1} that are sensitive to ^{54}Fe- and ^{34}S-substitutions.[18]

Finally, RR spectroscopy can also be used to identify and analyze products of the oxygen requiring reactions. For instance, in Chapter 3, our RR data indicate that one oxygen atom of molecular oxygen is incorporated as the μ-oxo bridge in the dinuclear iron center of ribonucleotide reductase. As also mentioned in Chapter 3, RR spectroscopy was used to identify an Fe-catecholate moiety[19] and the source of oxygen in the reaction between O_2 and the Phe122Tyr mutant of ribonucleotide reductase R2.

2. Oxygen Carriers: Hemoglobin, Hemerythrin, and Hemocyanin

All aerobic organisms utilize oxygen and require respiratory proteins to carry out the binding, transport, and storage of oxygen. Three types of respiratory proteins have been used by nature, all containing metal cofactors. Hemoglobin contains a *b*-type heme prosthetic group (Fe-protoporphyrin IX, see Figure 5A), hemerythrin (Hr) a dinuclear iron center and hemocyanin (Hc) a dinuclear copper center.[5]

Among the three, hemoglobins are by far the most widespread, occurring in all mammals and vertebrates, and in many invertebrates. They are usually tetrameric proteins consisting of $\alpha_2\beta_2$ subunits each of molecular weight $\sim$16,000 daltons. Vertebrate muscle tissue also contains a monomeric oxygen storage/transport protein,

myoglobin, that is very similar to a hemoglobin monomer. Hemoglobin and myoglobin have been extensively studied by X-ray crystallography and various spectroscopic techniques including RR spectroscopy.[20-24]

Oxygen binding by these globins can be described as an "oxidative-addition" reaction. Deoxyglobins contain reduced hemes [Fe(II)]; when they bind O_2, they are oxidized to ferric hemes while the dioxygen is reduced to superoxide (equation 1).

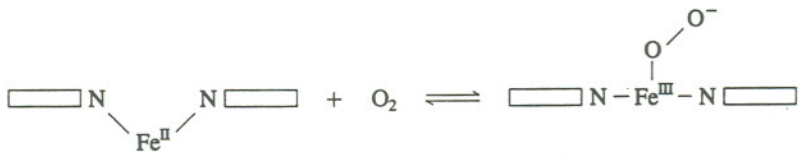

(1)

The superoxide binds to the heme iron in an end-on fashion with one oxygen atom while the other oxygen accepts a hydrogen bond from the distal histidine.[5] The observation of an O-O stretch at $\sim 1130\ cm^{-1}$ in vibrational spectra of oxyhemoglobin and cobalt-substituted oxyhemoglobin is one of the strongest pieces of evidence that the bound dioxygen has been reduced to superoxide.[5,25]

Hemerythrin (Hr) occurs among several phyla of marine invertebrates. It contains no heme group, despite its name, rather, it contains a coupled dinuclear iron cluster that is bridged by a solvent-derived oxo group. Hemocyanin (Hc) is the respiratory protein of molluscs and arthropods. Like hemerythrin, it does not contain a heme group, rather a coupled dinuclear copper cluster. As in globins, oxygen binding in Hr and Hc are also "oxidative-addition" reactions. In the deoxy states, the metal centers in Hr and Hc are diferrous and dicuprous, respectively. In oxy proteins, they are oxidized to diferric and dicupric, respectively. Distinct from oxyhemoglobin, the bound dioxygen in both oxyHr and oxyHc is in the peroxide state (equations 2 and 3).[17]

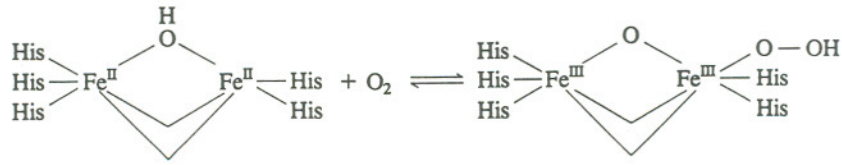

(2)

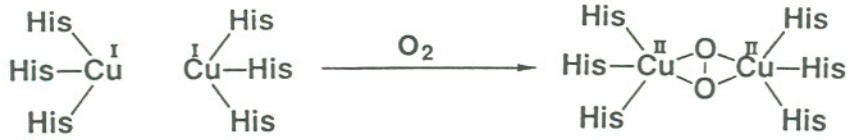

(3)

The active site structure of oxyhemocyanin is the subject of Chapter 4. As described there in greater detail, the salient features of oxygen binding in Hc are as follows: in deoxyHcs, the two Cu(I) ions are ligated to five or six histidines, depending on the phyla; in the oxyHcs, the dioxygen is reduced to peroxide that is bound symmetrically to the two Cu(II) ions in a μ-η^2:η^2 geometry, while the number of histidine ligands is unchanged.

Hemerythrins are usually found as homooctamers, although dimers, trimers, and tetramers are also known. As with hemoglobin, an analogous monomeric O_2 storage protein, myohemerythrin, has also been isolated. The basic monomer protein is a single polypeptide chain with a molecular weight of $\sim$13,000 daltons. This polypeptide contains two iron atoms and binds one molecule of oxygen.[25] The oxygen binding in most oligomeric Hr are noncooperative, except in hemerythrins from two brachiopods, *Lingula reevii* and *Lingula unguis*, which consist of two nonidentical subunits in an $\alpha_4\beta_4$ structure.[26] DeoxyHr is colorless while oxyHr exhibits intense absorption features at 330, 360, and $\sim$500 nm (Figure 2A).[16]

RR spectroscopy has provided definitive information about the active site structure of oxyhemerythrin. It has long been known that the iron atoms of deoxyHr are in the ferrous state and that oxyHr contains Fe(III) atoms.[27] RR spectroscopy provided the first direct and definitive evidence for the ferric-peroxide formulation. The first RR studies of oxyHr were reported by Dunn et al. in 1973. Two well-defined peaks at 503 and 844 cm^{-1} were observed in the spectrum when the protein was excited within the 500-nm absorption band.[28] These Raman features were identified as the Fe-O_2 and O-O stretching vibrations of a 2Fe(III)-peroxo moiety based on their shifts to 480 and 798 cm^{-1}, respectively, when the protein was oxygenated with $^{18}O_2$. As Table 1 shows, ν(O-O) is a good indicator of the oxidation state of dioxygen species and a frequency of 844 cm^{-1} clearly demonstrates that the

dioxygen moiety in oxyHr is a peroxide.

RR studies using mixed-label $^{16}O^{18}O$ hemerythrin offered further information about the peroxide geometry with respect to the dinuclear iron centers. As noted previously, a peroxide could coordinate to a dinuclear metal center in several ways (Figure 1).[29,30] The RR spectrum of oxyHr prepared with unsymmetrically labeled oxygen gas was used to distinguish among these possible structures. In the peroxide O-O stretching region, two peaks were observed at 825 and 818 cm^{-1}, corresponding to ^{16}O-^{18}O stretching vibrations, in addition to ^{16}O-^{16}O and ^{18}O-^{18}O vibrations (Figure 3, upper). In the 500-cm^{-1} region, two broad peaks were seen at 501 and 485 cm^{-1} for Fe-($^{16}O^{18}O$) stretching, whose envelopes also contained the Fe-$^{16}O_2$ and Fe-$^{18}O_2$ vibrations (Figure 3, lower).[29] These data clearly demonstrate that the two oxygen atoms of the peroxide are inequivalent. Thus, structures (a), (b), (c) in Figure 1 are inconsistent with the Raman data. Structure (d) is ruled out by X-ray crystallography of oxyHr (see below).[31,32] When exchanged with D_2O, ν(Fe-O_2) and ν(O-O) shifted to 500 and 848 cm^{-1}, respectively. These shifts suggested that the peroxide moiety is protonated (HOO^-) and, thus, the O_2 group must bind to the iron via a single oxygen atom.[14]

Two-electron oxidation of deoxyhemerythrin by ferricyanide leads to metHr. MetHr is capable of binding small anions such as azide and cyanide, resulting in azidomet- or cyanometHr. The various forms of metHr as well as oxyHr contain a μ-oxo bridge, as indicated by the short Fe-O-Fe bonds determined by EXAFS and X-ray crystal studies, by the presence of intense near-UV charge-transfer bands, and by the strong antiferromagnetic coupling between the two Fe(III) ions (-J = 77 cm^{-1} in oxyHr) determined from magnetic susceptibility studies. In addition, the Fe-O-Fe vibrations are active in RR spectra.[16,17] Met derivatives of hemerythrin have been extensively investigated.[27] However, since they are not physiologically active, these studies are not discussed in detail here.

The RR spectrum of oxyHr showed an intense feature at 486 cm^{-1} and a moderate peak at 753 cm^{-1} with near-UV excitation into the 350-nm $O^{2-} \rightarrow$ Fe(III) CT band. They were assigned to ν_s(Fe-O-Fe) and ν_{as}(Fe-O-Fe), respectively, by

comparison to those observed for model complexes and metHrs and, more definitively, by their shifts to 472 and 717 cm^{-1}, respectively, upon exchange of the bridging oxygen with $H_2{}^{18}O$ solvent (Figure 2B).[14] Compared to those of methemerythrins, the ν_s(Fe-O-Fe) of oxyHr is significantly lower in energy. For example, the symmetric Fe-O-Fe stretching mode of oxyHr is $\sim$20 cm^{-1} lower than that in azidometHr (486 vs. 507 cm^{-1}). The corresponding asymmetric stretching mode is 15 cm^{-1} lower (753 vs. 768 cm^{-1}). This decrease in vibrational frequencies has been attributed to hydrogen bonding between the oxo bridge and the hydroperoxide of oxyHr.[17] This hydrogen bond was verified by D-isotope shifts on ν_s(Fe-O-Fe), from 486 cm^{-1} (in H_2O) to 490 cm^{-1} (in D_2O). This isotopic shifts is unique to oxyHr, and is not observed in any of the methemerythrins, indicating that it is due to factors at the ligand binding site rather than general exchange of protein residues. The frequency increase of ν_s(Fe-O-Fe) in D_2O indicates that the deuterium bond is weaker than the analogous hydrogen bond and that the Fe-O-Fe frequency is approaching that of the non hydrogen-bonded metHrs.[17]

X-ray crystal structures have provided detailed structural information of hemerythrin including the dinuclear iron centers. The structures of deoxyHr and oxyHr had been solved to 3.9-Å and 2.2-Å resolution, respectively, by 1985[31], and have been refined to 2.0 Å more recently.[32] The overall protein structures are the same as those of azidometHr determined previously by X-ray crystallography.[33,34] Each monomer of the octomer hemerythrin consists of four antiparallel α-helices. In all forms of hemerythrin, the dinuclear iron center is held by 7 protein ligands, 3 His to Fe1, 2 His to Fe2, two carboxylates (Glu and Asp) bridging the two iron atoms, and additionally, by a solvent derived μ-oxo (or μ-hydroxyl in deoxyHr) group that also bridges the two iron atoms (Figure 4A).

The main differences are found only in the active site. In the structures of deoxyHr, the Fe$\cdots$Fe separation and Fe-O distances are found to be larger than those in the oxidized forms of the protein. In the 2.0-Å structure of deoxyHr, the Fe-OH-Fe complex is asymmetric, with an average (over 8 subunits) Fe1-OH distance of 2.15 Å and average Fe2-OH distance of 1.88 Å, while the Fe$\cdots$Fe separation is 3.32

Å. These data, together with magnetic susceptibility data ($-J = \sim 15\ cm^{-1}$),[16] suggest that the group bridging the two Fe atoms in deoxyHr is a hydroxyl.[31,32]

The structure of the oxyHr clearly showed that the bound peroxo group is ligated to Fe2 and bends back towards the bridging oxygen. The average distance between the outer peroxy oxygen atom and the bridging oxygen atom is 2.8 Å, consistent with a hydrogen bond between those two atoms. The oxygen binding site is quite hydrophobic and there are no other groups in the active site that can hydrogen bond the peroxo moiety. The Fe-O-Fe moiety is believed to be quite symmetric with an average Fe-O distance of 1.84 Å. The two Fe(III) atoms are separated by 3.27 Å, and the Fe-O-Fe angle was determined as 125° (Figure 4A).[31,32] This latter value is in good agreement with the angle of 134° calculated from secular equations using ν_s(Fe-O-Fe) for ^{16}O and ^{18}O derivatives.[35]

Based on the information of the active site structures of the deoxy and oxy hemerythrins, the mechanism of conversion of deoxyHr to oxyHr has been proposed (Figure 4B). Upon dioxygen binding to Fe2, oxidation of the dinuclear ferrous center occurs, and the proton on the bridging hydroxyl group shifts to the dioxygen, leaving a μ-oxo bridge between the Fe atoms. The peroxo is then stabilized by a hydrogen bond back to the bridging oxygen atom (Figure 4B).[31] Due to the nonpolar nature of the environment, the peroxide is most readily released as a neutral dioxygen, thereby accounting for the reversibility of the reaction.

3. Oxygen Activation in Cytochrome P-450 Monooxygenases

Cytochrome P-450 is a collective name for monooxygenases containing *b*-type hemes (Figure 5A), which are noncovalently attached to the protein and have a cysteine thiolate as the fifth ligand (Figure 5B). This family of enzymes has very unusual spectral properties owing to the thiolate ligand. When the ferrous heme is complexed with carbon monoxide, the derivative exhibits a characteristic absorption maximum at ~450 nm, whence the name cytochrome P-450 (Figure 6C). Cytochrome P-450 monooxygenase systems are widely distributed in nature. More than 150 P-

450s have been found in animals, plants, yeasts and bacteria. In animals and plants, the enzyme system has been detected in all tissues examined. The eukaryotic P-450 systems are usually membrane bound while those of bacterial origin are generally soluble. Cytochrome P-450s catalyze hydroxylation of hydrocarbon groups of fatty acids, steroid rings, and many xenobiotics (Equation 4).

$$RH + O_2 + NADPH + H^+ \rightarrow ROH + H_2O + NADP^+ \qquad (4)$$

P-450s in liver also catalyze a wide variety of additional reactions, including epoxidations, dealkylations, deaminations, and dehalogenations.[36]

The mechanism of oxygen activation by P-450 has been extensively studied. However, since some crucial intermediates in the catalytic cycle have not been fully characterized due to their instability, some key steps in the mechanism have been rationalized by comparative studies with heme peroxidases and modeling studies.

The best characterized cytochrome P-450 system is the monooxygenase ($P\text{-}450_{cam}$) isolated from the soil bacteria *Pseudomonas putida*. The bacteria can utilize D-camphor as the sole carbon and energy source and the enzyme catalyzes 5'-exo-hydroxylation of D-camphor. The mechanistic steps of oxygen activation by $P\text{-}450_{cam}$ are summarized in Figure 7. The P-450 reaction cycle begins with binding of the substrate at the active site, which changes the resting, low-spin hexacoordinate ferric state (1) to high-spin pentacoordinate Fe(III)-substrate complex (2), concomitantly raising the redox potential from -300 mV to -170 mV and changing the Soret absorption maximum from ~417 nm to 391 nm (Figure 6). (2) accepts one electron and forms the high spin pentacoordinate ferrous enzyme-substrate complex (3). This reduced form of P-450 is able to bind O_2 reversibly, yielding the last stable intermediate, oxy-P-450 (4). One electron reduction of the oxy form gives rise to a peroxo intermediate (5). Cleavage of the O-O bond produces a high valent iron-oxo (ferryl) species with a porphyrin or protein π-cation radical (6), which is competent to abstract a hydrogen atom from the substrate to produce a substrate radical (7), then "oxygen rebound" results in the hydroxylation of substrate that is released as

product.[37-39]

Resonance Raman Studies. States 1 through 4 in Figure 7 are stable or relatively stable, and thus, have been well characterized by various spectroscopic techniques including UV-Vis, resonance Raman, infrared, EPR, NMR, EXAFS, Mössbauer, and MCD spectroscopy. It is impractical to review all of these studies in this section. Rather, RR investigations of the four physiologically active and stable species (Figure 8) of the P-450$_{cam}$ reaction cycle are outlined below.

Resonance Raman scattering is a highly sensitive probe of the heme environment and of the iron oxidation, spin and ligation states,[40] making it ideal for the analysis of the different species of the P-450 cycle. The first systematic RR studies of different P-450 states were reported in 1978.[41,42] Recently, RR spectra of various forms of P-450$_{cam}$ that were isolated from gene products overexpressed in *E. coli* cells have been reported.[43] The recent spectra, while identical to those reported earlier,[41] are now shown with higher resolution and clarity. Figure 9 shows the RR spectra of the ferric P-450$_{cam}$-substrate complex (or m^{os}) using various excitation wavelengths. Raman bands above 1300 cm^{-1} correspond to porphyrin ring modes that are sensitive to the spin and oxidation states of the hemes.[40] The oxidation state marker, ν_4, is seen at 1368 cm^{-1} with excitation on the higher energy side of the Soret band (λ_{max} = 391 nm, Figure 6B) and at 1372 cm^{-1} with excitation on the lower energy side of the Soret band. However, both of these frequencies are consistent with the ferric state. The spin/core size marker bands, ν_3 and ν_{10} (bands II and V in Figure 9), are seen at 1488 and 1623 cm^{-1}, respectively, normal for a high-spin, pentacoordinate ferric heme.

The camphor-free, resting-form of the enzyme (m^{o}), and the ferrous substrate P-450 complex (m^{rs}) were also investigated.[41,43] The Raman results are summarized in Table 2. The oxidation state marker, ν_4, and the spin/core size maker bands, ν_3 and ν_{10}, were reported at 1373, 1503, and 1635 cm^{-1}, respectively, reflecting the low-spin, hexacoordinate ferric heme for the substrate-free, oxidized enzyme. For the reduced enzyme-camphor complex, these marker bands were seen at 1345, 1466 and

1601 cm^{-1} (ν_4, ν_3 and ν_{10}, respectively), consistent with the high-spin, pentacoordinate ferrous heme.

Dioxygen binding comes as the next step. The first RR studies of the oxy complex were reported in 1986.[44] The oxy complex was stabilized at ~-60°C in the presence of the substrate but in the absence of an electron donor. The Raman spectra revealed the ν(O-O) at 1140 cm^{-1}, that shifts to 1074 cm^{-1} with $^{18}O_2$ oxygenated protein (Figure 10). The oxidation state marker, ν_4, is at 1376 cm^{-1}. Photostationary states involving the photolysis of O_2^- and partial heme reduction were also observed. Recently, another RR study of the oxy P-450 complex was reported.[45] The oxy P-450_{cam} was generated at room temperature and under catalytic conditions, i.e., in the presence of the substrate, D-camphor, and electron donors, β-NADH, putidaredoxin, as well as putidaredoxin reductase. The Raman spectra were obtained using a custom-designed mixed-flow transient Raman apparatus. Their Raman spectra are basically the same as reported earlier, with ν(O-O) at 1141 cm^{-1} and shifting to 1072 cm^{-1} with $^{18}O_2$. The oxidation state marker, ν_4, was reported at 1373 cm^{-1}. No ν(Fe-O_2) vibrations were identified by either group.[44,45]

The observed ν(O-O) at ~1140 cm^{-1} is comparable to those of oxy Co-substituted hemoglobin and myoglobin (1137 cm^{-1}), indicating that the dioxygen is bound as a superoxide.[45] The ν_4 oxidation marker at ~1375 cm^{-1} in the oxy complex is consistent with a ferric oxidation state of the heme. These results indicate a ferric-superoxide formulation of oxyP-450. Neither of these papers investigated the use of mixed-label O_2 ($^{16}O^{18}O$), thus the Fe-superoxide binding geometry is still not definitive. Presumably, the superoxide binds to the Fe in the end-on fashion, as in oxyglobins.

Resonance Raman studies also provided direct evidence for the Fe-Cys ligation in P-450 and chloroperoxidase.[46] The RR spectrum of oxidized P-450/substrate complex shows a medium intensity peak at 351 cm^{-1} when excited on the high energy side of the Soret absorption band (Figure 11). This 351-cm^{-1} peak shifted -4.9 and +2.5 cm^{-1}, respectively, when the protein was isolated from ^{34}S-enriched culture and substituted with ^{54}Fe. These results unambiguously demonstrate the existence of an

Fe-S linkage in the oxidized enzyme-substrate complex. The 351-cm^{-1} feature was assigned to Fe-S stretching, accordingly. Similarly, a peak at 347 cm^{-1} was identified as ν(Fe-S) of the Fe-Cys linkage in chloroperoxidase by its -4.9 isotopic shift with ^{34}S.[47]

X-Ray Crystal Structures. The cytochrome P-450_{cam} enzyme isolated from *P. putida* has been extensively studied by X-ray crystallography. Crystal structures are now available for various forms of P-450_{cam}, from substrate-free to camphor-bound, camphor with CO, as well as the protein bound with alternative substrates, norcamphor, camphane, adamantanone, adamantane, and thiocamphor.[48]

Figure 12A shows the X-ray structure of the camphor-bound complex. The enzyme has roughly a triangular shape. Helices represent the primary structural motif, containing ~50% of the total residues. The heme *b* is rather deeply buried and is sandwiched between helix L and I. The cysteinate ligand (Cys 357) comes from helix L. In the camphor-bound form, the heme is pentacoordinate and the camphor molecule is held in place by hydrophilic intermediates and by H-bonding of its carbonyl oxygen to Tyr 96. The substrate, camphor, sits just above pyrrole ring A with the iron atom facing the 5-exo position, which may explain the stereoselective hydroxylation of this enzyme (Figure 12B, right). The camphor-free P-450_{cam} is hexacoordinate with a water or a hydroxide ligand bound on the distal side. Another five water molecules form a H-bonded network and occupy the substrate binding pocket (Figure 12B, left). No large conformational changes are observed between these two structures.[49-51]

O-O Bond Cleavage, Heterolytic vs. Homolytic. The states subsequent to the oxy complex are much less well known. Transfer of the second electron to the oxy complex leads to the putative peroxy complex. It is believed that the rate-determining step in the oxygen activation cycle of P-450 is the reduction of the oxy complex. Therefore, the following steps and intermediates are not observable in the P-450 cam system. The existence of a peroxo intermediate comes from following

indirect evidence: 1) Hydrogen peroxide is produced in mutants of distal-pocket residues in the absence of substrate[52,53] or for substrates that lead to substantial uncoupling of the NADPH/O_2 from substrate hydroxylation (Equation 5);

$$NADPH + H^+ + O_2 \rightarrow NADP^+ + H_2O_2 \qquad (5)$$

2) P-450 forms reversible complexes with organic peroxides, and in the absence of the NADPH/O_2 system, H_2O_2 and organic peroxides support some of the P-450 oxidation reactions (equation 6).[39,54]

$$RH + XOOH \rightarrow ROH + XOH \qquad (6)$$

The next step, cleavage of the O-O bond and generation of an "active oxygen", is the least understood and most controversial process in the entire scheme. Although several early suggestions that cleavage of the O-O bond could be homolytic,[55,56] more recent experimental evidence favors heterolytic cleavage.

The crystal structures of cytochrome c peroxidase (CCP) provides a strong suggestion that polar residues within the active site facilitate the heterolytic cleavage of the O-O bond of hydrogen peroxide. The distal histidine (His 52) serves as a proton donor to the peroxide anion and works together with a charged residue (Arg 48) to polarize the O-O bond.[51] The crystal structures of P-450_{cam} indicate that the active site of P-450 is rather nonpolar compared to CCP and that there are no residues similar to the distal His and Arg found in CCP. These prompted the suggestion that only the proximal cysteine ligand was sufficiently required for O-O bond scission.[37] However, two polar groups, a hydroxyl and carboxylate from threonine 252 and aspartate 251 that are conserved among all known P-450 sequences,[57] are in the active site and strongly implicated in the O_2 activation and cleavage (Figure 13).

Site-directed mutagenesis has been used to study the importance of these polar residues. Replacing Thr 252 with an Ala or a Val affects O_2 binding only very little,

but decreases the monooxygenase activity drastically, increasing O_2 consumption with H_2O_2 released as product (Equation 5). In contrast, mutation of Thr 252 to Ser does not affect enzyme activity very much.[52] This suggests that the OH group of the Thr 252 is important in facilitating O-O bond cleavage (Figure 13).

Changing the carboxylate at position 251 (Asp 251) to an amide (asparagine) dramatically decreases the catalytic turnover of the systems. Kinetic studies showed that this decrease is not due to inhibition of substrate binding, ferric-ferrous reduction of the heme iron, or dioxygen binding. Rather, single-turnover stopped-flow experiments indicate that it is due to the 200-fold reduction in the coupled, second-electron transfer and the oxygen-oxygen bond scission step. Additionally, the data showed that the redox input is no longer completely coupled to substrate hydroxylation, rather, electron equivalents are appearing as hydrogen peroxide and water.[53]

Based on these observations, an enzyme mechanism for P-450 has been proposed as shown in Figure 13. Thr 252 forms a hydrogen bond to the bound dioxygen and stabilizes this state and the peroxo complex. It was proposed that Asp 182, Lys 178, Arg 186, Asp 251, and Thr 252 form a charge relay system in the distal pocket of P-450. In this model, Asp 251 functions as a proton shuttle between the solvent-accessible Asp182-Lys178-Arg186 network and Thr 252. The OH group of Thr 252 serves as a general-acid-catalyst and aids cleavage of the peroxo O-O bond. Without the hydroxyl group, rapid autoxidation reactions results in release of superoxide and peroxide with very little substrate hydroxylation. Hence it was concluded that the oxygen-oxygen bond scission needs a general-acid assist. Replacing Asp 251 with Asn alters the basicity of Thr 252 such that catalysis is drastically slowed.[54]

4. Oxygen Activation in Dinuclear Iron-Oxo Enzymes

Hemerythrin (Hr), and ribonucleotide reductase (RnR) are the best characterized Fe-O-Fe proteins. Methane monooxygenase (MMO) is also believed to

contain a similar cluster.[58] Recent work suggests that Δ^9 stearoyl-acyl protein desaturase from castor bean, an enzyme that catalyzes oxidative desaturation of long chain fatty acids, also contains an Fe-O-Fe cluster, as indicated by Mössbauer and resonance Raman studies.[59] Whereas Hr is an oxygen carrier, binding oxygen reversibly, the other three belong to a class of oxidases that consume oxygen in the catalysis. X-ray crystal structures of Hr and the iron-containing subunit R2 of RnR show little or no homology in iron ligation. The iron center in R2 is dominated by negatively-charged oxygen ligands whereas Hr has mostly neutral His ligands. On the other hand, R2, MMO, and the desaturase are highly homologous in the metal binding sphere (see Chapter 3).

Oxygen activation in these iron-oxo enzymes is of interest relative to the mechanisms proposed for heme proteins. It is particularly challenging to see if high valent iron-oxo (ferryl) species are involved in the reaction mechanism of these non-heme systems. Many of the proposed catalytic cycles are discussed in Chapter 3. Recently, a transient intermediate in the MMO catalytic cycle has been characterized by rapid quench Mössbauer spectroscopy. This intermediate, resulting from the reaction of reduced MMO with oxygen, was shown to contain a symmetric Fe^{IV}/Fe^{IV} cluster.[60] This study provides the first direct evidence that a high valent iron species (ferryl) is involved in oxygen activation in a non-heme iron enzyme. It validates the speculation that such high valent iron-oxo species may be a common intermediate in oxygen activation in both heme and non-heme iron enzymes.

5. Oxygen Activation in Multi-Copper Oxidases

Ascorbate oxidase, laccase, and ceruloplasmin belong to the group of enzymes usually referred to as multi-copper oxidases or "blue" copper oxidases, because all contain the strongly absorbing, type 1 Cu chromophore.[61] This group of enzymes contains all three types of copper ions and show very similar spectral properties related to each type. They all catalyze the four-electron reduction of dioxygen to water with concomitant one-electron oxidations of organic substrates (Equation 7).[62]

$$4AH + O_2 \rightarrow 2H_2O + 4A \qquad (7)$$

Ascorbate oxidase (AO) is found mainly in plants. It catalyzes the oxidation of L-ascorbate (vitamin C) and some aminophenols and polyhydroxy phenols. Because the highest AO activity is usually associated with those parts of plants that have the fastest growth, it has been suggested that the enzyme plays an important role in the mechanism of plant growth.[63] Laccase is widely distributed in higher plants and fungi, where it oxidizes monophenols, diphenols, polyphenols, and diamines, with a low specificity toward the nature of the reducing substrate. In Chinese and Japanese lacquer trees, laccase is found to be involved in the hardening process of the white latex. The enzyme catalyzes the oxidation of phenols to radicals, then the radicals polymerize spontaneously. In fungi, laccase is found to play important roles in lignin degradation.[64] Ceruloplasmin is present in the blood serum of all mammals and birds examined, and is presumed to be important to all vertebrates. Although its complete function is not fully understood, ceruloplasmin plays many important roles in physiological processes. For example, it is found to be involved in mobilization, transport, and homeostasis of copper; it also exhibits ferroxidase, amine oxidase, and possibly superoxide dismutase activities.[65,66]

The only structurally characterized multicopper oxidase is ascorbate oxidase. The X-ray structure of ascorbate oxidase from zucchini was reported by Messerschmidt et al. in 1989[67] and has been refined to 1.9 Å.[68] The protein consists of two identical subunits of 552 amino acids and each subunit is clearly divided into three domains each showing mainly β-sheet structure (Figure 14A). Each subunit has four catalytic coppers bound as a distinct mononuclear type 1 site, and a novel trinuclear cluster. The mononuclear copper is located in domain 3 and is a typical type 1 copper, with two histidines (His 447 and 514), a cysteine (Cys 509) and a methionine (Met 519) ligand in a strongly distorted tetrahedral geometry. A substrate binding site can be found near the type 1 copper site. The trinuclear cluster has eight histidines symmetrically supplied from domains 1 and 3 (Figure 14B). It may be subdivided into one type 2 and a pair of type 3 copper atoms. The type 3 pair is

bridged by a hydroxo or an oxo group and each of the type 3 copper atoms is ligated to three histidines. The type 2 copper is ligated to two histidines and also an OH^- or a water that is *trans* to the copper pair.[68] The original 2.5-Å resolution structure indicated that the two type 3 coppers in AO were equivalent, however, the higher resolution structure reveals that His 62 is ligated to Cu3 by its N_δ atom while all other histidine ligands of the trinuclear site are complexed via their N_ϵ atoms.[68]

An X-ray structure of the fully reduced form of ascorbate oxidase has been solved at 2.2-Å resolution by difference-Fourier techniques.[69] The structure shows that the geometry at the type-1 copper remains much the same compared to the oxidized form. However, the structural changes are considerable at the trinuclear copper site, as shown in Figure 15. On reduction the bridging oxygen ligand OH1 is released and the two copper atoms (Cu2 and Cu3) of the type 3 pair move towards their respective histidines and become three coordinate, the preferred stereochemistry for Cu(I). Cu2 and Cu3 are each trigonally planar coordinated by the histidine ligands with equal bond lengths and bond angles within the accuracy of the X-ray structure determination. The copper-copper distances increase from an average of 3.7 Å to 5.1 Å for Cu2-Cu3, 4.4 Å for Cu2-Cu4 and 4.1 Å for Cu3-Cu4. Cu4, the type 2 copper, remains virtually unchanged between the reduced and oxidized forms. It is in a T-shape threefold coordination not unusual for Cu(I) compounds.

A 2.6-Å resolution X-ray structure of the peroxide derivative of ascorbate oxidase was also reported.[69] Crystals of the peroxide form of the enzyme were prepared by soaking the native enzyme in 10 mM H_2O_2. The geometry at the type-1 copper site is not changed compared to the oxidized form. However, as in the reduced form, the structural changes at the trinuclear copper site are remarkable (Figure 16): (a) the peroxide binds terminally to Cu2 as a hydroperoxide; (b) the bridging oxygen ligand OH1 is absent; and (c) the copper-copper distances increase from an average of 3.7 Å to 4.8 Å for Cu2-Cu3 and 4.5 Å for Cu2-Cu4. The Cu3-Cu4 distance remains at 3.7 Å. Cu3 is three coordinate as in the reduced form, and the coordination geometry of the ligating N-atoms of the histidines can be described as a trigonal pyramid with the copper sitting atop the NNN-plane. The coordination

sphere around Cu4 is not strongly affected and is similar in all three forms. Cu2 is four coordinate in a distorted tetrahedral geometry, ligated to three N_ϵ atoms of the histidines, as in the oxidized form, and by one oxygen atom of the terminally bound peroxide molecule.

Based on the three-dimensional structures of the oxidized, reduced, and peroxide forms of ascorbate oxidase and available kinetic data, a catalytic mechanism has been proposed,[69,70] and is diagramed in Figure 17. The catalytic cycle starts from the resting form (a) in which all four copper ions are oxidized and Cu2 and Cu3 are bridged by an OH^- ligand (Cu2 and Cu3 are most likely the spin-coupled type-3 pair and Cu4 is the type-2 site). The first step is the reduction of the type-1 copper (Cu1) by the substrate in a one-electron-transfer step (b). Three further electrons are transferred through the protein, either via Cu2 or Cu3, until the enzyme is fully reduced (c). At this stage, the hydroxyl bridge between the copper pair has been released, the Cu2···Cu3 distance has increased to about 5.2 Å, and dioxygen binds to Cu2. Transfer of two electrons from the copper pair to the neutral dioxygen molecule leads to the formation of the hydroperoxide intermediate (d), as shown in Figure 16. A third electron may be transferred from Cu4 to the hydroperoxide intermediate, and a fourth electron from the type-1 copper to Cu2. With these additional electrons, the O-O bond is broken and the first water molecule is released (e). The catalytic cycle is completed by loss of the second water molecule and return to the fully oxidized copper centers (a).

No crystal structures are yet available for laccase and ceruloplasmin. However, their similar spectroscopic properties and amino acid sequence homologies suggest that these two proteins have structures similar to that of ascorbate oxidase. It is believed that these proteins have evolved from a common ancestor.[71] Comparison of their amino acid sequences shows highly conserved copper binding sites.[62] Laccase and ascorbate oxidase are more closely related to each other than to ceruloplasmin. Laccase has a total of four copper atoms, one type 1, one type 2 and a type-3 pair. Fungal laccase contains all the copper ligands of AO, with the exception of methionine at the type-1 copper. It is expected that the spatial structure

of laccase is very similar to that of AO, including the type-1 copper in domain 1 and the trinuclear center in domain 3. Previous chemical and spectroscopic studies on various derivatives of laccase and ascorbate oxidase indicate that the two type 3 copper atoms are inequivalent in both enzymes.[72,73] Another study on the mercury derivative of the protein revealed an H_2O ligand in the type 2 copper site.[74,75] These findings were all reflected in the X-ray structures of ascorbate oxidase.[67,68] Ceruloplasmin is thought to have six copper atoms, three type-1, one type-2, and a type-3 pair. As in AO and laccase, the type 2 and type 3 copper atoms are also believed to form a trinuclear cluster.[62]

Resonance Raman spectroscopy has been used to investigate the type 1 copper site of the multi-copper oxidase.[76-78] These studies reveal rich Raman spectra in the metal ligand vibrational region, a typical pattern for thiolate-coordinated, type 1 copper ions. However, no RR studies have been reported on the trinuclear copper cluster of the copper oxidases. The difficulty relates to the absorption properties and lability of the trinuclear cluster. The only chromophore characteristic of the trinuclear clusters is due to the ~330-nm absorption of the magnetically coupled type-3 pair. Type 2 Cu is not good RR chromophore, and Cu-imidazole bonds are not easily observed in RR spectroscopy without coupling to a strong chromophore. UV laser irradiation of type 3 sites leads to bleaching, and thus far, no time-resolved spectral studies of the peroxo adducts of laccase or AO appear to have been successful.

Chapter 5 of this dissertation presents RR studies of a hydroxo-bridged dinuclear copper complex,[79] that serves as a potential structural model for type-3 copper sites in the multicopper oxidases. RR and infrared spectra of the complex reveal a ν_s(Cu-OH-Cu) mode 465 cm^{-1}. Nevertheless, investigation of the Raman enhancement profile of the ν_s(Cu-OH-Cu) mode suggests that coupling to a chromophoric ligand such as phenolate may be important for the observation of M-OH vibrations in the RR spectra of such systems. Since there is no phenolate ligation of copper in the oxidases, it is likely to be very difficult to use Raman spectroscopy to study bridging OH^- groups in these proteins. However, a significant effort should be made to attempt to characterize the peroxo derivative at the heart of the catalytic

mechanism.

References

(1) Faústo da Silva, J.J.R., and Williams, R.J.P. (1991) *The Biological Chemistry of the Elements, The Inorganic Chemistry of Life*, Clarendon Press, Oxford

(2) Gutteridge, J.M., and Halliwell, B. (1990) in *Iron Transport and Storage* (Ponka, P., Schulman, H.M., and Woodworth, R.C., Eds.), pp 55-65, CRC Press, Boco Raton

(3) Long, D.A. (1977) *Raman Spectroscopy*, McGraw-Hill, New York

(4) Carey, P.R. (1982) *Biochemical Application of Raman and Resonance Raman Spectroscopy*, Academic Press, New York

(5) Loehr, T.M. (1988) In *Oxygen Complexes and Oxygen Activation by Transition Metals* (Martell, A.E., and Sawyer, D.T., Eds.), pp 17-32, Plenum, New York

(6) Sitter, A.J., Reczek, C.M., and Terner, J. (1985) *Biochim. Biophys. Acta* **828**, 229-235

(7) Hashimoto, S., Tatsuno, Y., and Kitagawa, T. (1986) *Proc. Natl. Acad. Sci. USA* **83,** 2417-2421

(8) Reczek, C.M., Sitter, A.J., and Terner, J. (1989) *J. Mol. Struct.* **214**, 27-41

(9) (a) Varotsis, C., and Babcock, G.T. (1990) *Biochemistry* **29**, 7357-7362; (b)Varotsis, C., Zhang, Y., Appleman, E.H., and Babcock, G.T. (1993) *Proc. Natl. Acad. Sci. USA* **90**, 237-241

(10) Ogura, T., Takahashi, S., Shinzawa-Itoh, K., Yoshikawa, S., and Kitagawa, T. (1990) *J. Biol. Chem.* **265**, 14721-14723

(11) Kahlow, M.A., Zuberi, T.M., Gennis, R.B., and Loehr, T.M. (1991) *Biochemistry* **30**, 11485-11489

(12) Backes, G., Ling, J., Loehr, T.M., David, S.S., Que, Jr., L., Crowder, M., Averill, B.A., and Sanders-Loehr, J. (manuscript in preparation)

(13) Shiemke, A.K., Loehr, T.M., and Sanders-Loehr, J. (1986) *J. Am. Chem. Soc.* **108**, 2437-2443

(14) Shiemke, A.K., Loehr, T.M., and Sanders-Loehr, J. (1984) *J. Am. Chem. Soc.* **106**, 4951-4956

(15) Sjöberg, B.-M., Loehr, T.M., and Sanders-Loehr, J. (1982) *Biochemistry* **21**, 96-102

(16) Sanders-Loehr, J. (1989) in *Iron Carriers and Iron Proteins* (Loehr, T.M., Ed.) pp 373-466, VCH, New York

(17) Loehr, T. M., and Shiemke, A. K. (1988) In *Biological Applications of Raman Spectroscopy* (Spiro, T.G., Ed.) vol. 3, pp 439-490, Wiley, New York

(18) Champion, P.M. (1988) In *Biological Applications of Raman Spectroscopy* (Spiro, T.G., Ed.) vol. 3, pp 249-292, Wiley, New York

(19) Ormö, M., deMare, F., Regnström, K., Åberg, A., Sahlin, M., Ling, J., Loehr, T.M., Sanders-Loehr, J., and Sjöberg, B.-M. (1992) *J. Biol. Chem.* **267**, 8711-8714

(20) Dickerson, R.E., and Geiss, I. (1983) *Hemoglobin*, Benjamin/Cummings, Menlo Park, CA

(21) Spiro, T.G. (1983) In *Iron Porphyrins* Vol II (Lever, A.B.P., and Gray, H.B., Eds), pp 89-159, Addison-Wesley, Reading, MA

(22) Yu, N.T., and Kerr, E.A. (1988) In *Biological Applications of Raman Spectroscopy* (Spiro, T.G., Ed.) vol. 3, pp 39-95, Wiley, New York

(23) Kitagawa, T. (1988) In *Biological Applications of Raman Spectroscopy* (Spiro, T.G., Ed.) vol. 3, pp 97-131 Wiley, New York

(24) Rousseau, D.L., and Friedman, J.M. (1988) In *Biological Applications of Raman Spectroscopy* (Spiro, T.G., Ed.) vol. 3, pp .133-215, Wiley, New York

(25) Sanders-Loehr, J. (1986) in *Frontiers in Bioinorganic Chemistry* (Xavier, A.V., Ed), pp 574-583, VCH, Weinheim

(26) (a) Zhang, J.-H., and Kurtz, D.M., Jr. (1991) *Biochemistry* **30**, 9121-9125;

(b) Kaminaka, S., Takizawa, H., Handa, T., Kihara, H., and Kitagawa, T. (1992) *Biochemistry* **31**, 6997-7002

(27) Wilkins, P.C., and Wilkins, R.G. (1987) *Coord. Chem. Rev.* **79**, 195-214

(28) Dunn, J.B.R., Shriver, D.F., and Klotz, I.M. (1973) *Proc. Natl. Acad. Sci. USA* **70,** 2582-2584

(29) Kurtz, D.M., Jr., Shriver, D.F., and Klotz, I.M. (1976) *J. Am. Chem. Soc.* **98**, 5033-5035

(30) Ahmad, S., McCallum, J.D., Shiemke, A.K., Appleman, E.H., Loehr, T.M., and Sanders-Loehr, J. (1988) *Inorg. Chem.* **27**, 2230-2233

(31) Stenkamp, R.E., Sieker, L.C., Jensen, L.H., McCallum, J.D., and Sanders-Loehr, J. (1985) *Proc. Natl. Acad. Sci. USA* **82**, 713-716

(32) Holmes, M.A., Le Trong, I., Turley, S., Sieker, L.C., and Stenkamp, R.E. (1991) *J. Mol. Biol.* **218**, 583-593

(33) Stenkamp, R.E., Sieker, L.C., Jensen, L.H., and Sanders-Loehr, J. (1981) *Nature* **291,** 263-264

(34) Holmes, M.A., and Stenkamp, R.E. (1991) *J. Mol. Biol.* **220**, 723-737

(35) Sanders-Loehr, J., Wheeler, W.D., Shiemve, A.K., Averill, B.A., and Loehr, T.M. (1989) *J. Am. Chem. Soc.* **111**, 8084-8093

(36) Coon, M.J., and White, R.E. (1980) In *Metal Ion Activation of Dioxygen* (Spiro, T.G. Ed.) pp 73-123, Wiley, New York

(37) Dawson, J.H. (1988) *Science* **240,** 433-439

(38) Coon, M.J., Ding, X., Pernecky, S.J., and Vaz, A.D.N. (1992) *FASEB J.* **6**, 669-673

(39) Black, S.D., and Coon, M.J. (1987) *Adv. Enzymol.* **60**, 35-87

(40) Spiro, T.G., and Li, X.-Y. (1988) In *Biological Applications of Raman Spectroscopy* (Spiro, T.G., Ed.) vol. 3, pp 1-37, Wiley, New York

(41) Champion, P.M., Gunsalus, I.C., and Wagner, G.C. (1978) *J. Am. Chem. Soc.* **100**, 3743-3751

(42) Ozaki, Y., Kitagawa, T., Kyogoku, Y., Imai, Y., Hashimoto-Yutsudo, C.,

and Sato, R. (1978) *Biochemistry* **17,** 5826-5831

(43) Wells, A.V., Li, P., Champion, P.M. (1992) *Biochemistry* **31,** 4348-4393

(44) Bangcharoenpaurpong, O., Rizos, A.K., Champion, P.M., Jollie, D., and Sligar, S.G. (1986) *J. Biol. Chem.* **261**, 8089-8092

(45) Egawa, T., Ogura, T., Makino, R., Ishimura, Y., and Kitagawa, T. (1991) *J. Biol. Chem.* **266**, 10246-10248

(46) Champion, P.M, Stallard, B.R., Wagner, G.C., and Gunsalus, I.C. (1982) *J. Am. Chem. Soc.* **104**, 5469-5472

(47) Bangcharoenpaurpong, O., Champion, P.M., Hall, K., and Hager, L.P. (1986) *Biochemistry* **25,** 2374-2378

(48) (a) Poulos, T.L., and Raag, R. (1992) *FASEB J.* **6**, 674-679; (b) Poulos, T.L., Finzel, B.C., and Howard, A.J. (1987) *J. Mol. Biol.* **192**, 687-700

(49) Poulos, T.L., Finzel, B.C., Gunsalus, I.C., Wagner, G.C.,and Kraut, J. (1985) *J. Biol. Chem.* **260,** 16122-16130

(50) Poulos, T.L., Finzel, B.C., and Howard, A.J. (1986) *Biochemistry.* **25**, 5314-5322

(51) Poulos, T.L. (1987) *Adv. Inorg. Biochem* **7,** 1-36

(52) Imai, M., Shimada, H., Watanabe, Y., Matsushima-Hibiya, Y., Makino, R., Koga, H., Horiuchi, T., and Ishimura, Y. (1989) *Proc. Natl. Acad. Sci. USA* **86**, 7823-7827

(53) Martinis, S.A., Atkins, W.A., Stayton, P.S., and Sligar, S.G. (1989) *J. Am. Chem. Soc.* **111**, 9252-9253

(54) Geber, N., and Sligar, S.G. (1992) *J. Am. Chem. Soc.* **114**, 8742-8743

(55) Blake, R.C., and Coon, M.J. (1980) *J. Biol. Chem.* **255,** 4100-4111

(56) White, R.E., Sligar, S.C. and Coon, M.J. (1980) *J. Biol. Chem.* **255,** 11108-11111

(57) Nelson, D.R., and Strobel, H.W. (1989) *Biochemistry 28,* 656-660

(58) Sanders-Loehr, J. (1989) in *Iron Carriers and Iron Proteins* (Loehr, T.M., Ed.) pp 373-466, VCH, New York

(59) (a) Fox, B.G., Shanklin, J., Somerville, C., and Münck, E. (1993) *Proc. Natl. Sci. USA* **90**, 2486-2490; (b) Fox, B.G., Ai, J., Loehr, T.M., and Sanders-Loehr, J., unpublished results.

(60) Lee, S.-K., Fox, B.G., Froland, W.A., Lipscomb, J.D., and Münck, E. (1993) *J. Am. Chem. Soc.*, in press

(61) Solomon, E.I., Penfield, K.W., and Wilcox, D.E. (1983) *Struct. Bonding (Berlin)* **53**, 1-57

(62) Messerschmidt, A., and Huber, R. (1990) *Eur. J. Biochem.* **187**, 341-352

(63) Mondovi, B., and Avigliano, L. (1984) In *Copper Proteins and Copper Enzymes* (Lontie, L. Ed.), Vol III. pp 101-118. CRC Press, Boca Raton, Florida

(64) Reinhammer, B. (1984) In *Copper Proteins and Copper Enzymes* (Lontie, L. Ed.) Vol III. pp 1-35, CRC Press, Boca Raton, Florida

(65) Ryden, L. (1984) In *Copper Proteins and Copper Enzymes* (Lontie, L. Ed.) Vol III. pp 37-100, CRC Press, Boca Raton, Florida

(66) Frieden, E. (1981) In *Metal Ions in Biological Systems* (Sigel, H., Ed.), Vol 13. pp 117-142, Marcel Dekker, New York

(67) Messerschmidt, A., Rossi, A., Ladenstein, R., Huber, R., Bolognesi, M., Gatti, G., Marchesini, A., Petruzzeli, R., Finazzi-Agro, A. (1989) *J. Mol. Biol.* **206,** 513-529

(68) Messerschmidt, A., Ladenstein, R., Huber, R., Bolognesi, M., Avigliano, L., Petruzzeli, R., Rossi, A., and Finazzi-Agro, A. (1992) *J. Mol. Biol.* **224,** 179-205

(69) Messerschmidt, A., Luecke, H., and Huber, R. (1993) *J. Mol. Biol.* **230**, 997-1014

(70) Messerschmidt, A. (1993) in *Bioinorganic Chemistry of Copper* (Karlin, K.D., and Tyeklár, Z. Eds.), pp 471-484, Chapman & Hall, New York

(71) Huber, R. (1989) *EMBO. J.* **8**, 2125-2147

(72) Cole, J.L., Clark, P.A., and Solomon, E.I. (1990) *J. Am. Chem. Soc.* **112**,

9534-9548

(73) Casella, L., Gullotti, M., Pallanza, G., Pintar, A. (1988) *Biochem. J.* **251,** 441-446

(74) Tamilarasan, R., and McMillin, D.R. (1989) *Biochem. J.* **263**, 425-429

(75) Morrie-Bebel, M.M., McMillin, D.R. (1986) *Biochem. J.* **235**, 415-420

(76) Siiman, O., Young, N.M., and Carey, P.R. (1976) *J. Am. Chem. Soc.* **98**, 744-748

(77) Blair, D.F., Campbell, G.W., Schoonover, J.R., Chan, S.I., Gray, H.B., Malmström, B.G., Pecht, I., Swanson, B.I., Woodruff, W.H., Cho, W.K., English, A.M., Fry, H.A., Lum, V., and Norton, K.A. (1985) *J. Am. Chem. Soc.* **107**, 5755-5766

(78) Woodruff, W.H., Dyer, R.B., and Schoonover, J.R. (1988) In *Biological Applications of Raman Spectroscopy* (Spiro, T.G., Ed.), vol. 3, pp . 413-438, Wiley, New York

(79) Ling, J., Farooq, A., Karlin, K.D., Loehr, T.M., and Sanders-Loehr, J. (1992) *Inorg. Chem.* **31**, 2552-2556

(80) Messerschmidt, A., Steigemann, W., Huber, R., Lang, G., and Kroneck, P.M.H. (1992) *Eur. J. Biochem.* **209,** 597-602

(81) Han, S., Ching, Y.-C., and Rousseau, D.L. (1990) *Nature* **348,** 89-90

Table 1

Vibrational Spectra of Oxygen Species and Oxygen Isotopic Effects

Species	Example	Vibration	$\upsilon^a(^{16}O_2)$	$\Delta\upsilon(^{18}O_2)$	$\Delta\upsilon(^{16}O^{18}O)$
O_2	O_2 gas	ν(O=O)	1555	-88	-43
Superoxo	$Fe^{III}(O_2^-)^b$	ν(O-O)	~1132	-66	-28, -32
(end on)		ν(Fe-O_2)	~567	-27	0, -27
Peroxo	$Fe^{III}(O_2^{2-})^c$	ν(O-O)	844	-48	-19, -25
(asym.)		ν(Fe-O_2)	503	-21	-2, -18
(sym.)	$Cu_2(O_2^{2-})^d$	ν(O-O)	750	-41	-21
		ν(Cu-O_2)	542	-23	-12
Ferryl	$Fe^{IV}=O^e$	ν(Fe=O)	790	-35	0, -35
Hydroxy	$Fe^{III}(OH)^e$	ν(Fe-OH)	450	-25	0, -25

[a] υ and $\Delta\upsilon$ are in cm^{-1};

[b] exemplified by hemoglobin, from Ref. 5;

[c] exemplified by hemerythrin, from Ref. 5;

[d] exemplified by hemocyanin, see Chapter 4;

[e] exemplified by cytochrome oxidase, from Ref. 9 and 81.

Table 2

Observed Heme Core Marker Bands for Cytochrome P-450$_{cam}$ [a]

Sample	ν_4	ν_3	ν_2	ν_{10}	Assignment[b]
P450 m^{o}	1373	1503	1584	1635	LS, 6C, Fe^{3+}
P450 m^{os}	1368 1372	1488	1570 1582	1623 1637	HS, 5C, Fe^{3+} LS, 6C, Fe^{3+}
P450 m^{rs}	1345	1466	1564	1601	HS, 5C, Fe^{2+}
P450 m^{r}	1345	1468	1563	1601	HS, 5C, Fe^{2+}

[a]All units are in cm^{-1}, λ_{ex} = 420 nm, data from References 41;

[b]LS, low spin; HS, high spin; 5C, 5-coordinate; 6C, 6-coordinate.

Figure Legends

Figure 1. Possible structures of dioxygen species coordinated to a dinuclear metal site (exemplified by dinuclear iron site). Adapted from references 29 and 30.

Figure 2. (A) Absorption spectra of oxy and deoxyhemerythrin; the ordinate is molar absorbance in $M^{-1}cm^{-1}/2Fe$. (B) Resonance Raman spectra of oxyhemerythrin in $H_2{}^{16}O$ (upper) and $H_2{}^{18}O$ (lower), obtained with 363.8-nm excitation. From reference 16.

Figure 3. Resonance Raman spectra of oxyhemerythrin prepared with mixed label oxygen (containing 58 atom % ^{18}O). Upper: in the ν(O-O) region the spectrum shows a doublet corresponding to two $\nu(^{16}O\text{-}^{18}O)$ (components b and c), in addition to the $\nu(^{16}O\text{-}^{16}O)$ (component a) and $\nu(^{18}O\text{-}^{18}O)$ (component d). Lower: in the ν(Fe-O) region, it shows two $\nu(Fe\text{-}^{16}O^{18}O)$ (components b and c), in addition to the $\nu(Fe\text{-}^{16}O_2)$ and $\nu(Fe\text{-}^{18}O_2)$ (components a and d, respectively). From reference 29.

Figure 4. (A) Active site structure of oxyhemerythrin, adapted from reference 32. (B) Proposed mechanism for conversion of deoxyhemerythrin to oxyhemerythrin. From references 31 and 32.

Figure 5. (A) Structure of heme *b* (Fe-protoporphyrin IX). (B) Structure of heme *b* in cytochrome P-450 and chloroperoxidase.

Figure 6. Absorption spectra of various states of cytochrome $P\text{-}450_{cam}$, the substrate-free Fe(III) enzyme (m^o), the substrate-bound Fe(III) enzyme (m^{os}), the substrate-bound Fe(II) enzyme (m^{rs}), and the substrate-bound oxy-Fe(II) enzyme (m^{rs}/o_2), adapted from reference 41 and 44.

Figure 7. Proposed mechanism for cytochrome P-450 catalyzed hydroxylation of organic substrates by molecular oxygen. States 1 through 4, the substrate-free Fe(III) enzyme, the substrate-bound Fe(III) enzyme, the substrate-bound Fe(II) enzyme, and the substrate-bound oxy-Fe(II) enzyme, respectively, have been well characterized. Other intermediates have not been characterized and are placed in square brackets. Adapted from references 37-39.

Figure 8. The cytochrome P-450_{cam} reaction cycle consists of the four relatively stable intermediates: m^{o}, m^{os}, m^{rs}, and m^{rs}/o_2 as in Figure 6 and states 1 to 4 in Figure 7, respectively. From reference 41.

Figure 9. Resonance Raman spectra of substrate-bound Fe(III) form (m^{os}) of cytochrome P-450_{cam} with various excitations. From reference 41.

Figure 10. Resonance Raman spectra of substrate-bound oxy-Fe(II) form (m^{rs}/o_2) of cytochrome P-450_{cam}. (A) $m^{rs}/^{16}o_2$ and (B) $m^{rs}/^{18}o_2$. From reference 44.

Figure 11. Resonance Raman spectra of substrate-bound Fe(III) form (m^{os}) of cytochrome P-450_{cam} with UV (363.8 nm) excitation; the inset on the left shows the ^{56}Fe-^{54}Fe and ^{32}S-^{34}S difference spectra, respectively, in the 350-cm^{-1} region. From reference 46.

Figure 12. X-ray crystal structure of cytochrome P-450_{cam}. (A) The protein structure, α-helices are shown as rods and β-sheets as flat arrows. From reference 49. (B) The edge-on views of the active-site region, left, the substrate-free structure shows the axial aqua ligand that links to the network of hydrogen-bonded water molecules; right, the camphor-bound structure shows location of the substrate and the hydrogen-bond between

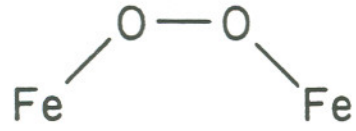

a.

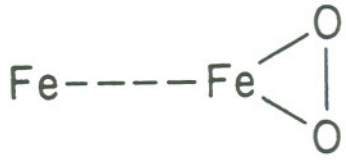

b.

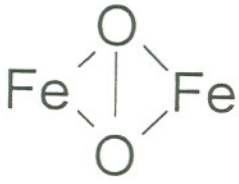

c.

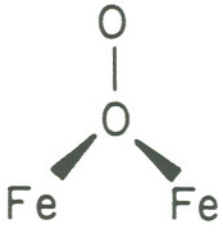

d.

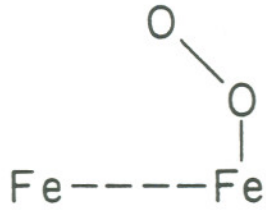

e.

Figure 1

A).

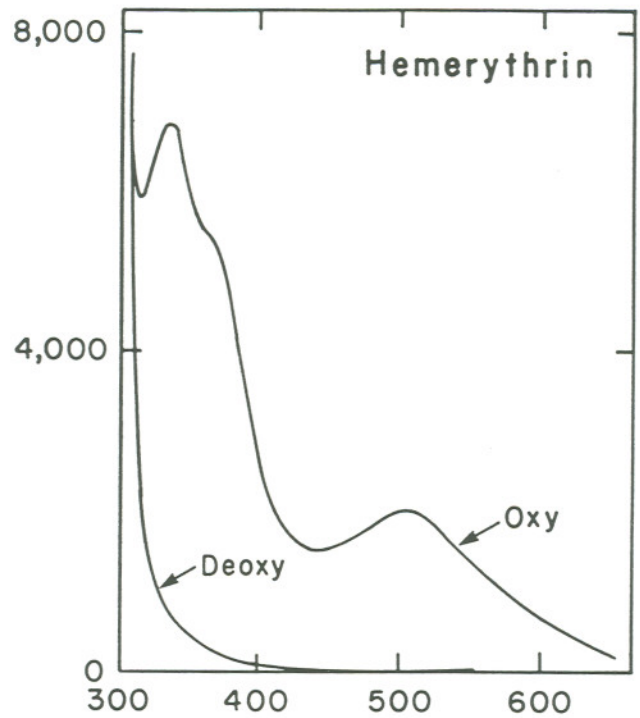
8,000
4,000
0
300
400
500
600
Hemerythrin
Oxy
Deoxy

B).

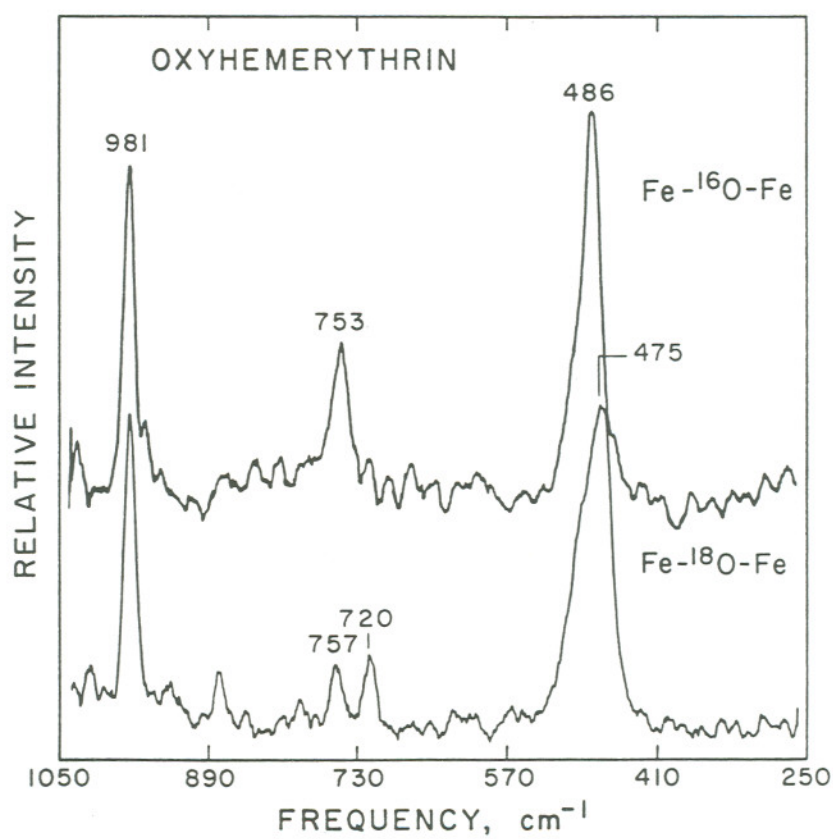
OXYHEMERYTHRIN
981
753
486
475
720
757
Fe-16O-Fe
Fe-18O-Fe
RELATIVE INTENSITY
1050
890
730
570
410
250
FREQUENCY, cm-1

Figure 2

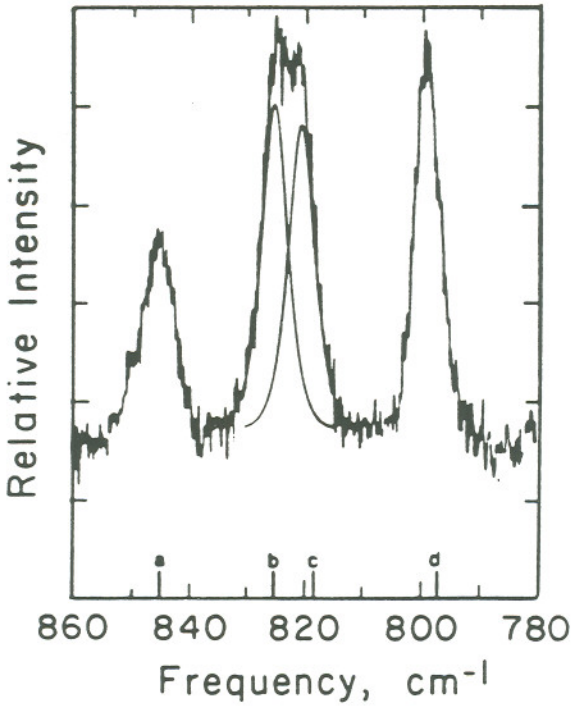
Relative Intensity
a
b
c
d
860
840
820
800
780
Frequency, cm-1

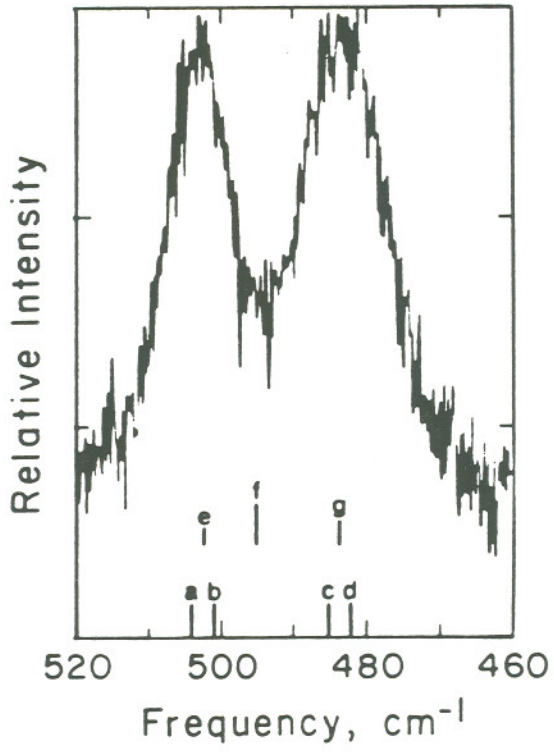
Relative Intensity
e
f
g
a
b
c
d
520
500
480
460
Frequency, cm-1

Figure 3

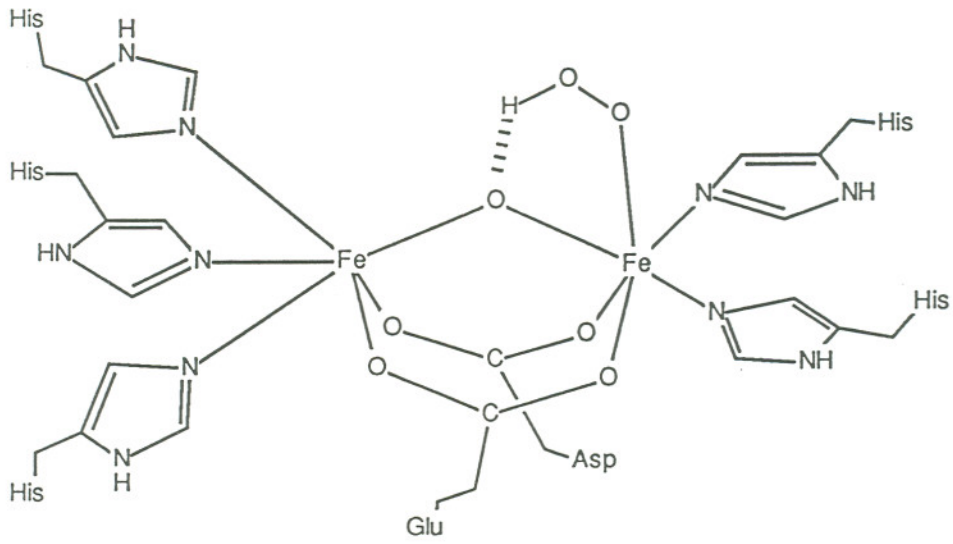
His
His
HN
His
NH
His
NH
His
Fe
Fe
Asp
Glu

A

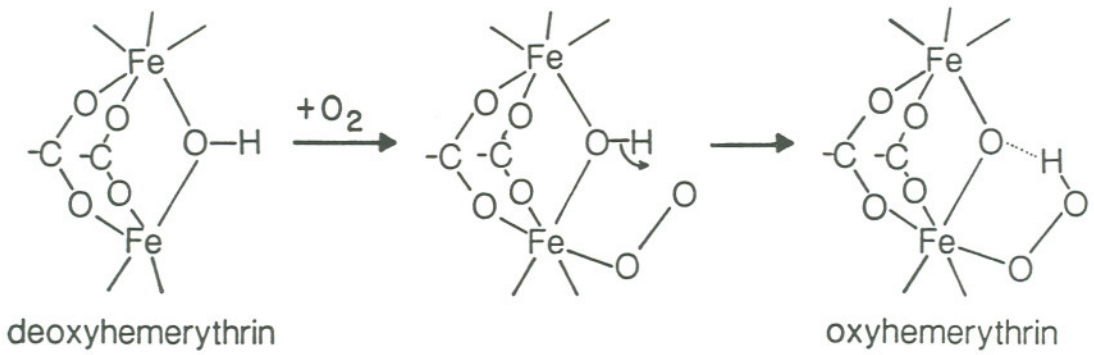
Fe
+O2
O—H
Fe
O—H
Fe
H
deoxyhemerythrin
oxyhemerythrin

B

Figure 4

A).

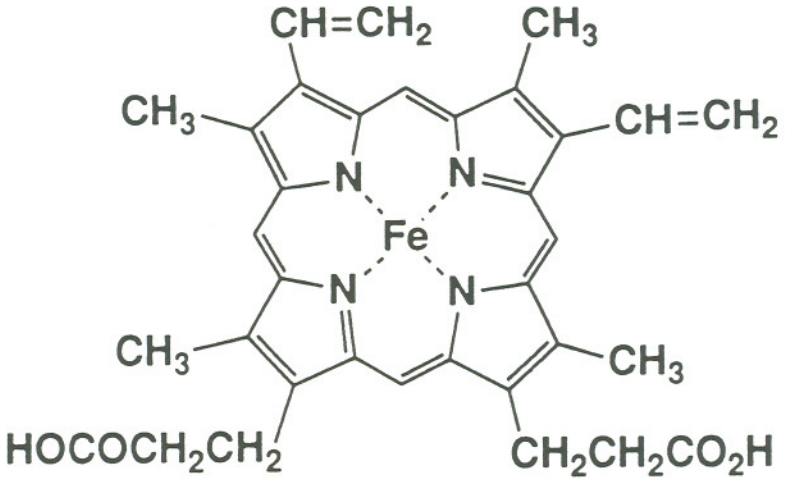
CH=CH2
CH3
CH3
CH=CH2
N
N
Fe
N
N
CH3
CH3
HOCOCH2CH2
CH2CH2CO2H

B).

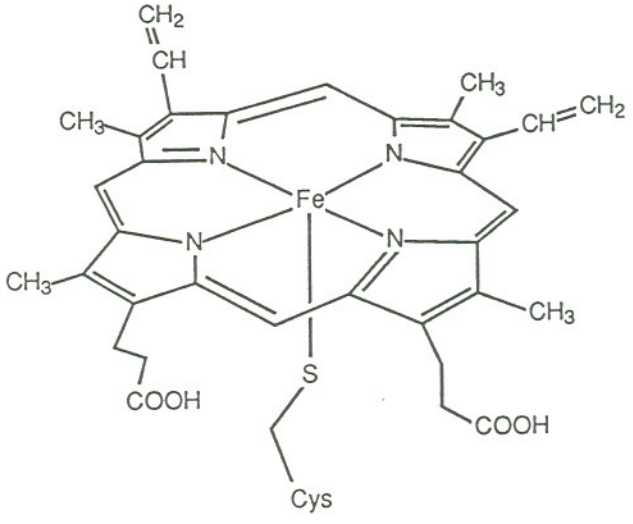
CH2
CH
CH3
CH3
CH=CH2
N
N
Fe
N
N
CH3
CH3
S
COOH
COOH
Cys

Figure 5

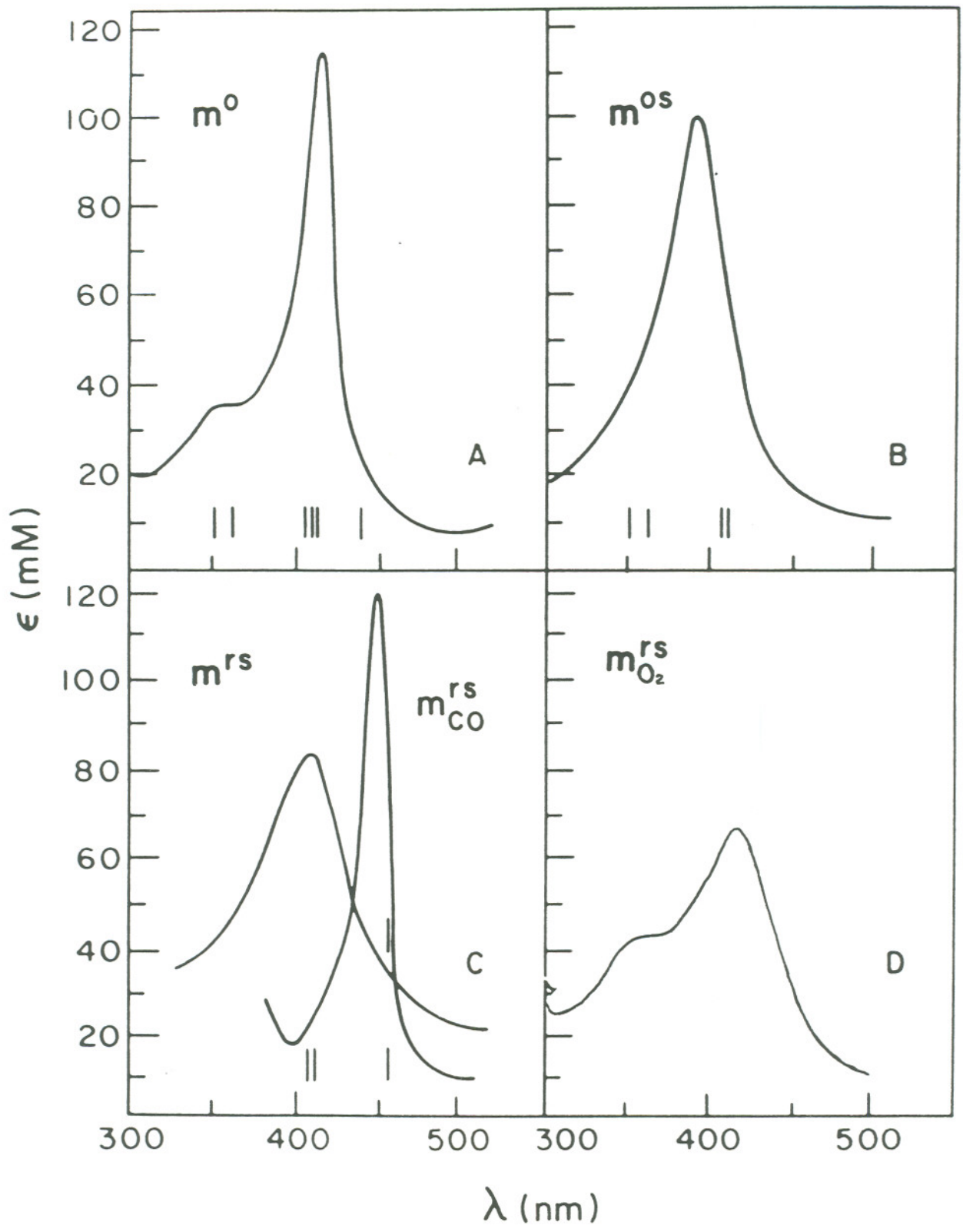
120
100
80
60
40
20
ε (mM)
m^o
A
m^os
B
m^rs
m^rs_CO
C
m^rs_O2
D
300
400
500
λ (nm)

Figure 6

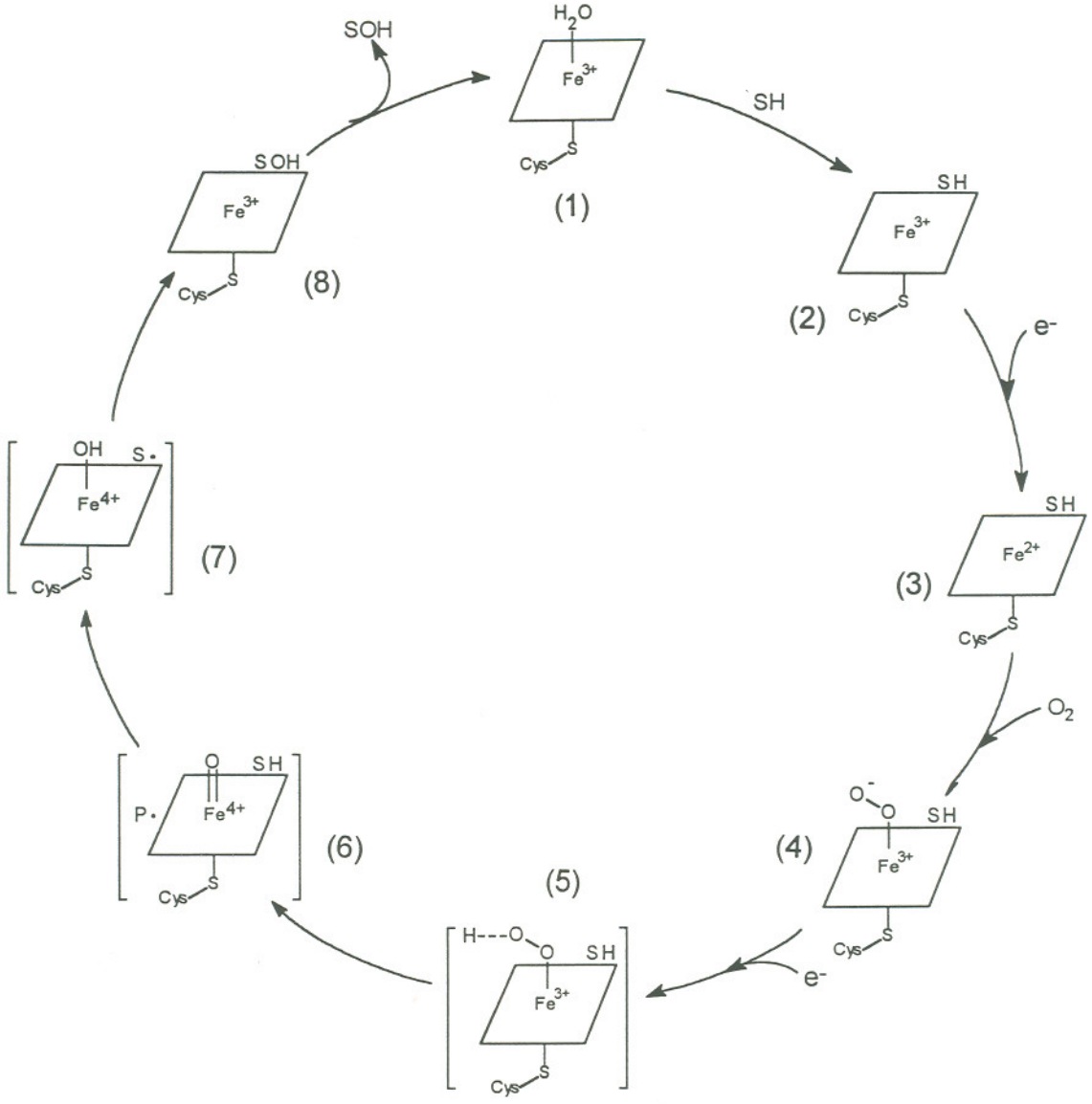
H2O
Fe3+
Cys
S
(1)
SH
SH
Fe3+
(2)
e-
SH
Fe2+
(3)
O2
O
O
SH
Fe3+
(4)
e-
H---O
O
SH
Fe3+
(5)
O
SH
P.
Fe4+
(6)
OH
S.
Fe4+
(7)
SOH
SOH
Fe3+
(8)

Figure 7

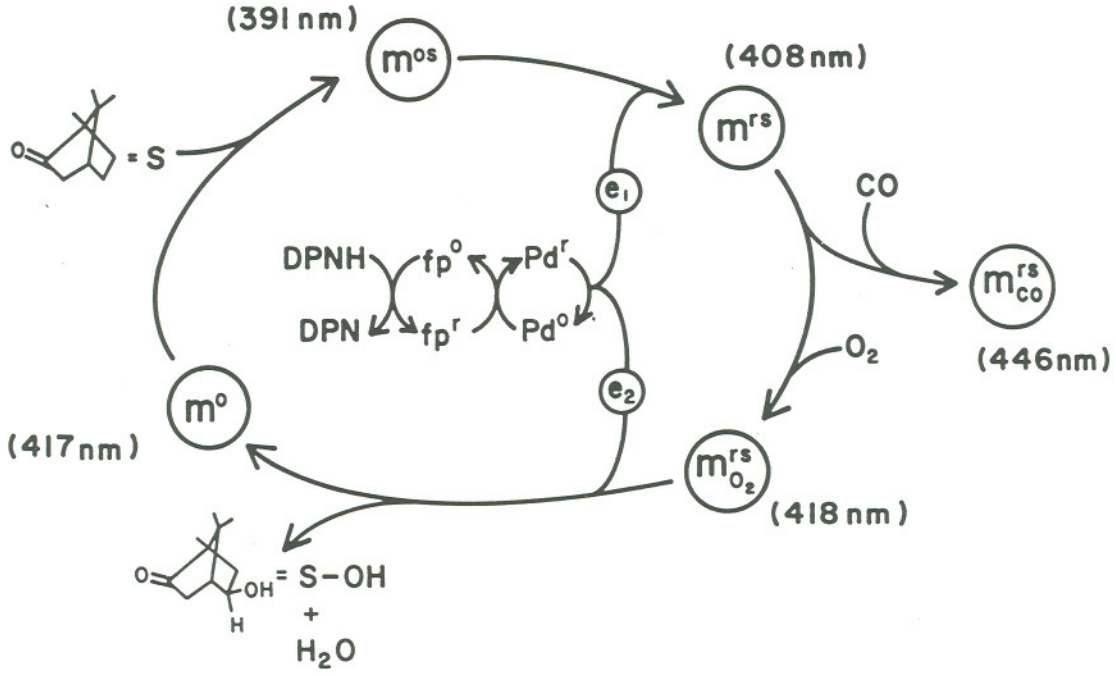
(391 nm)
m^{os}
(408 nm)
m^{rs}
= S
e_1
CO
DPNH
fp^o
Pd^r
DPN
fp^r
Pd^o
m^{rs}_{CO}
(446 nm)
O_2
e_2
m^o
(417 nm)
$m^{rs}_{O_2}$
(418 nm)
OH
H
= S-OH
+
H_2O

Figure 8

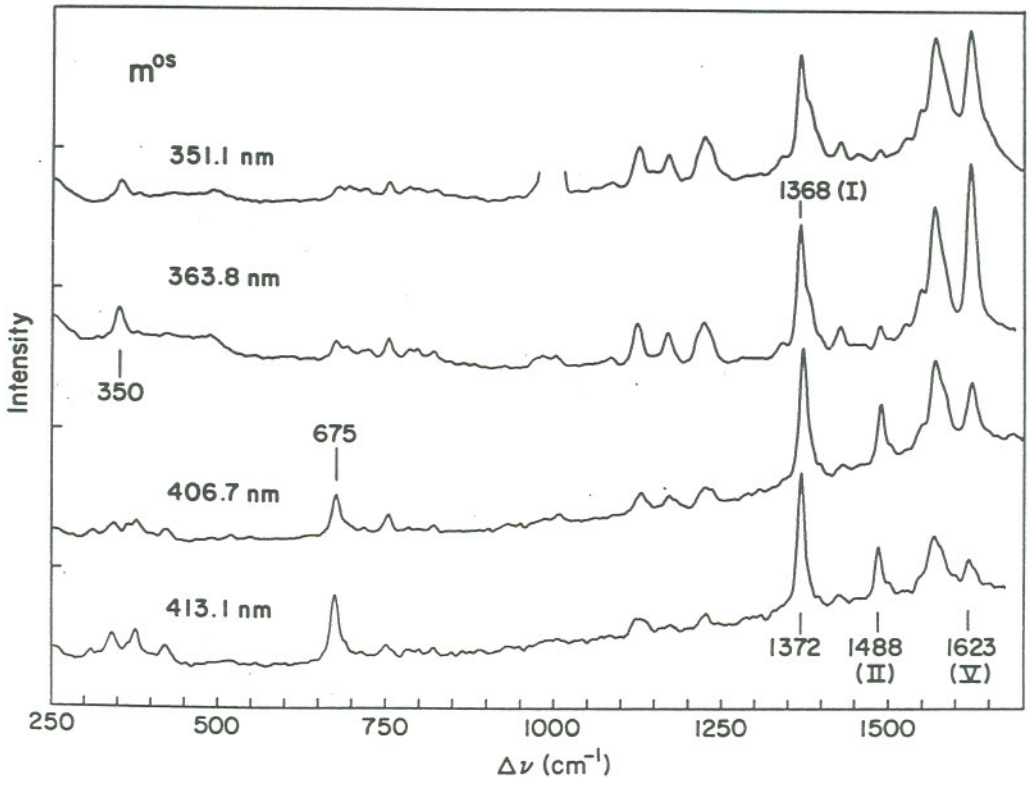
m^os
351.1 nm
1368 (I)
363.8 nm
350
675
406.7 nm
413.1 nm
1372
1488
(II)
1623
(V)
Intensity
250
500
750
1000
1250
1500
Δν (cm⁻¹)

Figure 9

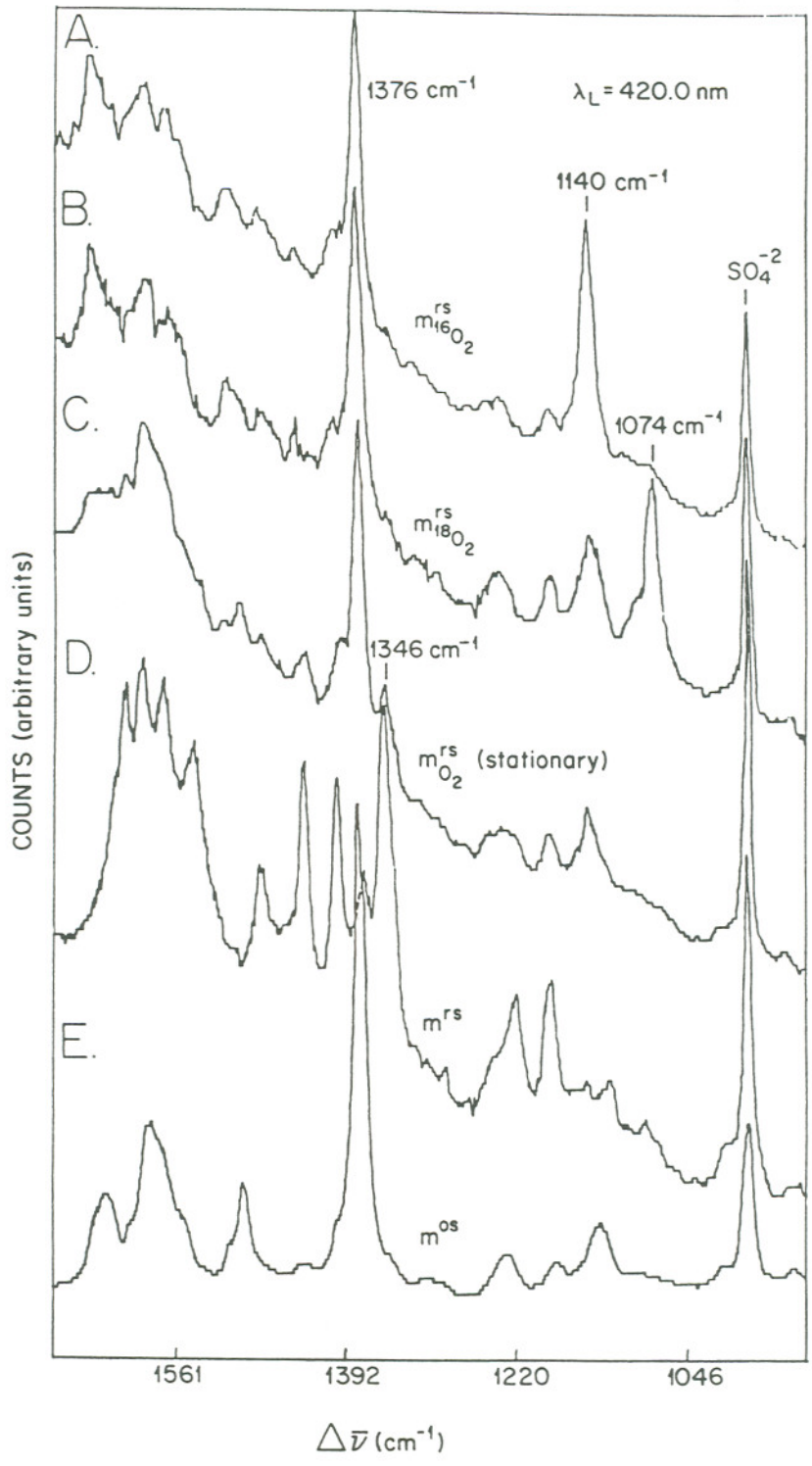
A.
1376 cm⁻¹
λL = 420.0 nm
1140 cm⁻¹
B.
SO4-2
m16O2rs
C.
1074 cm⁻¹
m18O2rs
D.
1346 cm⁻¹
mO2rs (stationary)
E.
mrs
mos
COUNTS (arbitrary units)
1561
1392
1220
1046
Δν̄ (cm⁻¹)

Figure 10

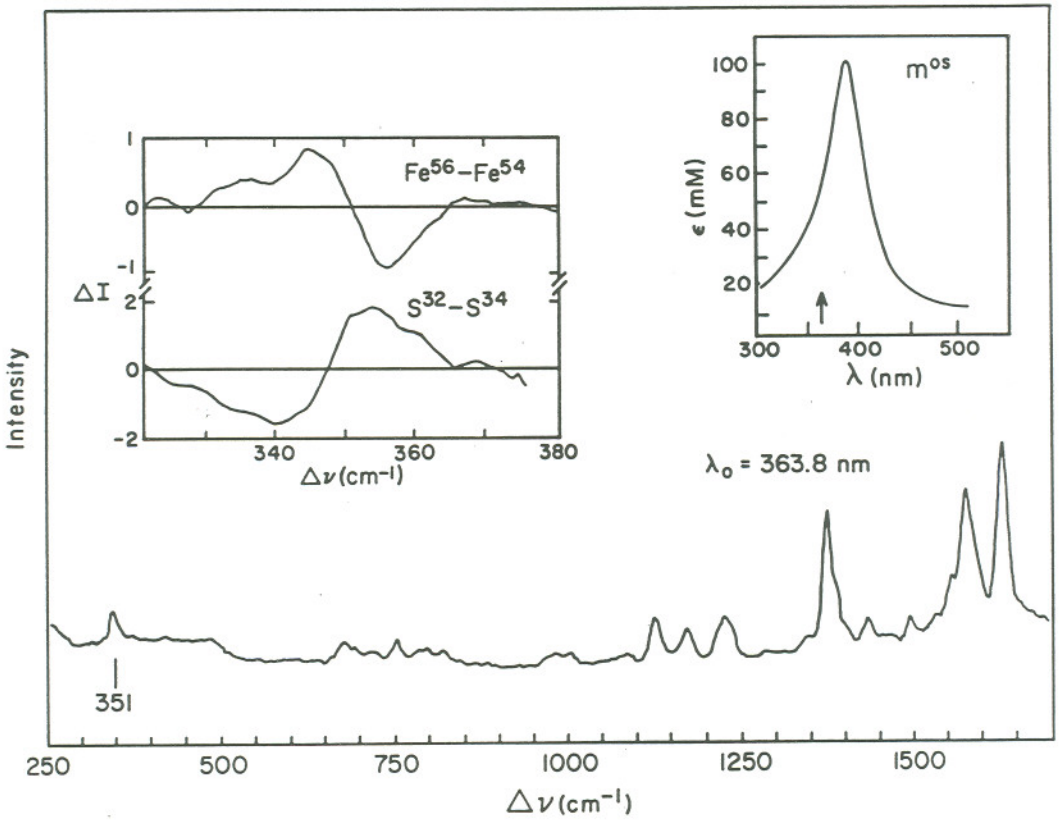
Intensity
ΔI
Fe56–Fe54
S32–S34
340
360
380
Δν(cm-1)
m os
ε (mM)
100
80
60
40
20
300
400
500
λ (nm)
λo = 363.8 nm
351
250
500
750
1000
1250
1500
Δν(cm-1)

Figure 11

A).

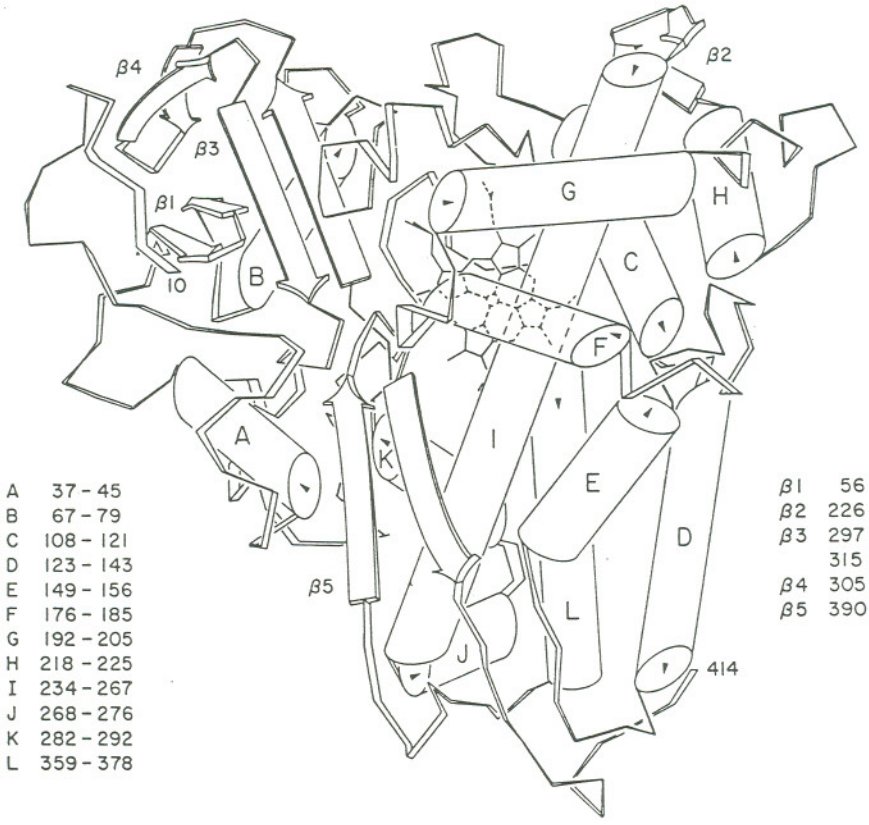
β4
β3
β1
10
B
β2
G
H
C
F
A
K
I
E
D
β5
L
J
414
A 37 - 45
B 67 - 79
C 108 - 121
D 123 - 143
E 149 - 156
F 176 - 185
G 192 - 205
H 218 - 225
I 234 - 267
J 268 - 276
K 282 - 292
L 359 - 378
β1 56 - 62
β2 226 - 233
β3 297 - 301
315 - 320
β4 305 - 312
β5 390 - 400

B).

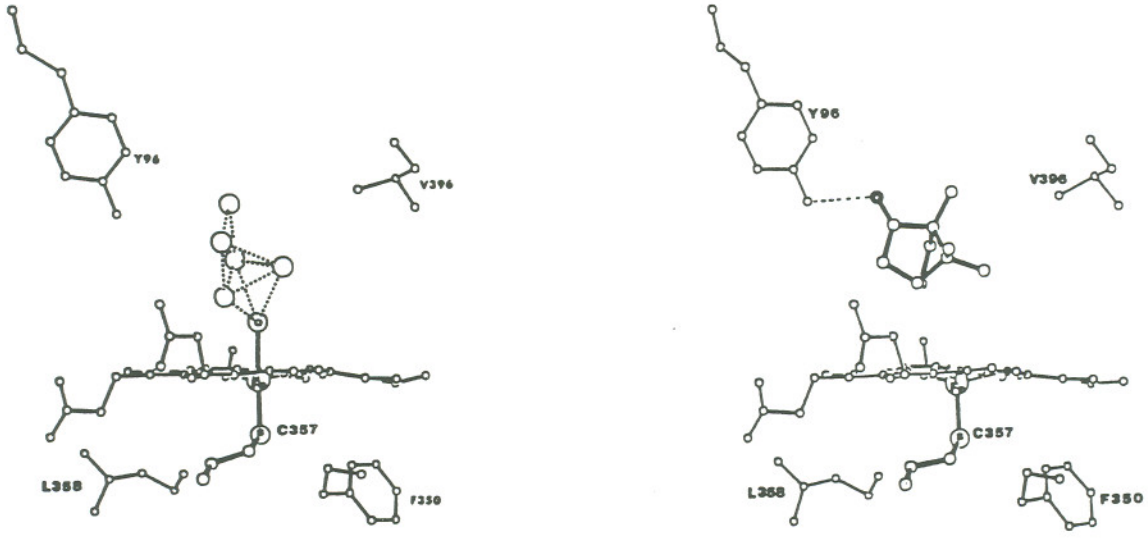
Y96
V396
C357
L358
F350
Y96
V396
C357
L358
F350

Figure 12

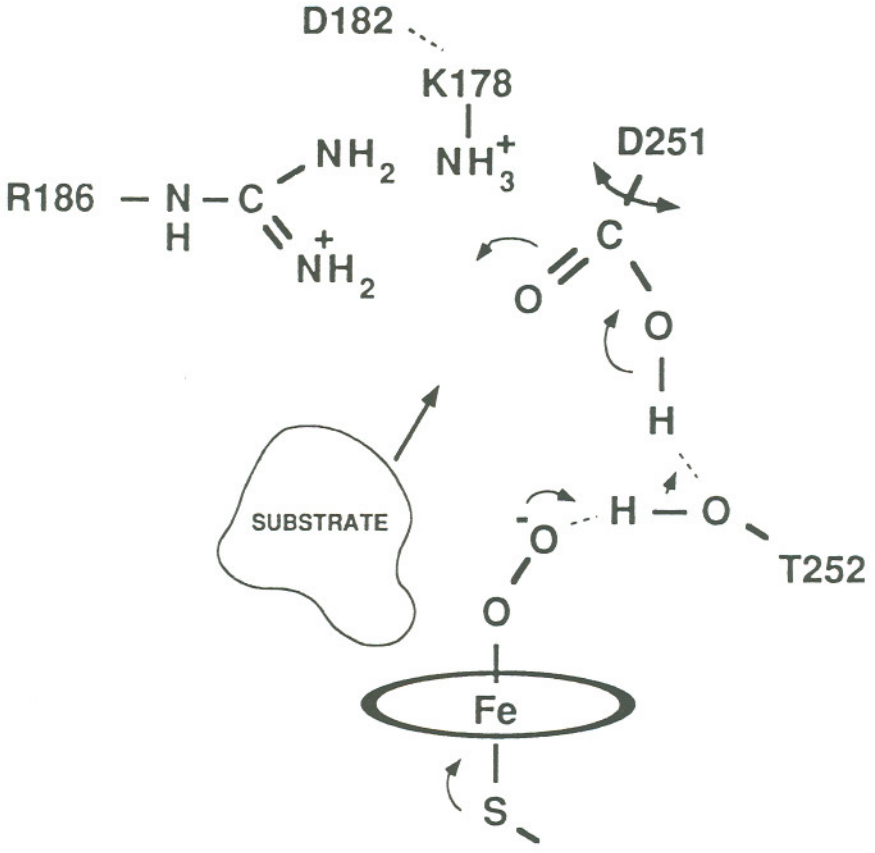

Figure 13

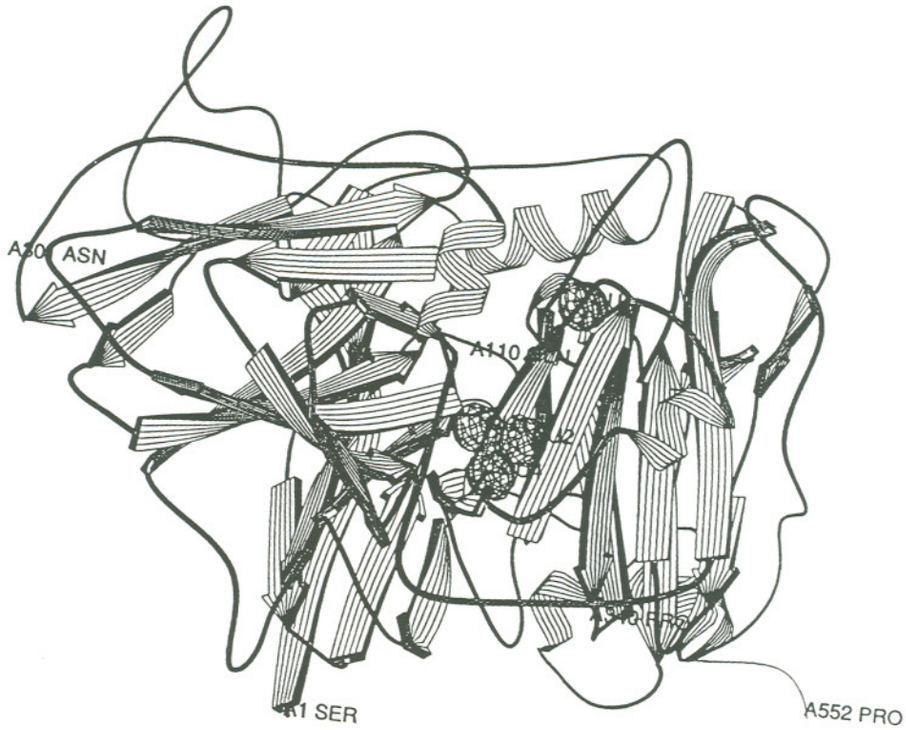
A30 ASN
A110
A552 PRO

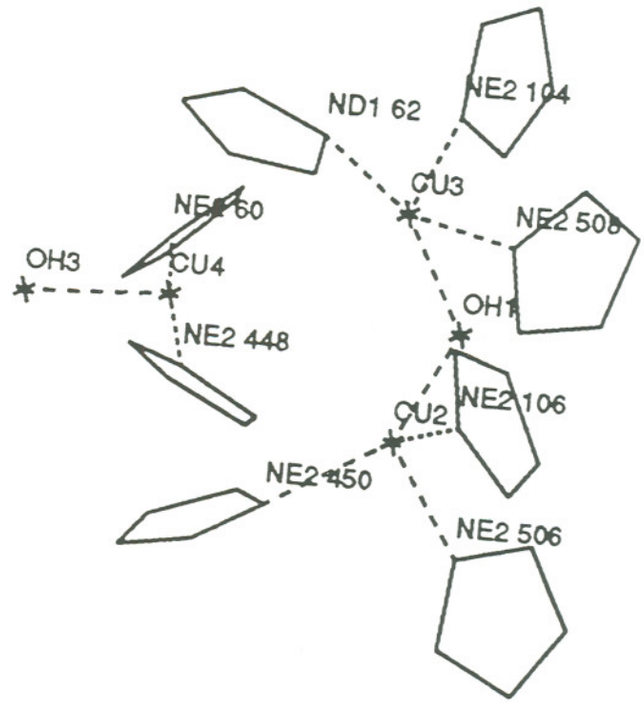
ND1 62
NE2 104
CU3
NE2 508
OH3
CU4
NE2 448
OH1
NE2 106
CU2
NE2 450
NE2 506

Figure 14

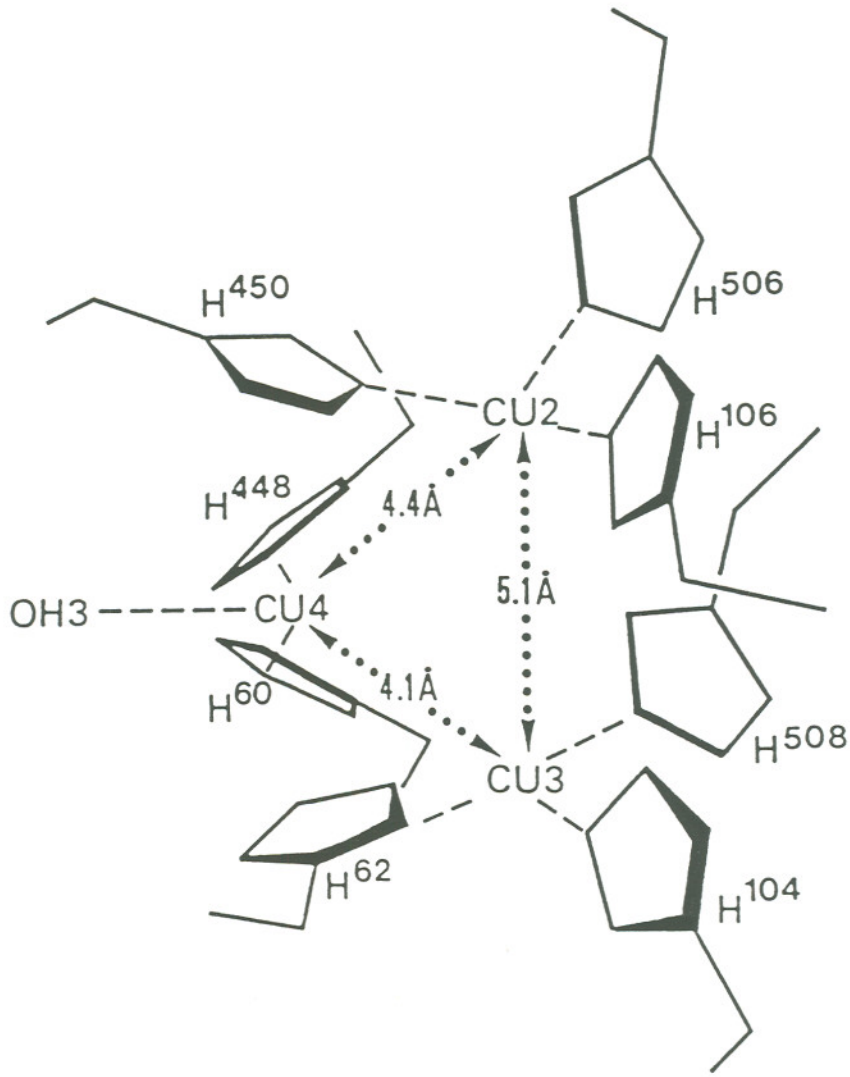
H450
H506
CU2
H106
H448
4.4Å
OH3
CU4
5.1Å
4.1Å
H60
H508
CU3
H62
H104

Figure 15

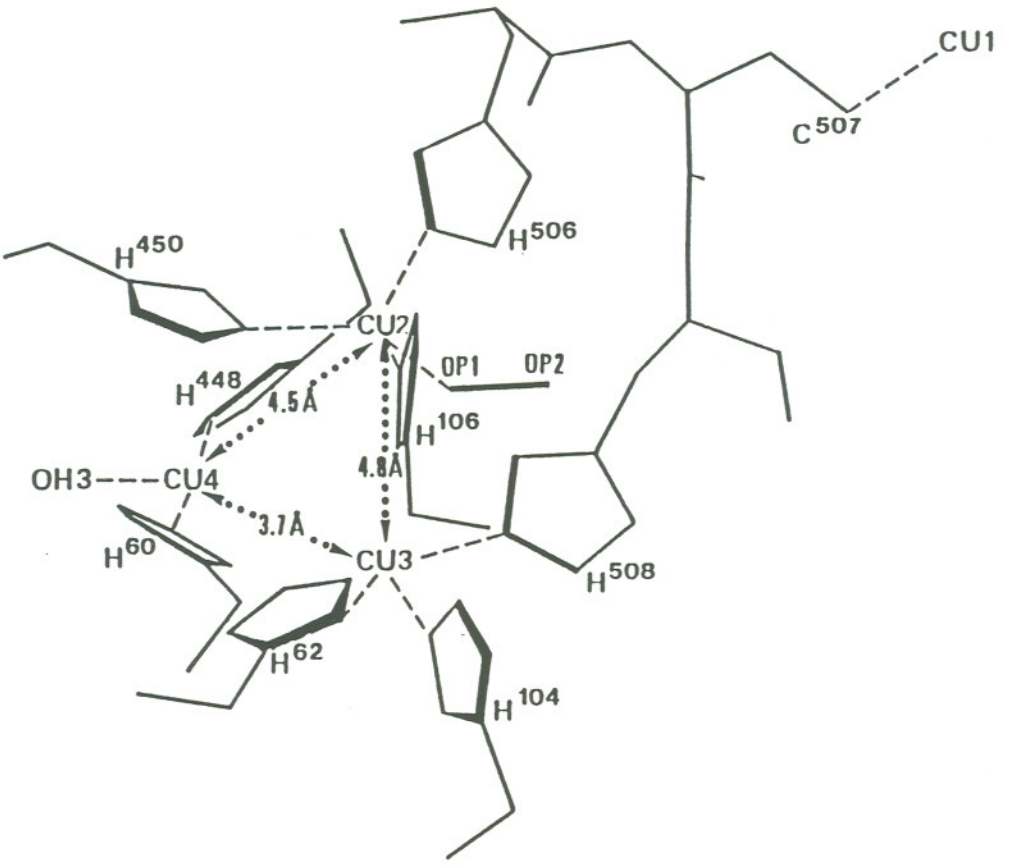
CU1
C507
H506
H450
CU2
OP1
OP2
H448
4.5Å
H106
4.8Å
OH3---CU4
3.7Å
H60
CU3
H508
H62
H104

Figure 16

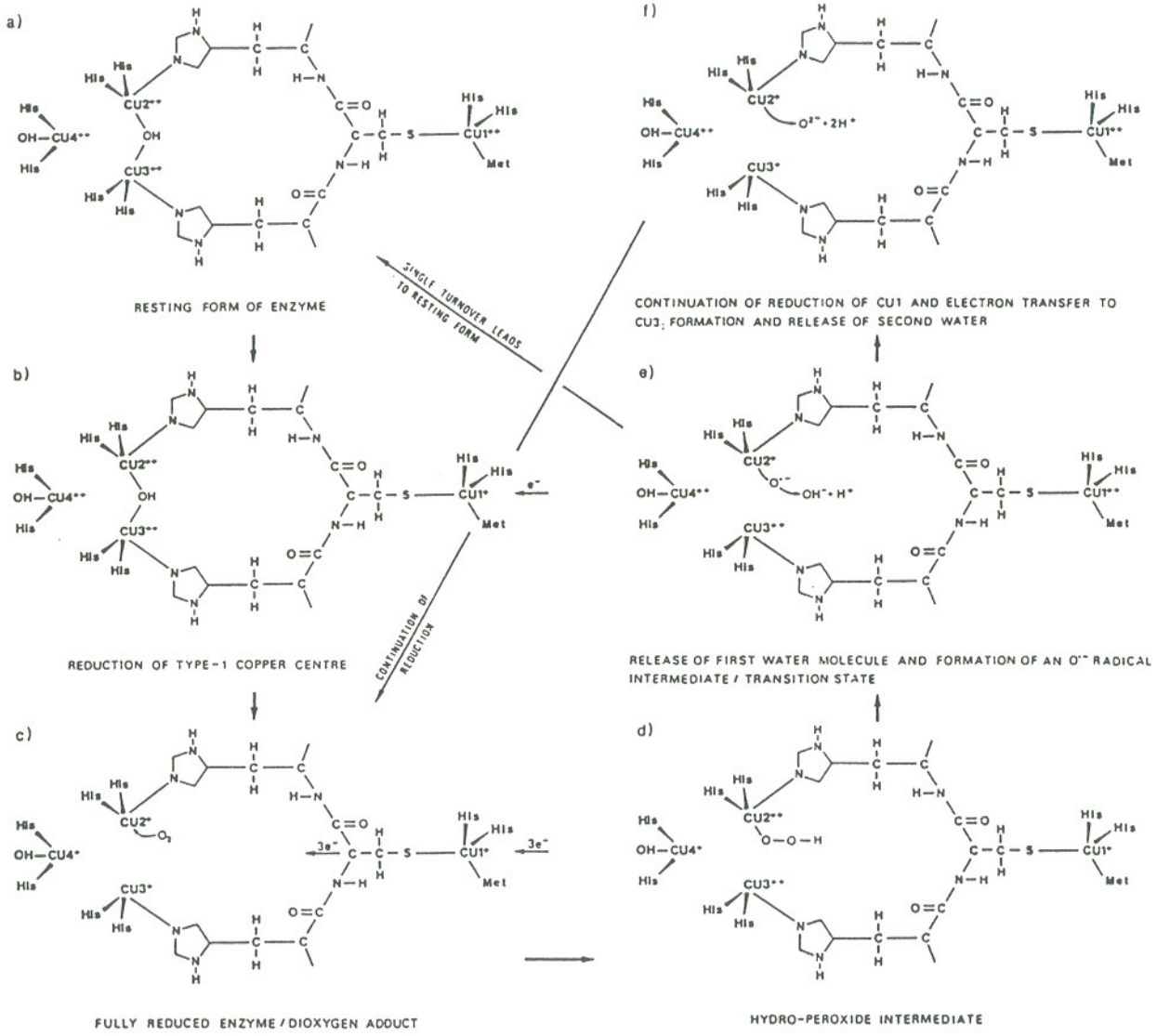
a)
RESTING FORM OF ENZYME
SINGLE TURNOVER LEADS TO RESTING FORM
b)
REDUCTION OF TYPE-1 COPPER CENTRE
CONTINUATION OF REDUCTION
c)
FULLY REDUCED ENZYME / DIOXYGEN ADDUCT
d)
HYDRO-PEROXIDE INTERMEDIATE
e)
RELEASE OF FIRST WATER MOLECULE AND FORMATION OF AN O⁻ RADICAL INTERMEDIATE / TRANSITION STATE
f)
CONTINUATION OF REDUCTION OF CU1 AND ELECTRON TRANSFER TO CU3; FORMATION AND RELEASE OF SECOND WATER

Figure 17

CHAPTER II
EXPERIMENTAL METHODS

O_2 Isotope Exchange

Preparation of $^{18}O_2$ and $^{16}O^{18}O$ Adducts of Hemocyanin. These experiments were carried out in two steps as indicated in equation 1:

(1)

First the purified hemocyanin ($^{16}O_2$) was reduced to CO-Hc by flushing with carbon monoxide gas. Then the resulting CO-Hc was reoxygenated with isotopically labeled oxygen ($^{18}O_2$ or $^{16}O^{18}O$).[1, 2] Molluscan Hc has a similar affinity for O_2 and CO with a K_f of $\sim 2\times10^5$ M^{-1}.[6] The CO displacement procedure is used because it is easier than trying to prepare deoxyHc by evacuation and flushing with N_2.

Since carbon monoxide is extremely toxic, the experimental apparatus was set up in a hood as shown in Figure 1.[3] The sample contained 200 μl concentrated Hc ($\sim$4 mM in Cu) in 0.1 M Tris-Cl, 0.05 M Mg^{2+}, 0.01 M Ca^{2+} (pH 7.8) and was placed in flask A. During the experiment, the sample was cooled by a small ice bath sitting on a stirrer to keep protein denaturation to a minimum and for more efficient gas exchanges. The protein was gently stirred except when it was exposed to vacuum (see below). Since the whole process took about two hours, water had to be removed and ice added about every 10 minutes.

For the deoxygenation step, CO gas was supplied from a small cylinder and its flow was adjusted by a regulator on the cylinder and fine adjusted by valve V3. A small serum bottle (E) containing ~50 ml Tris buffer was placed in the gas line to prevent the sample from drying by the gas flow and also to indicate the gas flow. With valve V1 open, and V2 closed, V3 was opened and the sample was flushed with CO. The CO flow was adjusted to ~1 bubble per second. CO passed through connections D and C, and into the oxyHc sample. A needle (B) was inserted into flask A through a serum stopper for CO to exit. The blue color of the sample gradually turned greenish and then nearly colorless, indicative of complete replacement of O_2 by CO in about 35 minutes. After complete deoxygenation, the CO valve V3 was closed. The needle B was gently removed and a little bit of liquid glue (Uhu) was quickly applied to seal the hole. The glue was allowed to dry for about 10 minutes. With V1 and V2 closed, the CO supply was disconnected at D, and the gas flask (F) containing O_2 isotope was connected to C.

After the glue was dry, vacuum was applied to remove as much CO as possible. With V1 and V4 closed, V2 was opened and the system was evacuated for ~10 minutes. Since the protein was vulnerable to bubbling, the sample was exposed to the vacuum only gently and briefly. First the stirrer was turned off. Then V1 was partially opened and closed after the sample was exposed to vacuum for 10 seconds. The stirrer was run again for ~5 minutes to release CO. The system was then exposed to vacuum again for 5 seconds. This last procedure was repeated one more time. With V1 closed, the system was then evacuated for another 10 minutes to remove any residual CO. Finally, with V2 closed, V4 was opened to allow labeled O_2 to be drawn into the system by the low pressure. V1 was then opened. The stirred protein quickly turned a blue color, indicative of successful reoxygenation. V4 was closed after 5 minutes.

The sample was left for 20-30 minutes to allow for complete reoxygenation. Then the sample was transferred to capillaries or an anaerobic sample holder (Figure 2) using a gas-tight syringe (20 μl sample plus 30 μl O_2 gas) connected to needle B. To avoid back exchange of the isotopically labelled oxyHc with air, the capillaries

were flushed with argon before, and flame-sealed after adding sample, as described in reference 3. The anaerobic sample holder was loaded in a N_2-atmosphere glove box. The capillary procedure suffers from the difficulty of transferring such a concentrated solution with a gas-tight syringe. The glove box procedure suffers from the difficulty that the oxyHc tends to lose O_2 in an N_2 atmosphere. The extent of oxygenation of the sample is also influenced by the gas pressure in the O_2 flask (generally less than 1 atm). The pressure can be increased by freeze-trapping the gas in a smaller-volume container. An improved procedure for introducing O_2 under pressure is suggested at the end of the next section.

Preparation of $^{18}O_2$ Adduct of Ribonucleotide Reductase. Oxygen activation of the R2 protein of ribonucleotide reductase (Y122F and F208Y mutants) requires that the apoprotein be reacted with an anaerobic solution of Fe(II) prior to addition of O_2. The sequence of the reaction is shown in equation 2 for a monomer of apoR2:

$$\text{ApoR2} + 2\text{Fe}^{\text{II}} \longrightarrow [(\text{Fe}^{\text{II}})_2]\ \text{Reduced R2} \xrightarrow[2e^-]{O_2} [\text{Fe}^{\text{III}}\text{-O-Fe}^{\text{III}}]\ \text{Oxidized R2} + H_2O \qquad (2)$$

A buffer solution containing 50 ml of 0.05 M Tris (pH 7.6), was placed in a glass-stoppered container and argon gas was bubbled through the buffer vigorously for about one hour, via a small tygon tubing inserted down to bottom of the tube (Figure 3A). Then the argon tubing was removed and weighed solid ascorbic acid and solid ferrous ammonium sulfate were added to the solution sequentially to give final concentrations of 11 mM and 40 mM, respectively. The solid was mixed and dissolved by inverting the stoppered container. The argon gas was reintroduced and the solution was gently bubbled for 5-10 minutes. This Fe^{2+} solution was ready for use.

In a setup as shown in Figure 3B, argon gas was bubbling through the large serum bottle that contained ~100 ml buffer with reducing agent (dithionite) to scavenge

O_2 and humidify the gas. The flushing gas was passed through the small serum bottle for about 1/2 hour. Then 100 μl concentrated apoprotein ($\sim$2 mM) was added to the small bottle via a plastic tubing that ran though the exit needle (gas flow off). The other end of the tubing was connected to a Pipetman. The purpose of this procedure was to avoid contact between the protein and the metal needle. The solution of apoR2 was flushed with argon for another 20 minutes, with gentle stirring. Then 25 μl of the anaerobic Fe^{2+}/ascorbate solution was added into the protein via a gas-tight syringe to give a sample $\sim$8 mM in Fe and $\sim$1.6 mM in R2. This ferrous protein was incubated and flushed with argon for another 20 minutes, with gentle stirring. Then it was ready for oxygenation.

As shown in Figure 3C, a short piece of glass tubing whose one end was covered with a serum stopper was clamped to the side arm of the $^{18}O_2$ flask. This extended side arm was flushed with argon gas for $\sim$10 minutes using an inlet and an outlet needle through the serum stopper. Then the inlet needle was removed, a 2.5 ml gas-tight syringe previously flushed with argon was attached to the outlet needle, $\sim$1.5 ml argon gas was pulled out using the syringe and a partial vacuum was created; the syringe and outlet needle were removed. Next the valve on the gas flask was opened to let $^{18}O_2$ into the side arm. The valve was then closed.

The argon was ejected from the syringe. The syringe was reinserted into its needle and 500 μl $^{18}O_2$ was withdrawn from the side arm. The $^{18}O_2$ was immediately injected into the R2 sample (from which inlet and outlet needles had been removed). A yellow color appeared immediately. Samples were transferred to capillaries and sealed. For the Y122F mutant, the capillaries were frozen in liquid nitrogen immediately, and the whole process including reaction, transfer, and sealing of the samples took 2 minutes. These frozen samples in capillaries were ready for Raman spectral analysis.

Compared to the oxygenation procedure for hemocyanin (*vide supra*), the procedure described above is much simpler and consumes much less precious $^{18}O_2$ gas. This procedure is especially suitable for the systems with high oxygen affinity like reduced R2 protein. The hemocyanin procedure (Figure 1) could be adapted to this

technique by closing valve V1 after evacuation and injecting the isotope gas through stopper B instead of attaching the O_2 flask at D.

Raman Spectroscopy

For solution samples, Raman spectra were usually obtained on ~20 μL samples in capillaries using a 90° scattering geometry. This geometry usually gives better signal/noise than in 150° backscattering. The samples are cooled by a copper rod which is dipped into an ice bath in a Dewar (Figure 4).[3] The L-shaped copper rod has a sample channel with diameter of ~ 2.0 mm into which is inserted a glass capillary. Near the end of channel there is a small hole (~3 mm dia.) for the incident beam to pass through the sample in the bottom of the capillary. Perpendicular to it is a larger V-shaped hole through which the Raman scattered light can exit and be collected. The horizontal exposed part of the rod is covered with Tygon tubing for insulation and is clamped to an adjustable platform.[4] A muffin fan with moderate speed is usually employed to prevent condensation on the sample and around in the exit hole. The sample cooling apparatus reduces protein denaturation without sacrificing Raman signal intensity. For example, a CCl_4 sample gave rise to the same photon counts with or without the copper cooling rod under the same conditions. This setup also helps to align samples with weak signals. If a sample does not give strong Raman signals, a solvent (CCl_4 or indene) capillary is placed inside the cooling rod and the laser optics are tuned for maximum Raman scattering. The solvent capillary is then replaced by a sample capillary, without further adjustment, yielding an optimum alignment for the sample.

As described in Chapter 3, good quality Raman spectra of ribonucleotide reductase R2 DOPA 208 protein were obtained using the 90° scattering geometry and the ice bath-cooled setup. In these experiments, the protein was relatively stable upon exposure to 647-nm laser excitation and the sample was much less fluorescent in solution than in the frozen state. In Chapter 4, the same setup was used to acquire visible excitation RR spectra of hemocyanin. Hemocyanin is stable to ~520-nm laser

excitation and has much lower fluorescence and background scattering in solution than in the frozen state.

In most other experiments, the proteins were less stable to the heating effects of laser irradiation, especially when UV (~350 nm) and violet (~410 nm) excitations were employed. Thus, the samples were cooled either by a closed-cycle helium refrigerator or in a copper cold finger immersed in liquid N_2 in a Dewar flask.[3] In these cases, the Raman data were collected in a 150° backscattering geometry. The helium refrigerator gives better quality spectra because of the lower temperature, absence of interference from glass bands, and greater ease of laser alignment on the sample. This method was used for UV-excitation of hemocyanin (to study Cu-L modes) and of ribonucleotide reductase R2 (to study the Fe-O-Fe mode). The capillary method was only used for samples requiring rapid freezing (as in the reaction of Apo F122Y R2 with $^{18}O_2$).

For studies with solid model compounds, the sample was ground and mixed with $NaNO_3$ (or Na_2SO_4) in a mortar. The mixture was then packed onto a metal disc with a circular sample groove using a hand pressed die.[4] The metal disc was mounted to a motor which itself was mounted to an adjustable platform. Raman spectra were recorded in a 150° backscattering geometry with the sample disc spinning at moderate speed (~ 200-300 rpm) to prevent the sample from overheating. A thorough analysis of the effect of grinding conditions on Raman intensities showed that sulfate salts are more sensitive to the amount of grinding and that nitrate salts are better internal standards.[4]

Most of the Raman data in this dissertation were acquired with a modified Jarrell-Ash 25-300 Raman spectrophotometer interfaced to a Intel 310 computer.[5] The source of incident radiation was provided by several lasers: Spectra-Physics 164-05 (Ar^+) and 2025-11 (Kr^+) and Coherent Innova 90-6 (Ar^+) and 599-01 dye laser with rhodamine 6G. A thermoelectrically cooled RCA C31034 photomultiplier tube was the detector whose output was connected to an ORTEC model 9302 amplifier/discriminator. Raman spectra were collected and processed using either a Fortran program running on the Intel 310 computer connected to a Tektronix 4054A graphics terminal,[5] or using the LabCalc program (from Galactic Industries, Salem,

NH) on a Gateway 486 computer.

References

(1) Freeman, T.B., Sanders-Loehr, J., and Loehr, T.M. (1976), *J. Am. Chem. Soc.* **98**, 2809-2815

(2) Thamann, T.J., Sanders-Loehr, J., and Loehr, T.M. (1977), *J. Am. Chem. Soc.* **99**, 4187-4189

(3) Loehr, T.M., and Sanders-Loehr, J. (1993) *Methods Enzymol.* **226**, 431-470

(4) Sharma, K.D. (1988), Ph.D. Dissertation, Oregon Graduate Center

(5) Loehr, T.M., Keyes, W.E., and Pincus, P.A. (1979) *Anal. Biochem.* **96**, 456-463

(6) Bonaventura, C., Sullivan, B., Bonaventura, J., and Bourne, S. (1974) *Biochemistry* **13**, 4784-4789

Figure Legends

Figure 1. Apparatus for deoxygenation and reoxygenation of hemocyanin. The internal volume is made as small as possible to minimize amount of O_2 gas that will be lost from flask F during each round of flushing. Flask A (not drawn to scale) has an internal volume of ~ 2 ml.

Figure 2. Anaerobic sample holder for Displex.

Figure 3. Apparatus for reacting reduced R2 with $^{18}O_2$.

Figure 4. An ice/water bath cooling setup for capillary samples used in a 90°-scattering geometry, adapted from reference 3.

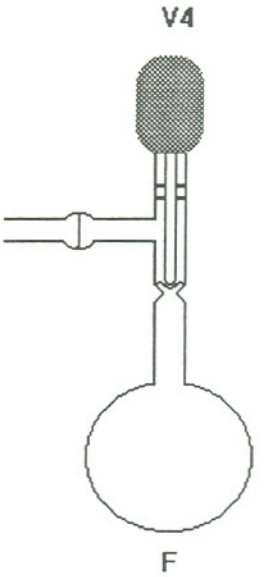

Flask Containing Isotopic O_2

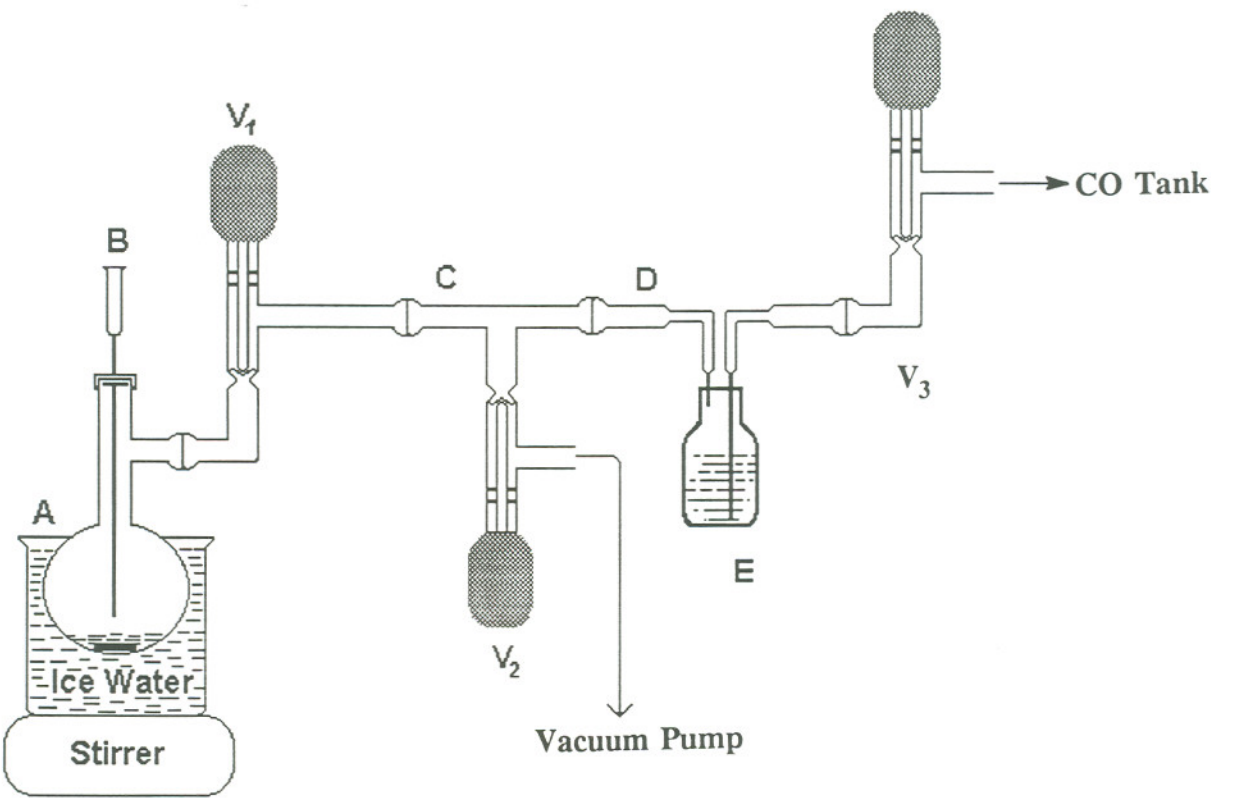

Figure 1

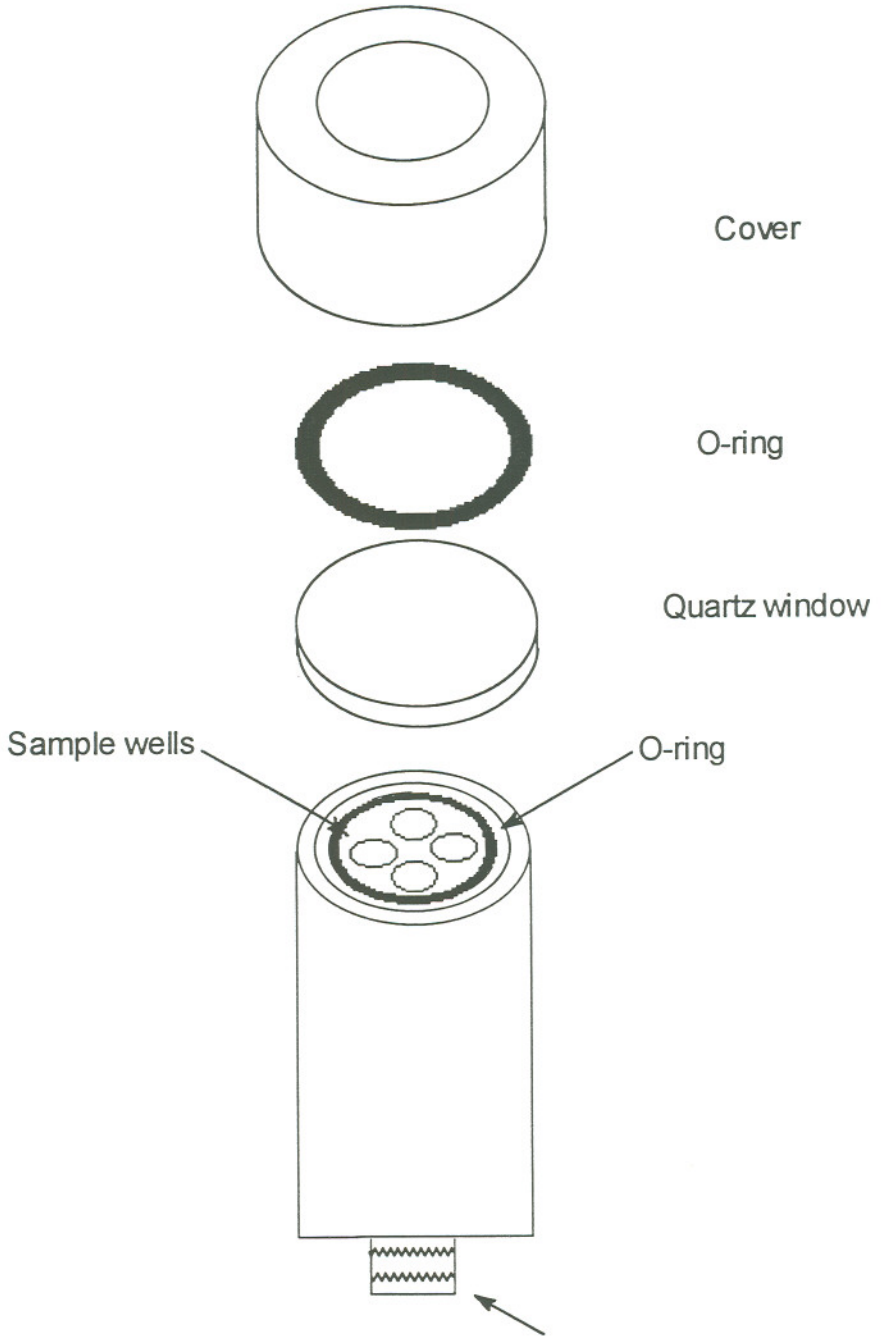
Cover
O-ring
Quartz window
Sample wells
O-ring
To be mounted to cold tip of the Displex.

Figure 2

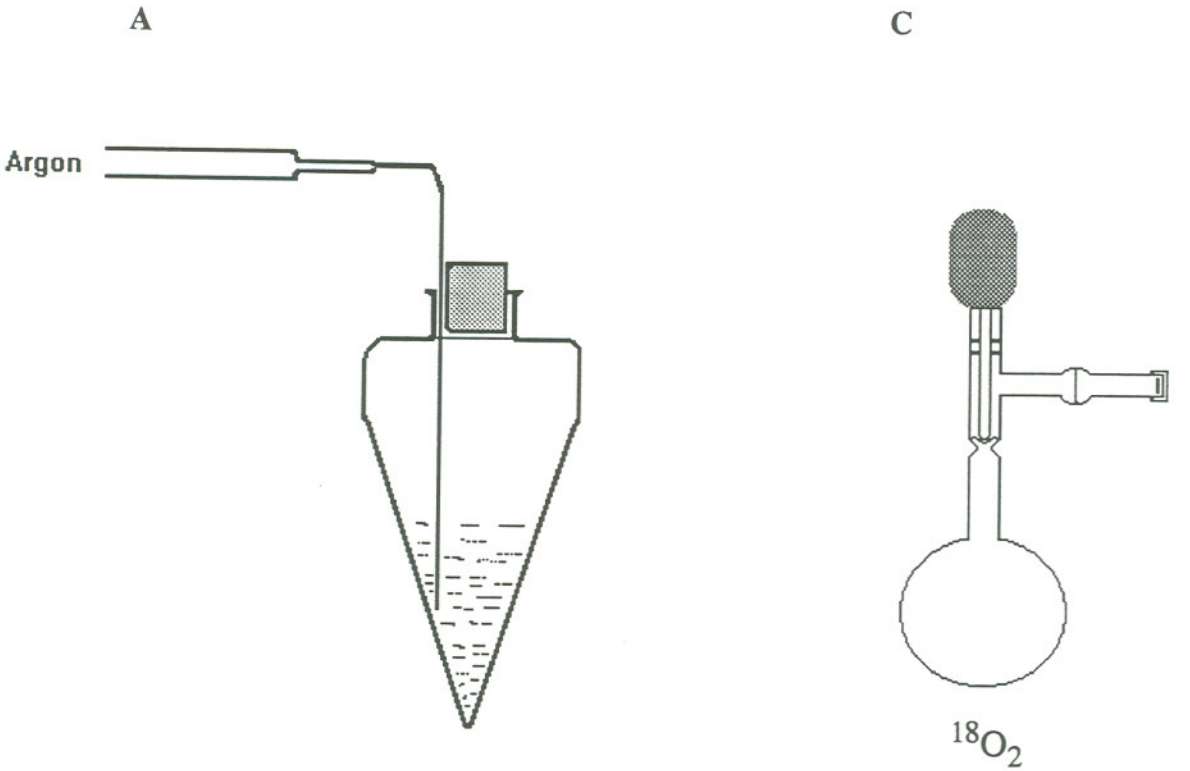

Figure 3

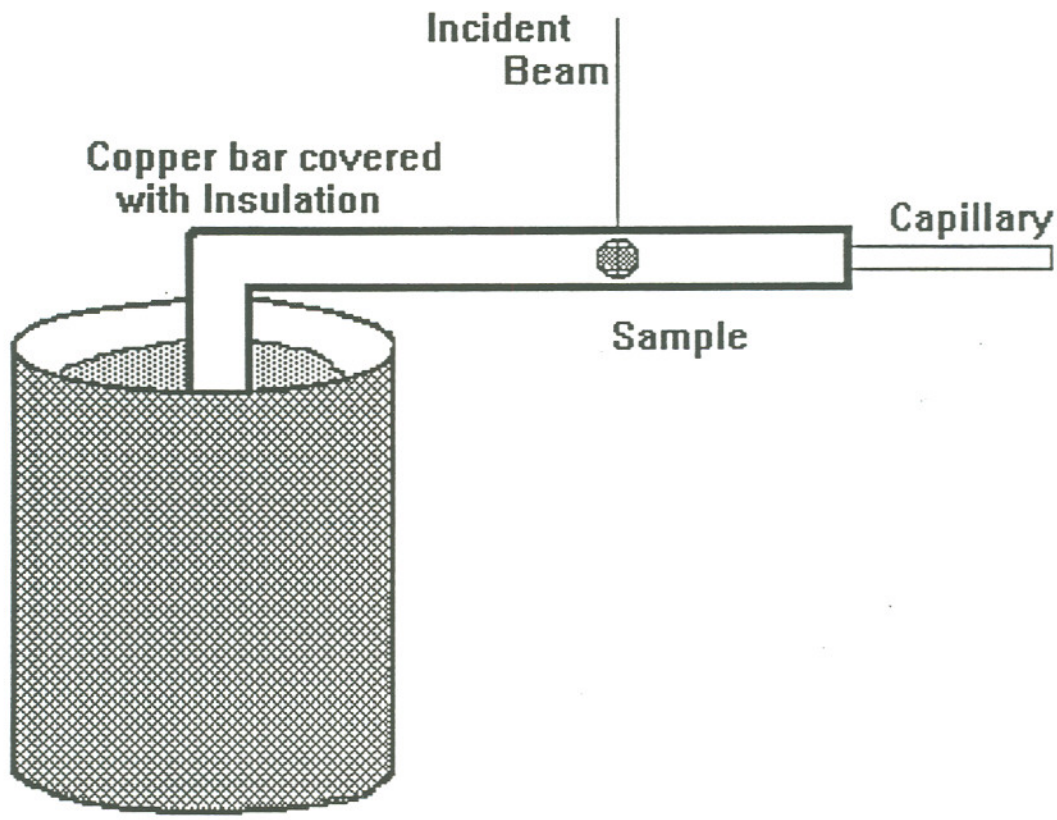
Incident
Beam
Copper bar covered
with Insulation
Capillary
Sample

Figure 4

CHAPTER III

RESONANCE RAMAN STUDIES OF RIBONUCLEOTIDE REDUCTASE MECHANISMS FOR OXYGEN ACTIVATION*

Abstract

Resonance Raman spectroscopy has been used to study oxygen activation in the R2 subunit of ribonucleotide reductase, which has an Fe-O-Fe center and a stable tyrosyl radical in its native form. Site-directed mutagenesis has been used to convert the radical residue into a phenylalanine. The resulting Y122F mutant, having the identical dinuclear iron center as native R2 but lacking the Tyr radical, is far more stable to laser irradiation than the native form. Thus, this mutant was used to study the oxygen activation mechanism as a model for wild-type R2. Apo-Y122F R2 was reacted with Fe(II) and $^{18}O_2$, then the sample was quickly frozen. Raman spectra of this sample clearly show that the bridging oxygen of the Fe-O-Fe moiety originates from O_2, thereby proving that dioxygen binds to the diiron center during activation. A chemical mechanism for the O_2 activation by the R2 system is proposed in which O_2 is reduced to peroxide and bridges the diferric center, followed by heterolytic cleavage of the O-O bond and generation of a high valent iron-oxo species (ferryl). The ferryl intermediate provides oxidizing power to generate the Tyr radical. Site-directed mutagenesis has also been used to convert Phe 208, a residue adjacent to the diiron

---

*This work was performed in collaboration with Dr. Margareta Sahlin and Dr. Britt-Marie Sjöberg of the University of Stockholm.

site, to a tyrosine. The phenolic sidechain is oxidized *in vivo* to a dihydroxyphenylalanine (DOPA) which in turn chelates to one of the iron atoms [*J. Biol. Chem.* **267**, 8711-8714 (1992)]. In order to probe the mechanism for the catechol formation, apo-F208Y plus Fe(II) was oxidized with $^{18}O_2$ in H_2O or O_2 in $H_2{}^{18}O$, respectively. Our Raman data indicate that the second O atom in DOPA 208 originates from H_2O rather than O_2. A chemical mechanism for formation of the DOPA 208 is proposed and discussed. It is believed that the ferryl intermediate oxidizes Tyr 208 to a radical which then recombines with a solvent-exchangeable OH^- associated with the dinuclear iron center.

Introduction

Ribonucleotide reductases (RnRs) are key enzymes in the biosynthesis of DNA. They catalyze the conversion of all four ribonucleotides to corresponding deoxyribonucleotides, the first step of the DNA synthesis. Four types of RnRs are known: (1) enzymes that contain a non-heme dinuclear iron center, (2) enzymes utilizing 5'-deoxyadenosylcobalamin cofactors (coenzyme B_{12}), (3) Mn-dependent enzymes,[2] and (4) an enzyme obtained from *Escherichia coli* grown under anaerobic conditions which appears to require S-adenosylmethionine and an as yet unidentified metal cofactor for catalytic activity.[3] Despite the vast difference in the cofactor requirements, RnRs, of category 1 and 2 seem to share a common mechanism in ribonucleotide reduction, in which redox-active dithiols and a protein free radical are involved. However, the nature of the radical and how it is generated distinguish the various reductases.[4] The RnRs of aerobically grown *E. coli* and many other bacteria, as well as those found in mammalian cells and eukaryotic viruses, belong to the first category. They consist of a large subunit (R1) and a small subunit (R2), each of which is a homodimer forming an $\alpha_2\beta_2$ structure. The R1 subunit contains substrate binding, regulatory, and catalytic sites, whereas the R2 subunit contains two dinuclear iron centers and one to two stable tyrosyl radicals, the latter of which is essential for enzymatic activity. Although the tyrosyl radical was originally believed to be involved

directly in ribonucleotide reduction, more recent studies suggest that it transfers its oxidizing equivalent to an amino acid residue in R1 and makes the latter to a radical via a long-range electron transfer, and that the latter radical initiates ribonucleotide reduction (see below).[4,5]

Extensive biophysical investigations of the R2 subunit of RnR from *E. coli* have contributed significantly to our understanding of the system. Resonance Raman studies revealed that the enzyme has an oxo-bridged dinuclear iron center, by observing ν_s(Fe-O-Fe) and ν_{as}(Fe-O-Fe) at 493 and 756 cm^{-1}, respectively; these frequencies shift to 480 and 731 cm^{-1}, respectively, upon exchange with $H_2{}^{18}O$.[6,7] The presence of the oxo bridge was also indicated by strong antiferromagnetic coupling ($-J = 110\ cm^{-1}$), large quadrupole splitting in the Mössbauer spectrum, and EXAFS observation of a short Fe-O distance of 1.78 Å.[8] The free radical in R2 was originally discovered from its EPR spectrum.[9] It was identified as a Tyr by deuterium substitution experiments[10] and located at Tyr-122 by site-directed mutagenesis.[11] Raman spectroscopy confirmed the presence of the tyrosyl radical by observation of a resonance-enhanced ν(C-O) at 1498 cm^{-1} in native R2, which disappeared in metR2. It was suggested that the tyrosyl radical is in its deprotonated form by the low ν(C-O) frequency.[12] The formulation as a neutral radical was also confirmed by ENDOR spectroscopy.[13] While the number of radicals and iron atoms per subunit had been difficult to establish, careful quantitative studies revealed that there are 4 iron atoms (i.e., two diiron-oxo clusters) per R2 protein.[14]

Recently, the X-ray crystal structure of the R2 protein was reported.[15] This structure is in very good agreement with above-mentioned biophysical data. It was demonstrated that indeed each R2 monomer has a dinuclear iron center, in which the two irons are bridged by an oxo and a carboxylate group, and each iron is additionally ligated to N_δ of a His sidechain, a H_2O molecule, and two oxygen atoms from carboxylate sidechains (Figure 1). The distance between the two Fe atoms is 3.3 Å. The ligation of the diiron center in R2 is more oxygen-dominated compared to methemerythrin in which the diferric iron center is ligated to five His.[8] The radical-bearing residue, Tyr 122, is in the vicinity of the iron center; its OH group is only 5.3

Å away from the nearer iron atom (Fe1). The diiron site is embedded in a hydrophobic pocket, consisting of sidechains from Tyr 122, Phe 208, Phe 212, Ile 231, and Ile 234, that is believed to stabilize the radical.[4]

The catalytic mechanism for ribonucleotide reduction has been well studied by Stubbe and others.[2] As shown in Figure 2, it is believed that a protein radical (X•) functions as a catalyst and initiates the reaction by abstracting the 3'-H from the substrate, generating a substrate radical. This then facilitates the elimination of the 2'-OH group as water to produce a cation radical intermediate. The latter is then reduced by the redox active dithiols of protein R1 to a deoxyribonucleotide radical. In the last step, the same hydrogen atom abstracted in the first step returns to the 3'-position, regenerating the protein radical and giving rise to the final product, a 2'-deoxyribonucleotide.

The chemical mechanism of formation of the tyrosyl radical is less well understood. The formation of the Tyr radical in active R2 *in vivo* is O_2 dependent.[16] The same active R2 can also be prepared *in vitro* (a) by reacting apo-R2 with Fe(II) and O_2,[17] or (b) by reacting metR2 with H_2O_2 or single oxygen-atom donors such as chloroperoxybenzoic acid, monoperoxyphthalate, or iodosobenzene.[18,19] Methane monooxygenase (MMO) is another nonheme iron enzyme believed to have a dinuclear iron center similar to that of R2, and like R2, it also functions as an oxygen activator.[8,20] In contrast, MMO has a substrate binding pocket that accepts a number of different substrates; it can convert methane to methanol or insert an oxygen atom into a variety of alkanes, alkenes, ethers, and aromatic or heterocyclic compounds.

The chemistry of dioxygen activation by diiron-oxo enzymes has long been of interest. Although lacking in direct experimental evidence, various mechanisms have been proposed, from Fenton-type chemistry involving hydroxyl radicals to mechanisms involving either homolytic or heterolytic cleavage of the dioxygen.[2,4] A plausible mechanism for oxygen activation in both R2 and MMO has the following elements: (1) the dioxygen binds to the diferrous center and is reduced to peroxide; (2) heterolytic cleavage of the peroxide results in a high valence species (ferryl) as the oxidizing agent.[21,22] Such high valence species have long been known to be involved in heme

chemistry and now seem feasible for non-heme iron systems as well.

The relatively stable compounds I and II in horseradish peroxidase and cytochrome *c* peroxidase both contain Fe(IV)=O species, and similar intermediates are believed to be involved in the chemistry of P-450 monooxygenases and chloroperoxidase.[23,24] Ferryl [Fe(IV)=O] species have also been characterized as intermediates in cytochrome *c* oxidase[25] and cytochrome *d* oxidase.[26] High valent metal-oxo (M=O) species have also been observed in a number of porphyrin complexes with metal ions such as Fe, Mn, and Cr.[27] Recently, a high-valent $Fe^{IV}\cdots Fe^{IV}$ intermediate was identified in MMO using rapid freeze-quenching in combination with Mössbauer spectroscopy.[28] A similar non-heme Fe(IV) species has been identified in the reaction of the dinuclear iron complex of TPA [tris(2-pyridylmethyl)amine] with H_2O_2. This species is capable of catalyzing some MMO-type reactions.[29] An Fe^{V}=O species has been proposed to explain the selective oxidation of saturated hydrocarbons in iron-containing Gif-type systems.[30] These results show that such high-valent iron-oxo species can exist in non-heme environments and that they are capable of hydrocarbon oxidation. In recent work on the R2 subunit of RnR, two intermediates in the tyrosyl radical formation were successfully characterized by EPR and Mössbauer spectroscopy.[31,32] Although neither intermediate contains high-valent iron, they could still have been formed via a transient ferryl intermediate.[21]

In this report, we present resonance Raman studies of oxygen activation by the R2 subunit using $^{18}O_2$. These data definitively prove, for the first time, that the oxygen atom in the Fe-O-Fe moiety originates from molecular oxygen (equation 1).

$$\text{ApoR2} + 2Fe^{2+} + {}^{*}O_2 + 2H^{+} + 2e^{-} \rightarrow [Fe^{3+}\text{-}{}^{*}\text{O-}Fe^{3+}]\text{R2} + H_2{}^{*}O \quad (1)$$

The fact that the activation results in incorporation of one ^{18}O atom of dioxygen strongly indicates that the O_2 is coordinated to the diiron center during O-O bond cleavage. Based on these Raman data and results previously published, a chemical mechanism for the O_2 activation is proposed and discussed, in which a peroxo and a

ferryl intermediate are involved.

Mutation of Phe 208, a residue in the hydrophobic pocket surrounding the iron/radical site (Figure 1), into Tyr turns R2 into a suicidal enzyme. During the reaction of apoprotein with Fe(II) and O_2, Tyr 208 is oxidized to DOPA (di-o-hydroxyphenylalanine). The DOPA 208 then deprotonates and becomes a bidentate ligand to the iron center, depleting the native enzymatic activity and giving rise to a blue color.[33] The X-ray crystal structure of the F208Y mutant shows that the DOPA is located at residue 208 and that both of its oxygen atoms are ligated to Fe1.[34] Nascent apo-F208Y mutant protein has been successfully purified from overproducing cells grown in iron-depleted medium. Reacting the apo-F208Y protein with O_2 and Fe(II) gives rise to the same blue Fe-catecholate protein. Here, we also present our new results using different oxygen isotopes. We have evidence from resonance Raman spectroscopy, that the second oxygen atom in DOPA-208 originates from solvent rather than molecular oxygen. Thus, it appears that the dinuclear iron center in the F208Y mutant is behaving as a tyrosine oxidase.

Experimental

Protein Purification. Samples of ribonucleotide reductase were provided by Drs. Margareta Sahlin and Britt-Marie Sjöberg (University of Stockholm). Wild-type, Y122F, and F208Y R2 proteins were purified according to standard procedures as described earlier.[35] Apo Y122F R2 was prepared by treating the isolated protein with chelating agent.[17] Apo F208Y R2 was isolated by growing *E. coli* in low iron medium as described in Reference 34.

Oxidation in the Presence of Oxygen Isotopes. The apo R2 mutant proteins (Y122F and F208Y) were concentrated to ~2 mM in 0.05 M Tris-Cl (pH 7.6). Solid ferrous ammonium sulfate and ascorbic acid were dissolved in anaerobic buffer to give final concentrations of 40 mM and 11 mM, respectively. This solution was added slowly to the aerobic stirred protein via a gas-tight syringe to give a sample 8.0 mM in

Fe and ~1.6 mM in oxidized R2. For oxidation with $^{18}O_2$, the protein sample (~100 μL) was first made anaerobic by flushing with argon, then mixed with the iron ascorbate solution. After 10 more minutes of flushing, 500 μL of $^{18}O_2$ (99 atom%, ICON) was added via a gas-tight syringe. The yellow color of oxidized protein appeared immediately. The Y122F sample was transferred to a capillary and frozen in liquid nitrogen within two minutes of $^{18}O_2$ addition. For oxidation of F208Y in the presence of $H_2{}^{18}O$, the apo F208Y protein was first exchanged with buffer prepared in $H_2{}^{18}O$ (97 atom %, YEDA, Israel) by 5-fold dilution and reconcentration using a Microcon concentrator.

Resonance Raman Spectroscopy. Raman spectra were recorded on a computerized Jarrell-Ash spectrophotometer using an RCA C31034A photomultiplier tube and an ORTEC model 9302 amplifier-discriminator. The excitation source was a Spectra-Physics 2025-11 (Kr^+) laser. For the R2 Y122F samples, spectra were obtained with 413.1-nm excitation in a 150°-backscattering geometry; the samples in capillaries were frozen by immersion in liquid nitrogen and held inside a copper-rod cold finger placed in a Dewar filled with liquid nitrogen.[36] For the R2 F208Y samples, spectra were obtained in a 90°-scattering geometry, and the samples in capillaries were cooled by a copper rod immersed in an ice bath. The Raman frequencies were corrected using indene as a standard[37] and are accurate to ± 1 cm^{-1}.

Results

Origin of Oxo Bridge in R2 Mutant (Y122F). Oxo-bridged dinuclear-iron complexes and proteins usually have intense absorption in the near-UV region (300-380 nm) that have been assigned $O^{2-} \rightarrow$ Fe(III) CT. Excitation into this electronic transition usually yields strong ν_s(Fe-O-Fe) and weaker ν_{as}(Fe-O-Fe) at ~500 and ~750 cm^{-1}, respectively, in the Raman spectra.[8, 38] Previous resonance Raman studies of the R2 subunit of RnR have identified ν_s(Fe-O-Fe) at 493 cm^{-1}.[6,7] The same vibrational frequency is observed for met R2, in which the Tyr 122 radical has been reduced by

hydroxyurea, and for Y122F R2, in which the Tyr at position 122 has been replaced by Phe.[7,12] Each of these changes in residue 122 is accompanied by a successive increase in the stability of the dinuclear iron center with respect to photodecomposition during laser irradiation.[12] However, the constancy of ν_s(Fe-O-Fe) at 493 cm^{-1} shows that the ground-state structure of the diiron site is unaffected by alterations in residue 122, whose closest distance to the iron center is ~5 Å.[15] Furthermore, in all three cases, ν_s(Fe-O-Fe) shifts to 497 cm^{-1} after equilibration in D_2O, suggesting that the same H-bonds to the bridging oxo group are present in the native, met, and Y122F forms of R2.

The bridging oxo group in native and met R2 has been found to be capable of slow exchange with solvent oxygen.[6] Its shift of -13 cm^{-1} in $H_2{}^{18}O$ leads to a calculated Fe-O-Fe angle of 138°,[7] in good agreement with the 130° angle determined by EXAFS.[39] The rate of oxo-bridge exchange could be measured using protein precipitated in 60% $(NH_4)_2SO_4$ and was found to have a $t_{1/2}$ of 15 min. at 4 °C.[6] Given this slow rate of exchange, we thought that it might be possible to determine the origin of the oxygen atom in the Fe-O-Fe moiety during the reaction of apo-R2 with Fe(II) and O_2. In order to prevent solvent exchange of the μ-oxo group, the R2 sample was frozen in liquid nitrogen immediately after it was exposed to O_2. In order to further optimize Fe-O-Fe stability during Raman excitation, the experiment was performed on the Y122F mutant of protein R2.

The Y122F mutant protein ($^{16}O_2$ oxidized) exhibits ν_s(Fe-O-Fe) at 500 cm^{-1} in the Raman spectrum obtained at 90 K (Figure 3A). This frequency is 7 cm^{-1} higher than that observed at 293 K,[12] but close to the 496-cm^{-1} value obtained for native and met R2 at 90 K.[6] Oxidized protein was also prepared by reacting reduced Y122F R2 with $^{18}O_2$, followed by quick freezing of the sample in liquid nitrogen. This sample shows an ill-resolved doublet in the Raman spectrum (Figure 3B), whose major component at ~487 cm^{-1} is assigned to ν_s(Fe-^{18}O-Fe). The shoulder at 500 cm^{-1} is apparently due to ν_s(Fe-^{16}O-Fe). The isotopic shift of -13 cm^{-1} is exactly the same as that previously observed for met R2 in $H_2{}^{18}O$.[7] These Raman data clearly indicate that one ^{18}O atom of $^{18}O_2$ ends up as the bridging oxygen in the Fe-O-Fe cluster. The

ν_s(Fe-^{16}O-Fe) component can be accounted for by back exchange of the Fe-^{18}O-Fe moiety with solvent ($H_2{}^{16}O$) during the ~2-min. period prior to freezing and by local heating during laser irradiation (the intensity of the 500 cm^{-1}-component was proportional both to time of exposure and laser power, Figure 3C). These data provide, for the first time, direct experimental evidence that O_2 can be the source of the bridging oxygen in an Fe-O-Fe cluster in a protein.

Origin of Catecholate Oxygen in R2 Mutant (DOPA 208). Native R2 has a conserved Phe at position 208 in the hydrophobic pocket between the radical and the iron site (Figure 1). To investigate the importance of the hydrophobic residues in the oxygen activation by R2, Phe 208 was converted to a tyrosine by site-directed mutagenesis.[33] The resultant protein isolated from the R2 F208Y mutant has prominent absorption bands at 460 and 720 nm, the latter of which is reminiscent of an iron(III)-catecholate complex.[40] Previous resonance-Raman studies revealed that the mutant protein contains an iron(III)-catecholate complex with bidentate ligation of the catecholate from a comparison of the RR spectrum with those of known iron-catecholate complexes (Table 1). As a result, the 720-nm absorption band was assigned to catecholate → Fe(III) CT.[33] The recently reported X-ray crystal structure of the F208Y mutant shows that the catecholate group of DOPA-208 is indeed coordinated to Fe1 in a bidentate fashion.[34] Previously, we proposed that the conversion of Tyr 208 to DOPA involved a self-hydroxylating monooxygenase reaction,[33] but the new data reported here indicate that it has, in fact, a tyrosine oxidase activity.

We have been able to investigate the source of oxygen in the DOPA-208 moiety by growing cells in an iron-depleted medium. The resultant protein that is obtained from these cells is >90% in the apo form with unreacted Tyr 208. The apo protein was reacted with Fe(II) plus $^{16}O_2$ (air) and $^{18}O_2$, respectively. The air-activated protein shows the identical Raman spectrum to that of the isolated R2 F208Y mutant reported previously, with prominent features at ~512, 592, 619, 1146, 1265, 1320, 1350, and 1475 cm^{-1}, characteristic of catecholate ligation (Figure 4A). Much to our surprise, the $^{18}O_2$-activated protein showed an RR spectrum identical to that of the

$^{16}O_2$-reacted protein (Figure 4B). The Fe-O and C-O stretching vibrations of an Fe-catecholate complex are expected to be in the 500-600- and 1200-1300-cm^{-1} regions, respectively, and are expected to shift to lower energy if an ^{18}O atom is incorporated into the DOPA-208 moiety. However, the absence of isotopic shifts with $^{18}O_2$ strongly suggested that the second oxygen of the DOPA-208 should come from solvent rather than from molecular oxygen.

Evidence for a solvent origin of the hydroxyl group in DOPA-208 was obtained by reacting R2 F208Y apoprotein with Fe(II) and air in $H_2{}^{16}O$ or $H_2{}^{18}O$ buffer. The peaks at 512 and 592 cm^{-1} from the protein oxidized in $H_2{}^{16}O$ (Figure 4A, 5A) clearly shift to 499 and 484 cm^{-1}, respectively, when the protein is oxidized in $H_2{}^{18}O$ (Figure 4C, 5B). The 619-cm^{-1} band also shifts to 617 cm^{-1} in the $H_2{}^{18}O$ sample (Figure 5B). Each of these modes is likely to have Fe-O vibrational character. However, in the region above 700 cm^{-1}, the Raman spectra of the two preparations are essentially identical (Figure 4C). Thus, none of the resonance-enhanced modes in the 1200-1400 cm^{-1} region have a significant C-O stretching contribution.

To test the solvent exchangeablity of the oxygen atom of oxidized DOPA-208, protein isolated from cells grown in an iron-rich medium was incubated in $H_2{}^{18}O$ buffer. The Raman spectrum of this material (Figure 5C) is identical to that of the protein in buffer prepared from normal H_2O (Figure 5A). This indicates that neither of the oxygen atoms in the DOPA moiety are solvent exchangeable and that the observed ^{18}O shifts shown in Figure 5B must occur during oxidation in $H_2{}^{18}O$. The lack of solvent-exchangeable oxygens in the RR spectrum is also in agreement with the X-ray structure which shows no μ-oxo bridge or aqua ligands in the DOPA-208 protein.

An alternative explanation for the solvent origin of the hydroxyl group is that the proposed ferryl intermediate undergoes oxygen exchange at the pH of 7.6 used in the F208Y reconstitution experiments. Such ferryl oxygen exchange has been observed for compound II of horseradish peroxidase and bovine liver catalase at neutral pH, but not at alkaline pH ($pH > 9$).[41,42] It was suggested that at neutral pH, a protonated distal histidine H-bonds to the ferryl and facilitates its exchange with

solvent H_2O. To investigate the possibility of acid catalysis of ferryl oxygen exchange, we assembled the apo F208Y with Fe(II) and $^{18}O_2$ at pH 8.9. The resultant DOPA-208 protein showed an identical Raman spectrum to that prepared at neutral pH (data not shown). Thus, even at pH 9, there is no detectable oxygen incorporation into the catechol from molecular oxygen.

Assignment of Catecholate Vibrations. The appearance of several ^{18}O-sensitive vibrational modes at 512, 592, and 619 cm^{-1} in the DOPA-208 protein is not unexpected. Earlier studies of metal oxalate complexes by metal substitution and normal coordinate analysis have shown that chelate rings in 1,2-dioxo-metal complexes give rise to two or more mixed modes in which the M-O stretch is coupled with motion of the chelate ring.[43] A similar mixing of chelate-ring deformation modes with the M-N stretch has been documented for oxamide and biuret complexes of copper.[44] Resonance Raman spectra for a number of iron-coordinated catecholates in proteins and model compounds are listed in Table 1. All of these samples exhibit a set of two to three resonance-enhanced features near 520, 600, and 620 cm^{-1} that are also likely to be due to coupling of the Fe-O stretch with deformations of the catecholate chelate ring.

There are several other possible explanations for the observation of two principal Fe-O modes at 512 and 592 cm^{-1} with ^{18}O shifts of -13 and -8 cm^{-1}, respectively. (i) The crystal structure of DOPA-208 R2 suggests inequivalent Fe-O distances of 1.97 and 2.26 Å.[34] The longer distance is due to the oxygen at C4 being weakly coordinated to the other iron atom (Figure 7). If the difference in bond length were great enough to destroy the symmetry of the complex, then only a single Fe-O mode would be expected with an isotope shift of -23 cm^{-1} (for the band at 512 cm^{-1}). This is clearly not the case. (ii) They might be assigned to ν_{as}(O-Fe-O) and ν_s(O-Fe-O) modes of an isolated O-Fe-O moiety. From the X-ray structural data,[34] the O-Fe-O angle is estimated as $\sim 82°$. Using the secular equation,[45] these vibrations at 512 and 592 cm^{-1} should downshift by 12 and 13 cm^{-1}, respectively, when one of the oxygen atoms is substituted with ^{18}O. This is close to the observed downshifts of 13 and 8

cm^{-1}, respectively. (iii) Alternatively, the 592-cm^{-1} band could be due to an O-Fe-O bending mode. Preliminary calculations show that such a δ(O-Fe-O) with an O-Fe-O angle of 82° should have a -8 cm^{-1} shift when one of the oxygens is replaced by ^{18}O. However, it is unlikely that a bending mode would be at as high an energy or have as high a Raman intensity as a stretching mode.

Previous studies of the [Fe(PDA)cat$^-$] complex indicated that the Raman features at 523, 633, 1154, 1250, 1308, 1469, and 1573 cm^{-1} (Table 1) are all catecholate vibrational modes, because they are all affected by deuteration of the catecholate ring protons.[40] The 1154, 1250, 1469, and 1573 cm^{-1} peaks were assigned to a C-H bend, a C-O stretch, and two C-C stretches, respectively, by analogy to those observed for iron-phenolate complexes.[40] Although we do not have any doubt that all these high frequency features are due to catecholate ring modes, the fact that we did not observe any isotopic shift for these features in the ^{18}O-incorporated protein makes assignment of the feature $\sim$1250 cm^{-1} to a C-O stretch questionable. It is likely that this feature is also due to a catecholate ring mode. More extensive studies using ^{18}O-labeled iron catecholate model compounds and normal coordinate analysis is desirable and required for more detailed assignments of Fe-O and C-O vibrations of these systems.

Discussion

Oxygen Activation in R2 F122Y. The Raman data presented in this study clearly show that one of the oxygen atoms of O_2 is inserted into the Fe-O-Fe moiety. This result strongly suggests that the O_2 is coordinated to iron during the oxidation reaction. A mechanism for oxygen activation in R2 (Y122F mutant) is proposed in Figure 6. The preliminary X-ray crystal structure of reduced R2 shows that the two Fe(II) ions are bridged by Glu 238 and Glu 115 and each metal ion is additionally ligated to a His and a monodentate carboxylate.[46] This metal site is very similar to the dimaganous substituted R2, except that the diferrous form lacks coordinated water molecules.[47] Each Fe is 4-coordinate and the structure is consistent with Mössbauer

spectroscopic observations that the two diferrous iron atoms appear to have equivalent environments.[14] The dioxygen binds and oxidizes the diferrous center and itself is reduced to a peroxide. This reaction is accompanied by a rearrangement of the carboxylate ligands to the diiron center: Glu 238 becomes monodentate to Fe2, Asp 84 becomes bidentate to Fe1. At the same time, a water molecule coordinates to each of the ferric ions. Such changes in the coordination of carboxylate ligands have been observed in model compounds and have been referred to as a "carboxylate shift".[48] Crystal structures of different forms of R2, i.e., dimanganese, met, and DOPA-208 R2 show that similar carboxylate shifts also occur in the biological system. For example, Glu 238 also bridges the divalent metal ions in Mn(II)-R2, is monodentate to Fe2 in met R2, and is bidentate to Fe2 in DOPA-208 R2. Asp 84 is a monodentate ligand to Fe1 in reduced R2, bidentate to Fe1 in met R2 and again monodentate in DOPA-208 R2.[15,34,46,47] It is remarkable that the same protein ligands can adopt so many different coordination modes to accommodate the changing metal environments.

In our proposed mechanism, the peroxo intermediate undergoes heterolytic O-O bond cleavage, releasing a water molecule and forming a ferryl intermediate. The ferryl intermediate accepts one electron from exogenous ascorbate and another electron from an endogenous residue, Z, to generate the free radical "intermediate X" that has been observed by rapid freeze-quench EPR spectroscopy.[31,32] X can accept another electron from ascorbate to form the stable diferric-oxo product, met R2 (Y122F). In wild type R2, the electron which reduces X is proposed to come from Tyr-122, generating the stable tyrosyl radical.[31,32] As a potential model for this reaction, diferric complexes stabilized by dinucleating ligands have been shown to form peroxide adducts that are capable of carrying out one-electron oxidations of phenols.[49]

There is, as yet, no direct experimental proof for the existence of a peroxo species. However, previous studies showing that met R2 can react with H_2O_2 to produce the tyrosyl-122 radical, strongly argue for its existence.[18,19] Oxyhemerythrin, a possible model for the peroxo intermediate in R2,[4] has a hydroperoxide terminally ligated to the diferric iron center.[50] The diferrous center in deoxy Hr is OH-bridged and has only one exogenous ligand coordination site at Fe2. In contrast, the irons in

reduced R2 are only 4-coordinate, with two potential additional coordination sites on each iron atom. Thus, it is plausible that peroxide bridges the two Fe(III) atoms in R2. The peroxide could link the two iron atoms in a μ-1,2 fashion, as proposed for several diiron peroxo complexes.[49] However, based on our Raman result that the μ-oxo of F122Y R2 is quantitatively produced from molecular oxygen (Figure 3), we believe that the peroxide bridges the two Fe(III) atoms in a μ-1,1 fashion (Figure 6). The other oxygen atom of peroxide could associate with the hydrogen of a coordinated water molecule, facilitating the subsequent O-O bond cleavage.

A μ-1,1 peroxo structure has been proposed previously for R2.[51] A similar type of reaction intermediate appears to form in the O_2-dependent oxidation of the diferrous complex, $[Fe_2(O_2CH)_4(BiphMe)_2]$.[52] The latter reaction with $^{18}O_2$ also engenders quantitative incorporation of ^{18}O into the Fe-O-Fe moiety of the diferric product, $[Fe_2{}^{18}O(O_2CH)_4(BiphMe)_2]$. Ferrous porphyrin complexes in nonaqueous solvent react with $^{18}O_2$ to produce documented peroxo and ferryl intermediates which finally transfer both of the oxygen atoms into Fe(III)-O-Fe(III) products.[53] However, in the latter case the peroxide is more likely to bridge two irons in a μ-1,2 fashion and the high-valent metal-oxo intermediate is likely to exchange with solvent if any water is present in the system. Finally, additional evidence for our proposed mechanism for selective incorporation of O_2 into the μ-oxo bridge of the R2 protein (Figure 6) comes from studies with $^{17}O_2$. Rapid freeze-quench trapping of the X intermediate reveals an Fe(III)-^{17}O complex, presumably Fe(III)-^{17}O-Fe(III), that does not exchange readily with solvent.[54]

It has been speculated that a high valent iron-oxo complex, produced by heterolytic cleavage of the bound peroxo species, is involved in the mechanisms of R2 and MMO,[21,22] like those in heme peroxidases and P-450 monooxygenases.[23] In horseradish and cytochrome *c* peroxidases, the heterolytic scission of the O-O bond is believed to be facilitated by a "push/ pull" mechanism, "pushed" by electron donation from the proximal His ligand and "pulled" by the polar network of the distal histidine and an arginine.[23] In cytochrome P-450 monooxygenases and chloroperoxidase (CPO), the O-O cleavage is believed to be achieved by the stronger "push" of the

proximal cysteinate ligand,[23] and a weaker pull from a polar network of a distal threonine and aspartate (Chapter 1, Figure 13). The iron center in R2 also has a number of negatively-charged ligands (four carboxylates) which could be providing a similar kind of "push" to generate and stabilize a high valent iron-oxo intermediate. Finally, the fact that single oxygen-atom donors such as peracids are capable of reacting with metR2 to generate the tyrosyl radical also suggests the involvement of a ferryl species.[19]

Although a ferryl intermediate has been observed for MMO,[28] it may be too short-lived to be detected in RnR. Nevertheless, it is likely to be the precursor of the X intermediate that has been isolated by Stubbe and coworkers.[31,32] The X intermediate is competent to oxidize Tyr 122 to a radical and has a formal oxidation state of one above metR2. However, only Fe(III) was detected by Mössbauer spectroscopy of the X intermediate and EPR spectroscopy revealed a free radical with a sharp singlet signal at g = 2.00. This EPR signal is different from that of the Tyr 122 radical, and, furthermore, is coupled to the diferric site, as evidenced by broadening of its signal upon ^{57}Fe substitution.

Mechanism of DOPA-208 Formation. A possible chemical mechanism for the formation of DOPA-208 is proposed in Figure 7. It is assumed that the initial reaction proceeds as in Figure 6, forming a peroxo species which decomposes to a ferryl. The ferryl intermediate oxidizes the Tyr-208 to a tyrosyl radical. The radical recombines with an iron-bound OH, forming DOPA-208. The catechol sidechain of DOPA is a strong chelator of Fe(III) and rapidly binds to Fe1. Since the terminal OH groups of the ferryl intermediate are initially derived from solvent (Figure 6), this mechanism explains the fact that the second oxygen atom of the DOPA-208 is incorporated from solvent rather than molecular oxygen. If correct, the diiron center in R2 F208Y is behaving formally as an oxidase, which uses O_2 as an electron acceptor, rather than as a monooxygenase, which would require insertion of an oxygen atom from O_2 into the substrate.

Since there are three relatively equivalent oxygens associated with the proposed

ferryl intermediate, any one of them could potentially be an oxygen donor. Our results for the Y122F mutant showing essentially complete incorporation of an oxygen from $^{18}O_2$ into the μ-oxo bridge (Figure 3) suggest that the ferryl intermediate undergoes reduction without significant exchange of the bridging oxygen. Assuming that the ferryl intermediate is reduced equally rapidly in the DOPA-208 mutant, it seems unlikely that the $H_2{}^{18}O$ incorporation into DOPA-208 can be accounted for by solvent exchange at the bridging position. Thus, one of the terminal OH groups is the more probable oxygen donor. If MMO (which is a true monooxygenase) forms a similar ferryl intermediate, then its $^{18}O_2$-derived μ-oxo group would be likely to serve as the oxygenating species.

An alternative mechanism for the reaction would involve only the Fe(IV)=O derived from O_2. In this case, a monooxygenase-type mechanism would only be consistent with the observed data if the ferryl intermediate (Fe=^{18}O) were able to exchange with solvent oxygen faster than it reacts with the substrate (Tyr-208). A number of ferryl and other high-valent metal-oxo species from heme proteins and model compounds have been observed to exchange with solvent.[41,42,55] In fact, in many reports on model complexes, the incorporation of an oxygen atom from labeled H_2O has been used to indicate the existence of a high-valent metal-oxo species as a reaction intermediate.[27c,55b,c] However, other studies have indicated that under catalytic conditions, the reaction of high-valent metal-oxo species with organic substrates is often faster than the rate of exchange with solvent.[55a] Our data on the lack of solvent ^{18}O exchange in Y122F and the lack of pH dependence for the oxygenation reaction in F208Y make it unlikely that a single Fe(IV)=O is involved in the RnR reaction.

High valent species in non-heme iron systems appear to be capable of either one electron abstraction to generate a radical or two-electron abstraction to generate a carbonium ion. Such a carbonium ion intermediate has been proposed in the MMO-catalyzed conversion of 1,1-dimethylcyclopropane to 3-methyl-3-buten-1-ol.[56] Studies on bleomycin-mediated oxidative degradation of a DNA analogue showed that the oxygen in the 4'-keto moiety derived from degradation of d(CGCGCG) comes from

solvent, rather O_2.[57,58] This points to the likelihood of a C-4' carbonium ion intermediate, produced by a two-electron stepwise oxidation of "active bleomycin". Bleomycin has also been demonstrated to catalyze production of ^{18}O-labeled *cis*-stilbene oxide from *cis*-stilbene and $^{18}O_2$, a typical epoxidation reaction.[59] In the case of R2 F208Y, it is possible that the ferryl intermediate undergoes a similar two-electron oxidation. The resulting carbonium ion on residue 208 would then be susceptible to nucleophilic attack by OH^- from solvent. A similar mechanism has been proposed for the formation of a hydroxymethyl derivative of the porphyrin of horseradish peroxidase when the enzyme is incubated with phenylhydrazine and H_2O_2.[60] However, when phenolates act as 2-electron donors, they tend to generate quinone methide intermediates which are most susceptible to nucleophilic addition at the C-7 position.[61] The position ortho to the phenolic oxygen is actually an unfavorable site for a nucleophilic reaction.[62] Thus, it is much more likely that Tyr 208 becomes oxygenated via a free radical intermediate. A similar free-radical mechanism has been proposed for the horseradish peroxidase-catalyzed conversion of phenol to catechol.[63]

In the studies on wild-type R2 and the Y122F mutant in the presence of excess Fe(II), the reaction forming the X intermediate (Figure 6) has an overall $t_{1/2}$ of $\sim$0.15 seconds at 4°C, indicating that any ferryl intermediate in the system has an even shorter half-life.[31,32] In contrast, the ferryl intermediate in MMO forms more slowly, reaching its maximum concentration in 4 seconds.[28] Studies of the reaction of the F208Y mutant with O_2 show that only 2 equivalents of Fe(II) are utilized per DOPA-208 produced.[34] This implies an even faster production of an Fe(III)-containing intermediate since endogenous electron donors are used in preference to exogenous Fe(II). In contrast, formation of the Fe(III)-catecholate complex is considerably slower, having a $t_{1/2}$ of 2.9 seconds at 22°C. These results suggest rapid formation of DOPA-208 (Met R2) with the final Fe chelation (Figure 7) being the rate-determining step. The chelation reaction may be limited by the need to disrupt stable Fe-O-Fe bonds whose exchange with solvent oxygen has a $t_{1/2}$ of 15 min at 25°C.[6]

As demonstrated above, the diiron center in R2 apparently has the ability to

oxidize a tyrosine to DOPA. Naturally, the question may be raised, why Tyr 122 is not oxidized to a catechol in native R2, or what factors protect it from being oxidized further than to the radical level, and why Tyr 208 was selected over a possible Tyr at position 122 in the F208Y mutant. The answers may lie in the hydrophobic pocket around the Tyr 122. The hydrophobic pocket, consisting of sidechains from Phe 208, Phe 212, Ile 231, and Ile 234, functions not only to maintain the tyrosyl radical stable for use in ribonucleotide reduction, but apparently, also to protect it from further oxidation and, thus, to keep the whole enzyme from self destruction. Since oxygen insertion requires close proximity of the hydrocarbon target, the fact that Tyr 122 is several Å removed from the dinuclear iron site would also help to prevent it from reacting with an Fe-coordinated oxo group. Furthermore, in native R2 the Tyr 122 is actually oxidized by X• rather than the ferryl intermediate,[31] which may also serve to protect the tyrosyl radical from recombining with an oxygenated species. Similar protein shielding and control of reactive species can also be found in heme peroxidases. As shown by the studies of Ator and Ortiz de Montellano, the high valent compound I of horseradish peroxidase definitely has the ability to oxidize substrates, but rarely inserts its oxygen directly into a substrate, presumably due to isolation of the high-valent species by protein shielding.[60]

Oxygen Activation in Other Oxo-Bridged Dinuclear Iron Enzymes.

Hemerythrin (Hr), and RnR R2 are the best characterized Fe-O-Fe proteins. MMO is also believed to contain a similar cluster. Recent work suggests that Δ^9 stearoyl-ACP desaturase from castor bean, an enzyme that catalyzes oxidative desaturation of long chain fatty acids, also contains an Fe-O-Fe cluster, as indicated by Mössbauer and resonance Raman studies.[64] Previously, Hr had been used as a biological model in probing structure and function of other iron-oxo proteins. However, while Hr is an oxygen carrier, binding oxygen reversibly, the other three are oxidases, consuming oxygen in the catalysis. X-ray crystal structures of Hr and R2 show little or no homology in iron ligation. The iron center in R2 is dominated by negatively charged oxygen ligands whereas Hr has mostly neutral His ligands. On the other hand, R2 and

MMO seem to be highly homologous in the metal binding domain.[20a]

A comparison of sequences of R2, MMO, Δ^9 desaturase, and other possible diiron-oxo proteins capable of reaction with O_2, namely, phenol hydroxylase and toluene-4-monooxygenase, also reveal the presence of a highly conserved metal binding motif (Figure 8). In each protein there are two Glu-X-X-His sequences in well-aligned regions suggestive of ligands being provided by an α-helix. Investigation of R2, MMO, and Δ^9 desaturase by circular dichroism spectroscopy reveals that they are all $>60\%$ α-helical.[20b,64a] These results indicate that R2, rather than Hr, is the appropriate model for the O_2-activating diiron proteins. Interestingly, a further sequence identity is observed between the biological reductant of R2, a flavin reductase from *E. coli*, and the reductant of the MMO hydroxylase, the flavin-containing protein C.[16]

It is likely that MMO, Δ^9 desaturase, and other diiron oxidases all have oxygen dominated, negatively charged ligands to the iron center and that these ligands also help to stabilize a high-valent iron-oxo intermediate generated in the catalytic reaction. However, one should keep in mind that these enzymes catalyze different reactions: tyrosyl radical generation (R2), hydroxylation (MMO), and oxidative desaturation (Δ^9 desaturase). These differences in reactivity are most likely controlled by structural variations in the diiron active site that determine whether a particular substrate is better oriented for electron abstraction or oxygen atom insertion.

References

1) (a) Oregon Graduate Institute of Science & Technology; (b) Stockholm University.

2) (a) Stubbe, J. (1990) *Adv. Enzymol.* **63**, 349-419; (b) Stubbe, J. (1990) *J. Biol. Chem.* **265,** 5329-5332

3) (a) Fontecave, M., Eliasson, R., and Reichard, P. (1989) *Proc. Natl. Acad. Sci. USA* **86**, 2145-2151; (b) Eliasson, R., Fontecave, M., Jörnvall, H.,

Krook, M., Pontis, E., and Reichard, P. (1990) *Proc. Natl. Acad. Sci. USA* **87**, 3314-3318

4) Fontecave, M., Nordlund, P., Eklund, H., and Reichard, P. (1992) *Adv. Enzymol.* **65,** 147-183

5) (a) Karlsson, M., Sahlin, M., and Sjöberg, B.-M. (1992) *J. Biol. Chem.* **267**, 12622-12626; (b) Climent, I., Huang, C. Y., and Sjöberg, B.-M. (1992) *Biochemistr* **31**, 4801-4807; (c) Mao, S.S., Yu, G.X., Chalfoun, D., and Stubbe, J. (1992) *Biochemistry* **31**, 9752-9759

6) Sjöberg, B.-M., Loehr, T.M., and Sanders-Loehr, J. (1982) *Biochemistry* **21,** 96-102

7) Sjöberg, B.-M., Sanders-Loehr, J., and Loehr, T.M. (1987) *Biochemistry* **26,** 4242-4247

8) Sanders-Loehr, J. (1989) in *Iron Carriers and Iron Proteins* (Loehr, T.M., Ed.) pp. 373-466, VCH Publishers, Inc., New York

9) Reichard, P., and Ehrenberg, A. (1983) *Science* **221,** 514-519

10) Sjöberg, B.-M., Reichard, P., Gräslund, A., and Ehrenberg, A. (1978) *J. Biol. Chem.* **243,** 6863-6865

11) Larsson, Å., and Sjöberg, B.-M. (1986) *EMBO J.* **5**, 2037-2040

12) Backes, G., Sahlin, M., Sjöberg, B.-M., Loehr, T.M., and Sanders-Loehr, J. (1989) *Biochemistry* **28,** 1923-1929

13) Bender, C.J., Sahlin, M., Babcock, G.T., Barry, B.A., Chandrashekar, T.K., Salowe, S.P., Stubbe, J., Lindström, B., Petersson, L., Ehrenberg, A., and Sjöberg, B.-M. (1989) *J. Am. Chem. Soc.* **111**, 8076-8083

14) Lynch, J.B., Juarez-Garcia, C., Münck, E., and Que, L., Jr. (1989) *J. Biol. Chem.* **264,** 8091-8096

15) Nordlund, P., Sjöberg, B.-M., and Eklund, H. (1990) *Nature* **345**, 593-598

16) Spyrou, G., Haggard-Ljungquist, E., Krook, M., Jörnvall, H., Nilsson, E., and Reichard, P. (1991) *J. Bact.* **173**, 3673-3679

17) Atkins, C.L., Thelander, L., Reichard, P., and Lang, G. (1973) *J. Biol. Chem.*

248, 7464-7472

18) Sahlin, M., Sjöberg, B.-M., Backes, G., Loehr, T.M., and Sanders-Loehr, J. (1990) *Biochem. Biophys. Res. Commun.* **167**, 813-818

19) Fontecave, M., Gerez, C., Atta, M., and Jeunet, A. (1990) *Biochem. Biophys. Res. Commun.* **168**, 659-664

20) (a) Nordlund, P., Dalton, H., and Eklund, H. (1992) *FEBS Letter* **307**, 257-262; (b) Smith, D.D.S., and Dalton, H. (1992) *Eur. J. Biochem.* **210,** 629-633

21) Que, L. Jr., (1991) *Science*, **253**, 273-274

22) (a) Fox, B.G., Borneman, J.G., Wackett, L.P., and Lipscomb, J.D. (1990) *Biochemistry* **29**, 6419-6427; (b) Wilkins, P.C., Dalton, H., Podmore, I.D., Deighton, N., and Symons, M.C.R. (1992) *Eur. J. Biochem.* **210,** 67-72

23) (a) Dawson, J.H. (1988) *Science* **240,** 433-439; (b) Poulos, T.L. (1987) *Adv. Inorg. Biochem.* **7,** 1-36

24) Erman, J.E., Vitello, L.B., Matthew, M. and Kraut, J. (1989) *Biochemistry* **29**, 7992-7995

25) Varotsis, C., Zhang, Y., Appleman, E.H., and Babcock, G.T. (1993) *Proc. Natl. Acad. Sci. USA* **90**, 237-241

26) Kahlow, M.A., Zuberi, T.M., Gennis, R.B., and Loehr, T.M. (1991) *Biochemistry* **30**, 11485-11489

27) (a) Watanabe, Y., and Groves, J.T. (1992) In *The Enzymes*, 3rd Ed (Sigman, D.S., Ed) Vol XX, pp 405-452, Academic Press, New York; (b) Czernuszewicz, R.S., Su, Y.O., Stern, M.K., Macor, K.A., Kim, D., Groves, J.T., and Spiro, T.G. (1988) *J. Am. Chem. Soc.* **110**, 4158-4165; (c) Groves, J.T., and Kruper, W.J., Jr. (1979) *J. Am. Chem. Soc.* **101,** 7613-7615

28) Lee, S.-K., Fox, B.G., Froland, W.A., Lipscomb, J.D., and Münck, E. (1993) *J. Am. Chem. Soc.*, in press

29) Leising, R.A., Brennan, B.A., Que, L., Jr., Fox, B.G., and Münck, E. (1991) *J. Am. Chem. Soc.* **113,** 3988-3990

30) Barton, D.H.R., Csuhai, E., Doller, D., Ozbalik, N., and Balavoine, G. (1990) *Proc. Natl. Acad. Sci. USA* **87**, 3401-3404

31) Bollinger, J.M., Jr., Edmondson, D.E., Huynh, B.H., Filley, J., Norton, J.R., and Stubbe, J. (1991) *Science* **253**, 292-298

32) Bollinger, J.M., Jr., Stubbe, J., Huynh, B.H., and Edmondson, D.E. (1991) *J. Am. Chem. Soc.* **113,** 6289-6291

33) Ormö, M., deMare, F., Regnström, K., Åberg, A., Sahlin, M., Ling, J., Loehr, T.M., Sanders-Loehr, J., and Sjöberg, B.-M. (1992) *J. Biol. Chem.* **267**, 8711-8714

34) Åberg, A., Ormö, M., Nordlund P., and Sjöberg, B.-M. (1993) *Biochemistry* (manuscript submitted)

35) Sjöberg, B.-M., Hahne, S., Karlsson, M., Jörnvall, H., Göransson, M., and Uhlin, B.E. (1986) *J. Biol. Chem.* **261**, 5658-5662

36) Loehr, T.M., and Sanders-Loehr, J. (1993) *Methods Enzymol.* **226**, 431-470

37) Hendra, P.J., and Loader, E.J. (1968) *Chem. Ind.* 718-719

38) Loehr, T. M.; Shiemke, A. K. (1988) In *Biological Applications of Raman Spectroscopy* (Spiro, T. G., Ed.), vol. 3, pp. 439-490, Wiley: New York

39) Bunker, G., Petersson, L., Sjöberg, B.-M., Sahlin, M., Chance, M., Chance, B., and Ehrenberg, A. (1987), *Biochemistry* **26,** 4708-4716

40) Cox, D.D., Benkovic, S.J., Bloom, L.M., Bradley, F.C., Nelson, M.J., Que, L., Jr., and Wallick, D.E. (1988) *J. Am. Chem. Soc.* **110,** 2026-2032

41) Chuang, W.-J., Heldt, J., and Van Wart, H.E. (1989) *J. Biol. Chem.* **264**, 14209-14215

42) Hashimoto, S., Tatsuno, Y., and Kitagawa, T. (1986) *Proc. Natl. Acad. Sci. USA* **83**, 2417-2421

43) (a) Fujita, J., Martell, A.E., and Nakamoto, K. (1962) *J. Chem. Phys.* **36,** 324-330; (b) Hester, R.E., and Plane, R.A. (1964) *Inorg. Chem.* **4,** 513-517

44) Thamann, T.J., and Loehr, T.M. (1980) *Spectrochim. Acta* **36A**, 751-760

45) Wing, R.M., and Callahan, K.P. (1969) *Inorg. Chem.* **8**, 871-874

46) Nordlund, P., Åberg, A., Eklund, H., Regnström, K., and Hajdu, J. Personal communication.

47) Atta, M., Nordlund, P., Åberg, A., Eklund, H., and Fontecave, M. (1992) *J.*

Biol. Chem. **267**, 20682-20688

48) Rardin, R.L., Tolman, W.B., and Lippard, S.J. (1991) *New J. Chem.* **15,** 417-430

49) Dong, Y., Ménage, S., Brennan, B.A., Elgren, T.E., Jang, H. G., Pearce, L.L., and Que, L., Jr. (1993) *J. Am. Chem. Soc.* **115,** 1851-1859

50) (a) Stenkamp, R.E., Sieker, L.C., Jensen, L.H., McCallum, J.D., and Sanders-Loehr, J. (1985), *Proc. Natl. Acad. Sci. USA* **82**, 713-716; (b) Holmes, A.M., Trong, I.L., Turley, S., Sieker, L.C., and Stenkamp, R.E. (1991) *J. Mol. Biol.* **218,** 583-593

51) Solomon, E.I., and Zhang, Y. (1992) *Acc. Chem. Res.* **25,** 343-352

52) Tolman, W.B., Liu, S., Bentsen, J.G., and Lippard, S.J. (1991) *J. Am. Chem. Soc.* **113,** 152-164

53) (a) Chin, D.-H., LaMar, G., and Balch, A.L. (1980) *J. Am. Chem. Soc.* **102,** 4344-4349; (b) Paeng, I.R., Shiwaku, H., and Nakamoto, K. (1988) *J. Am. Chem. Soc.* **110,** 1995-1996

54) Bollinger, J.M., Edmondson, D.E., Huynh, B.H., Filley, J., Norton, J.R., and Stubbe, J. (1991) *J. Inorg. Biochem.* **43,** 533

55) (a) Nam, W., and Valentine, J.S. (1993) *J. Am. Chem. Soc.* in press; (b) Groves, J.T., Haushalter, R.C., Nakamura, M., Nemo, T.E., and Evans, B.J. (1981) *J. Am. Chem. Soc.* **103,** 2884-2886; (c) Groves, J.T., Kruper, W.J., Jr., and Haushalter, R.C. (1980) *J. Am. Chem. Soc.* **102,** 6375-6377

56) (a) Ruzicka, F., Huang, D.-S., Donnelly, M.I., and Frey, P.A. (1990) *Biochemistry* **29**, 1696-1700; (b) Frey, P.A. (1990) *Chem. Rev.* **90,** 1343-1357

57) Rabow, L.E., McGall, G.H., Stubbe, J., and Kozarich, J.W. (1990) *J. Am. Chem. Soc.* **112,** 3203-3208

58) Sam, J.W., and Peisach, J. (1993) *Biochemistry* **32,** 1488-1491

59) Heimbrook, D.C., Carr, S.A., Mentzer, M.A., Long, E. C., and Hecht, S. M. (1987) *Inorg. Chem.* **26**, 3835-3836

60) Ator, M.A., and Ortiz de Montellano, P.R. (1987) *J. Biol. Chem.* **262**, 1542-

1551

61) Thompson, D.C., Thompson, J.A., Sugumaran, M., and Moldeus, P. (1992) *Chem.- Biol. Interactions* **86**, 129-162.

62) Wagner, H.U., and Gompper, R. (1974) in *The Chemistry of the Quinoid Compounds* (Patai, S. Ed.), pp 1145-1179, John Wiley: New York

63) Dordick, J.S., Klibanov, A.M., and Marletta, M.A. (1986) *Biochemistry* **25,** 2946-2951

64) (a) Fox, B.G., Shanklin, J., Somerville, C., and Münck, E. (1993) *Proc. Natl. Acad. Sci. USA* **90**, 2486-2490; (b) Fox, B.G., Ai, J., Loehr, T.M., and Sanders-Loehr, J., unpublished results.

65) Salama, S., Stong, J.D., Neilands, J.B., and Spiro, T.G. (1978) *Biochemistry* **17**, 3781-3785

66) Pyrz, J.W., Roe, A.L., Stern, L.J., and Que, L., Jr. (1985) *J. Am. Chem. Soc.* **107,** 614-620

67) Andersson, K.K., Cox, D.D., Que, L., Jr., Flatmark, T., and Haavik, J. (1988) *J. Biol. Chem.* **263**, 18621-18626

Table 1. Resonance Raman Spectra of Fe-Catecholates in Proteins and Model Complexes.

Sample[a]	Raman Frequency (cm^{-1})										Ref.
$Fe(cat)_3^{-3}$		533		621	1154	1262	1322	1359	1487	1572	65
$Fe(cat\text{-}d_4)_3^{-3}$				610		1206			1436		66
[Fe(salen)cat]$^-$		511		614	1145	1260	1324		1473		40
[Fe(salen)cat-d_4]$^-$				599			1202		1426		66
[Fe(PDA)cat]$^-$	310	523		633	1154	1250	1308		1469	1573	40
Tyr hydroxylase[b]		527	604	635	1130	1271	1320	1426	1476		67
Phe hydroxylase + cat		531		621	1151	1257	1313		1470	1568	67
R2 DOPA-208	322	512	592	619	1143	1263	1319	1350	1475	1569	this work

[a]cat = catecholate; [b]isolated as an iron-catecholate complex.

Figure Legends

Figure 1. Structure of the dinuclear iron site in the met R2 subunit of ribonucleotide reductase. Adapted from Reference 15.

Figure 2. Proposed mechanism for the reduction of ribonucleotides by ribonucleotide reductase. X denotes a protein residue capable of forming a transient radical. Adapted from Reference 2.

Figure 3. Resonance Raman spectra of the met form of R2 Y122F. A) Apo Y122F was reacted with Fe(II) in air ($^{16}O_2$). B) The Fe(II) protein was reacted with $^{18}O_2$ and frozen in liquid N_2 within 140 s to minimize exchange of the μ-oxo group with solvent. The sample underwent 20 minutes of laser exposure at 90 K. C) Spectrum of sample B upon an additional 20 minutes of laser exposure at 90 K. Laser warming of the sample apparently caused the Fe-^{18}O-Fe moiety to exchange with solvent ^{16}O. The spectra were obtained with 413.1-nm excitation (15 mW), scan rate of 0.5 cm^{-1}/s, resolution of 10 cm^{-1}, and accumulations of 16, 4 and 4 scans, respectively. Each spectrum has been subjected to a 21-point Savitsky-Golay smoothing.

Figure 4. Resonance Raman spectra of the DOPA-208 form of R2. Apo F208Y plus Fe(II) was oxidized by (A) air ($^{16}O_2$), (B) $^{18}O_2$, and (C) air in presence of $H_2{}^{18}O$. Spectra were obtained on samples in capillaries at 5 °C (90-degree scattering geometry) using 676.4-nm excitation (100 mW) at a scan rate of 1 cm^{-1}/s and resolution of 8 cm^{-1}, and each was an accumulation of 4 scans. Spectrum C has been subjected to a 15-point Savitsky-Golay smoothing.

Figure 5. Low frequency resonance Raman spectra of the DOPA-208 protein prepared by air oxidation of reduced F208Y in $H_2{}^{16}O$ (A) and $H_2{}^{18}O$ (B). The protein in (C) was purified from cells grown on high iron and then incubated for 24 hr in $H_2{}^{18}O$. Spectra were obtained on samples in capillaries at 5 °C (90-degree scattering geometry) using 676.4-nm excitation (30-50 mW) at a scan rate of 1 cm^{-1}/s and resolution of 8 cm^{-1} (10 cm^{-1} for spectrum C). Each spectrum was an accumulation of 8, 8, and 15 scans, respectively, and was subjected to a 15-point Savitsky-Golay smoothing.

Figure 6. Proposed mechanism for oxygen activation by R2 (Y122F mutant) using excess Fe(II) and ascorbate. The structure of metR2 is the same as in Figure 1. The structure of reduced R2 is from reference 43. The X intermediate containing a free radical, Z, is described in reference 30.

Figure 7. Proposed mechanism for the formation of DOPA-208 in R2 (F208Y mutant). The steps leading to the ferryl intermediate are the same as in Figure 6. The $^*OH$ moieties in the ferryl intermediate are derived from solvent. The structure of DOPA-208 R2 (ferric catecholate) is from reference 32.

Figure 8. Primary sequence identities of diiron-oxo enzymes capable of activating O_2. A) ribonucleotide reductase R2; B) methane monooxygenase; C) stearoyl-ACP desaturase; D) phenol hydroxylase; and E) toluene-4-monooxygenase. Adapted from reference 58a.

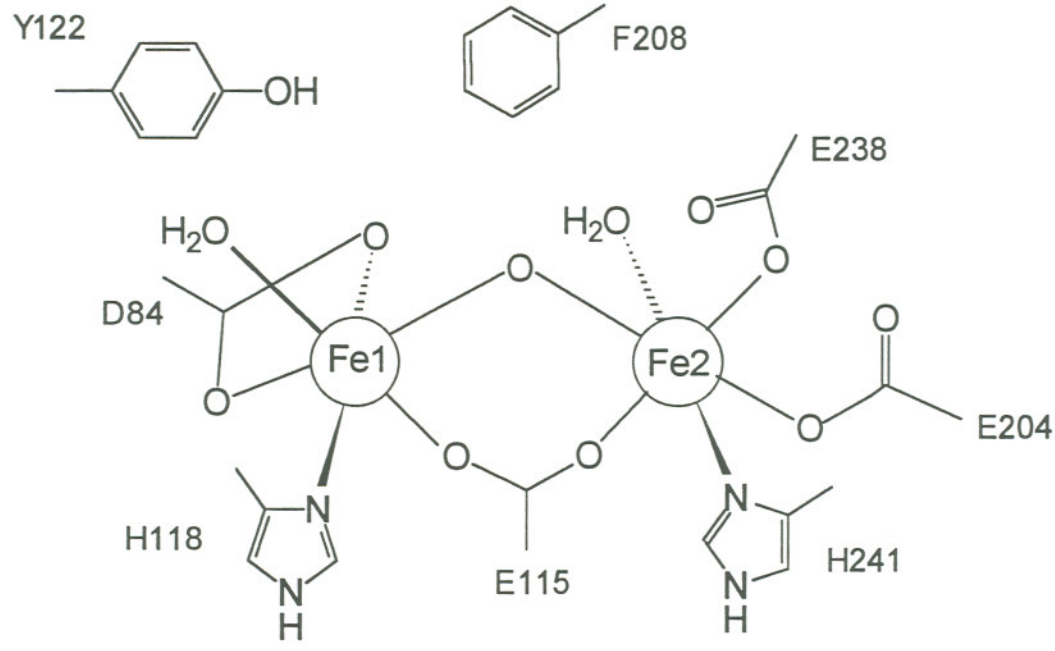

Figure 1

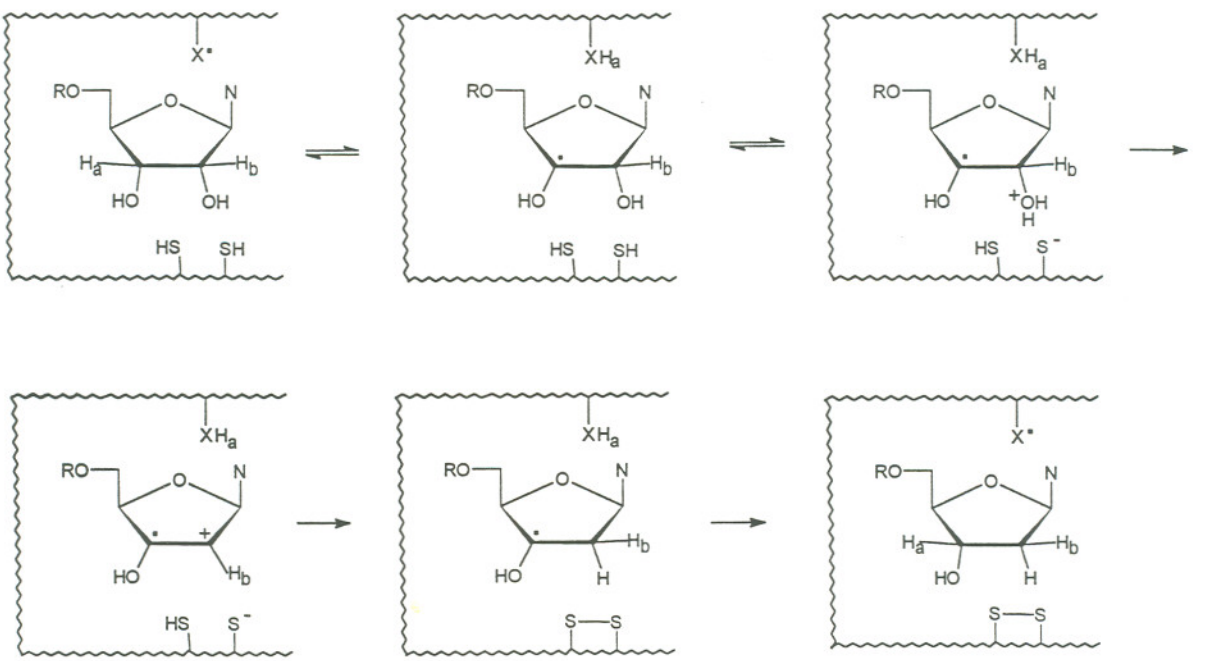

Figure 2

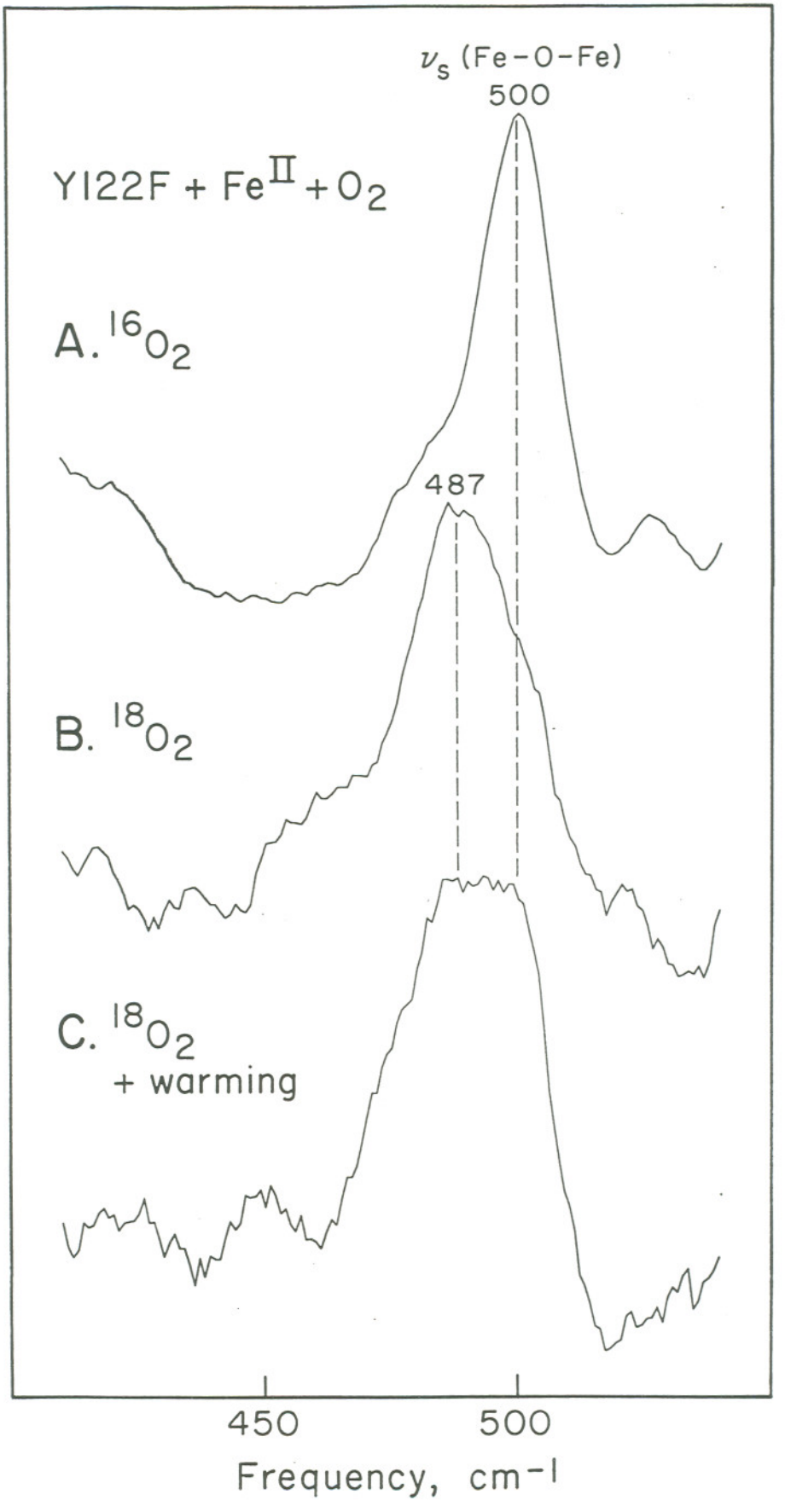
ν_s (Fe-O-Fe)
500
Y122F + Fe^{II} + O_2
A. $^{16}O_2$
487
B. $^{18}O_2$
C. $^{18}O_2$
+ warming
450
500
Frequency, cm^{-1}

Figure 3

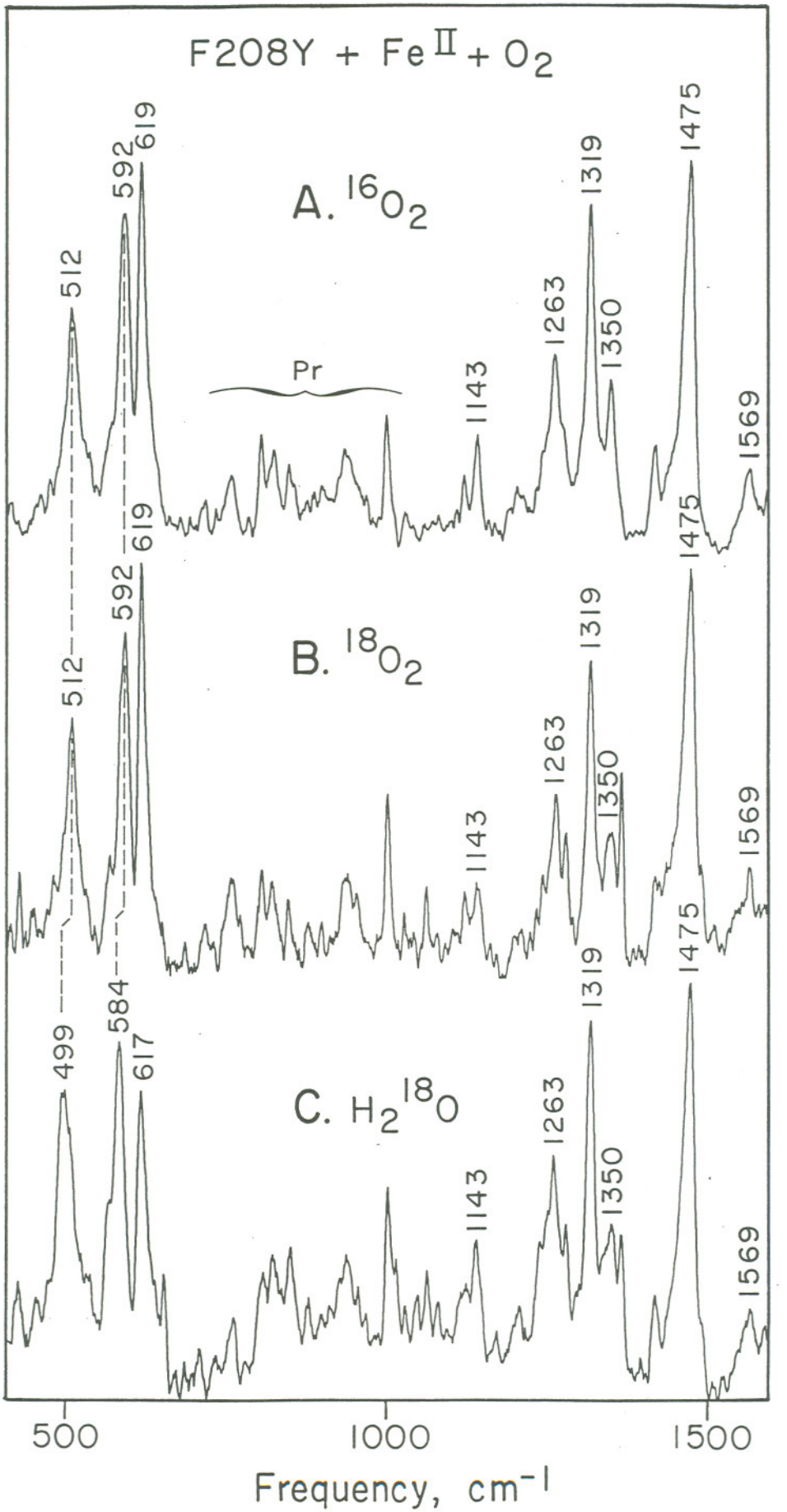
F208Y + Fe II + O2
A. 16O2
B. 18O2
C. H2 18O
512
592
619
499
584
617
Pr
1143
1263
1319
1350
1475
1569
500
1000
1500
Frequency, cm-1

Figure 4

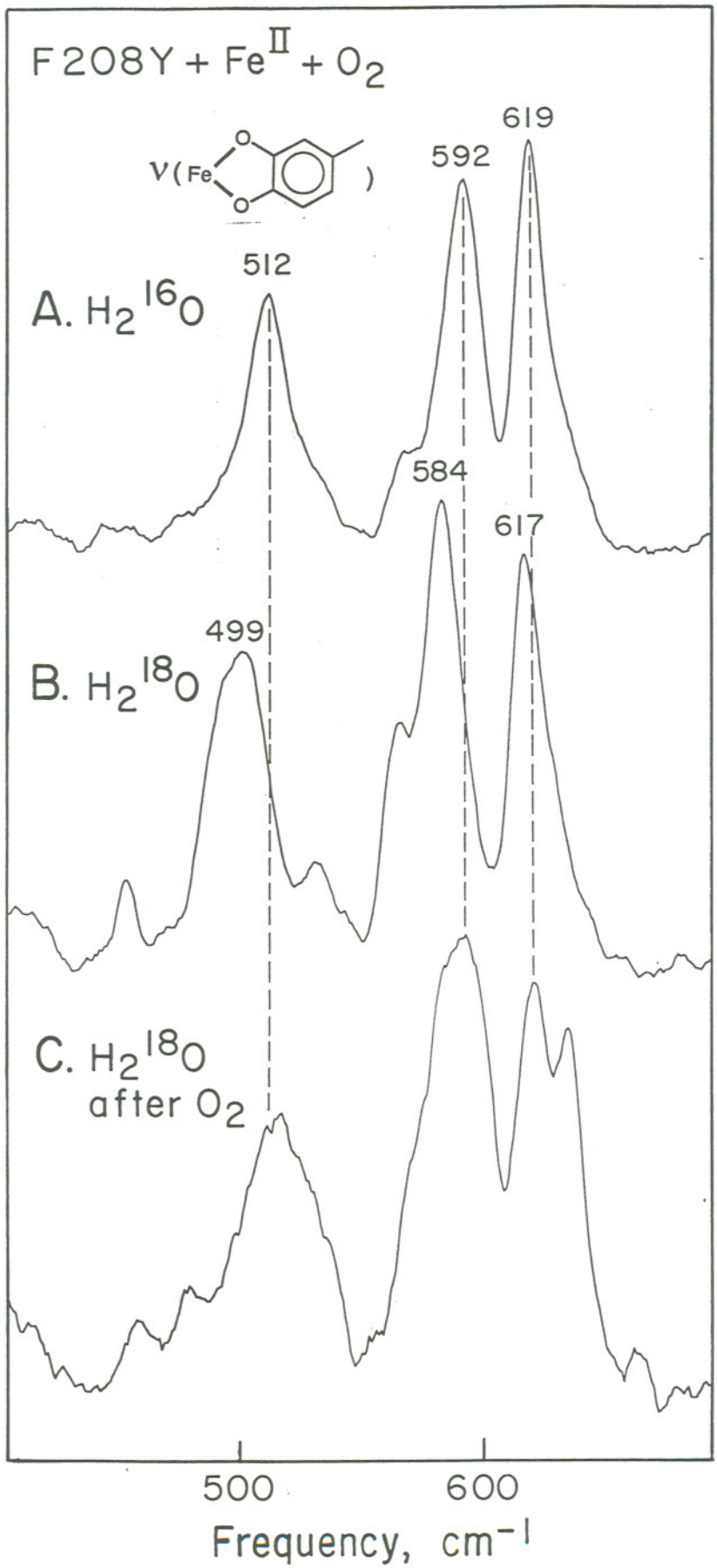
F208Y + Fe^II + O2
ν(Fe
)
619
592
512
A. H2 16O
584
617
499
B. H2 18O
C. H2 18O
after O2
500
600
Frequency, cm-1

Figure 5

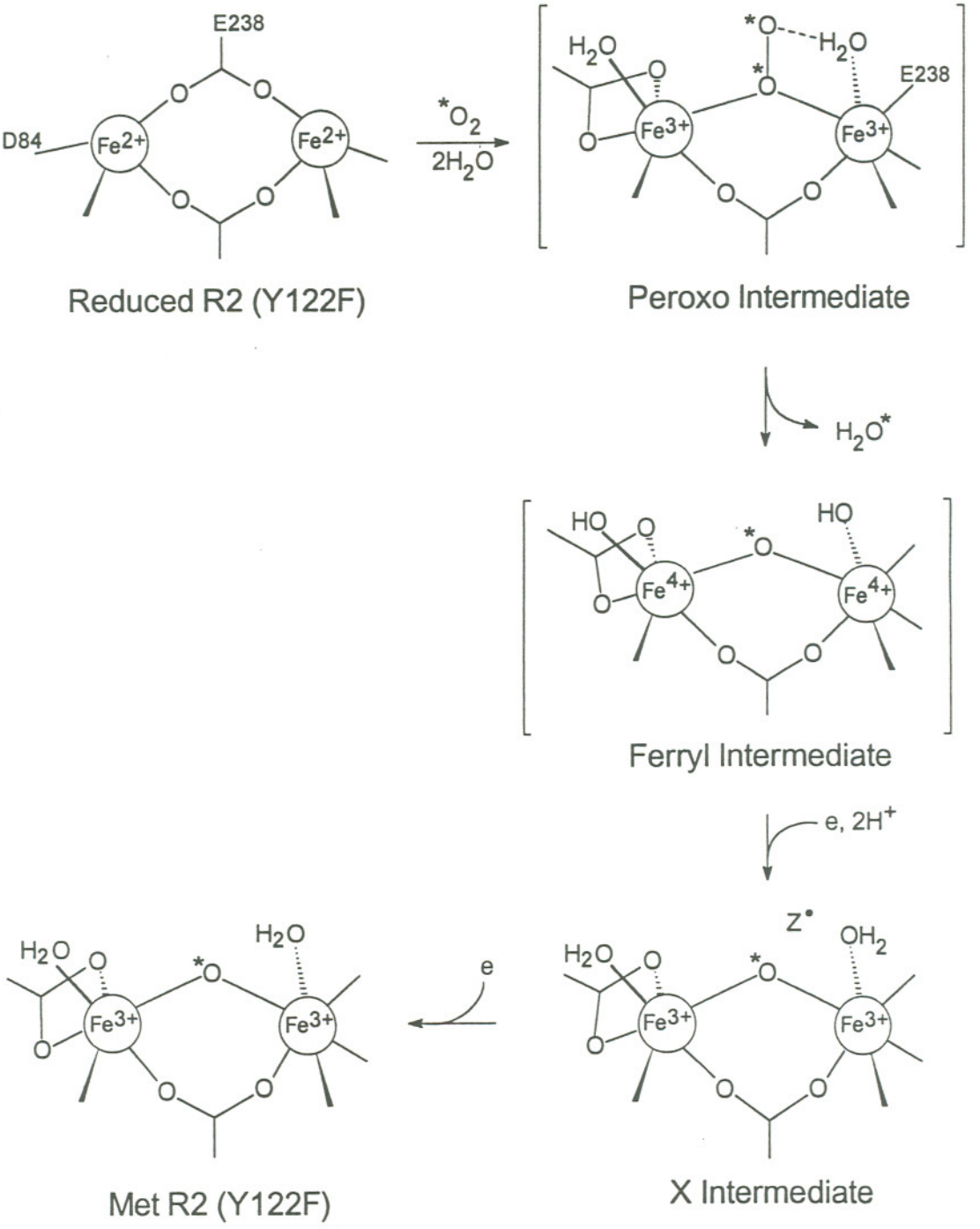
E238
D84
Fe2+
Fe2+
*O2
2H2O
H2O
*O
H2O
E238
Fe3+
Fe3+
Reduced R2 (Y122F)
Peroxo Intermediate
H2O*
HO
HO
Fe4+
Fe4+
Ferryl Intermediate
e, 2H+
Z•
OH2
H2O
H2O
e
Met R2 (Y122F)
X Intermediate

Figure 6

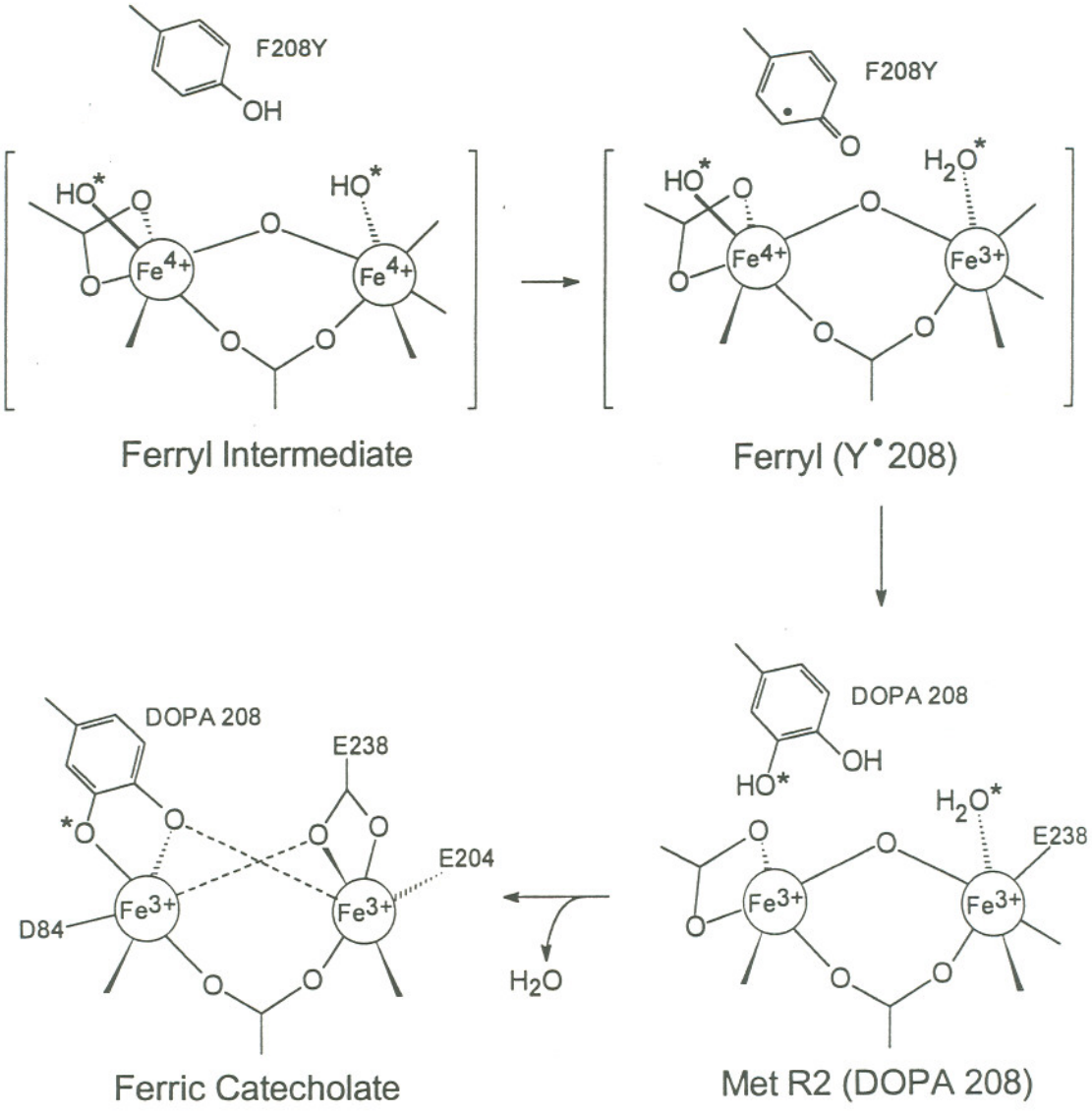
F208Y
OH
HO*
HO*
Fe4+
Fe4+
Ferryl Intermediate
F208Y
HO*
H2O*
Fe4+
Fe3+
Ferryl (Y•208)
DOPA 208
OH
HO*
H2O*
E238
Fe3+
Fe3+
Met R2 (DOPA 208)
H2O
DOPA 208
E238
*O
E204
D84
Fe3+
Fe3+
Ferric Catecholate

Figure 7

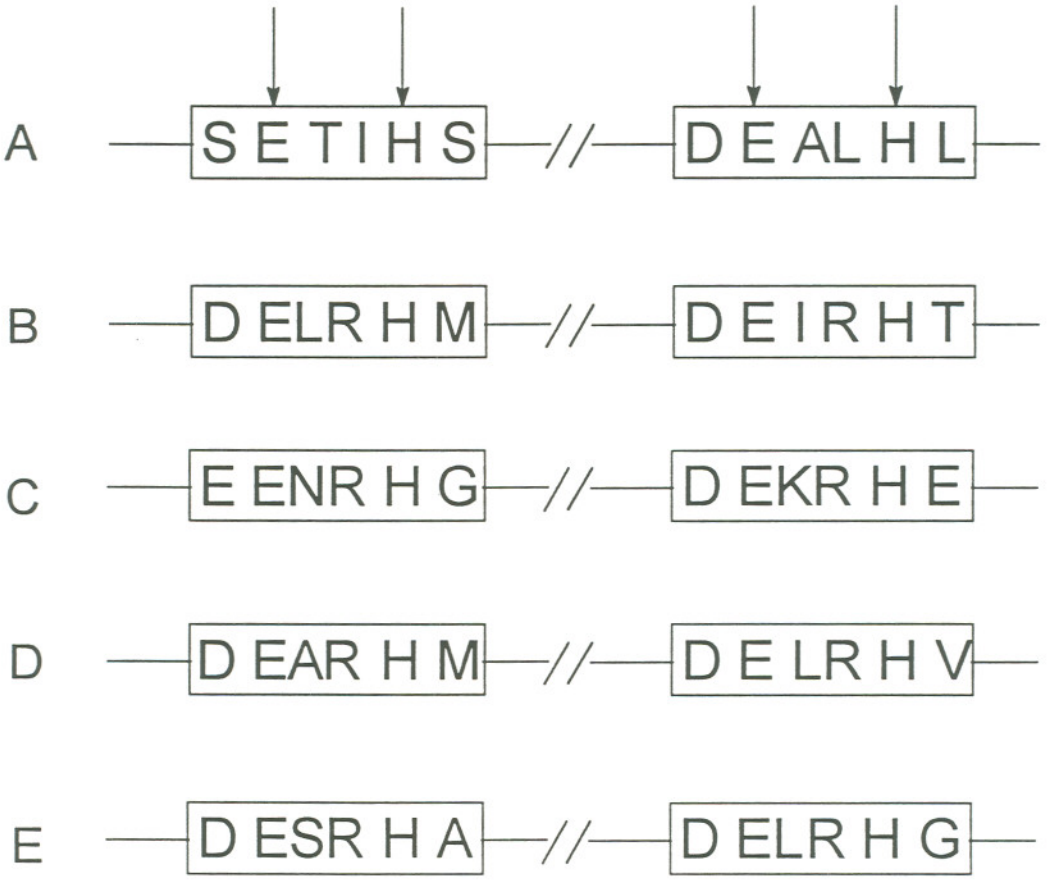
A
S E T I H S
D E AL H L
B
D ELR H M
D E I R H T
C
E ENR H G
D EKR H E
D
D EAR H M
D E LR H V
E
D ESR H A
D ELR H G

Figure 8

CHAPTER IV

RESONANCE RAMAN STUDIES OF OXYHEMOCYANINS. NEW INSIGHTS INTO THE DINUCLEAR COPPER SITE*

Abstract

Hemocyanins (Hcs) are copper-containing oxygen-transport proteins found in the hemolymph of molluscs and arthropods. Previous resonance Raman (RR) studies of oxyhemocyanin indicated that the dioxygen is symmetrically bound to the two Cu(II) ions, based on the oxygen isotope dependence of the peroxide O-O stretch (Thamann, T.J.; Loehr, J.S.; Loehr, T.M. *J. Am. Chem. Soc.* **1977**, *99*, 4187-4189). We have now identified a Cu-O (peroxide) stretch, $\nu_{as}(Cu_2O_2)$, at 542 cm^{-1} (519 cm^{-1} in $^{18}O_2$) and its first overtone, $2\nu_{as}(Cu_2O_2)$, at 1085 cm^{-1} (1039 cm^{-1} in $^{18}O_2$) in the RR spectra of oxyHc from *Octopus dofleini*. When the protein was oxygenated with $^{16}O^{18}O$, only a single $\nu_{as}(Cu_2{}^{16}O^{18}O)$ mode was observed at 529 cm^{-1}. These results provide more definitive evidence that the peroxo group is symmetrically bound to the Cu(II)'s. Oxyhemocyanins from both molluscs and arthropods exhibit similar $\nu_{as}(Cu_2O_2)$ and $2\nu_{as}(Cu_2O_2)$ Raman modes, suggesting that oxyHcs from both phyla have the same copper-peroxide structure: in both cases the Cu(II)'s are bridged solely by the peroxo in a $\eta^2{:}\eta^2$ geometry, as revealed by X-ray crystal structure of *Limulus*

---

*This work was performed in collaboration with Dr. Kamala D. Sharma,[1a] Lisa M. Nestor,[1b,c] Dr. Roman Czernuscewicz,[1d] Robert Fraczkiewicz[1d] and Dr. Thomas G. Spiro[1b]

polyphemus II oxyhemocyanin (Magnus, K.A.; Ton-That, H. *J. Inorg. Biochem.* **1992**, 47, 21). In the low frequency region (100-400 cm^{-1}) oxyHc from *Busycon canaliculatum* exhibits eight distinct vibrational modes, most of which are sensitive to ^{65}Cu or D substitution, rather than $^{18}O_2$. These peaks are assigned to $\nu_s(Cu_2O_2)$ and $\nu_{as}(Cu_2O_2)$ modes coupled with Cu-N(His) stretching vibrations. Comparisons of the low frequency RR spectra reveal that oxyHc from arthropod and mollusc have somewhat different Cu-ligand vibrational patterns, implying that molluscan Hc does not have all six of the histidine ligands found in arthropod Hc. Normal coordinate analysis yields an excellent match with the entire set of observed RR frequencies, thereby lending credibility to the spectral assignments.

Introduction

Properties of Hemocyanins. Hemocyanins (Hcs) are copper-containing oxygen-transport proteins found in the hemolymph of molluscs and arthropods.[2,3] They occur as multi-subunit aggregates. The molluscan Hcs are cylindrical molecules with 10-20 subunits of ~350,000 daltons. Each subunit, in turn, contains 7-8 covalently linked functional units, each of which contains two copper atoms and binds one O_2 molecule. The arthropodan Hcs are composed of hexamers or oligohexamers built from individual subunits, in which each subunit also contains two copper atoms and binds one oxygen molecule. The molecular weight of the minimum oxygen-binding functional unit or subunit varies from 50,000-55,000 in molluscs to 75,000 in arthropods. The oxygen binding in hemocyanins is cooperative and under allosteric control with both homotropic and heterotropic effectors. Besides dioxygen, the deoxy form of the protein also binds carbon monoxide, cyanide, and azide.[3]

Hemocyanins as isolated in their oxy form are blue in color due to the visible absorption band at ~570 nm (ϵ = 1,000 $M^{-1}cm^{-1}$ per 2 Cu). In addition to this feature, oxyHcs have another more intense absorption band at ~345 nm (ϵ = 20,000 $M^{-1}cm^{-1}$). Early resonance Raman (RR) studies showed that the 570-nm band should be assigned as peroxide → Cu(II) charge transfer (CT).[4] Theoretical analysis using a transition

dipole vector coupling model has further assigned the 345-nm band as a transition from the π_σ* orbital of peroxide to the d(x^2-y^2) orbital of Cu(II) and the 570-nm band as π_v* to Cu(II) d(x^2-y^2) CT.[5-7] Despite the presence of Cu(II), oxyHcs are EPR silent, due to strong antiferromagnetic coupling between the two Cu(II) ions ($J \geq 500$ cm^{-1} for *Limulus* oxyHc).[8] The strong coupling is now attributed to the bound peroxide (see below), although it was initially thought that an additional bridging group might also contribute.[5] The deoxy form of Hc is colorless and EPR inactive as well, the latter being due to the d^{10} configuration of the Cu(I) ions.

Tyrosinase is another coupled dinuclear copper protein, catalyzing the oxidation of monophenols and playing an essential role in melanin biosynthesis.[9] Tyrosinase also binds O_2 and forms a relatively stable dioxygen adduct. It has very similar spectroscopic and magnetic properties to hemocyanin, and thus, it is believed to have a similar active site structure to hemocyanin.[5]

Resonance Raman studies have established that in oxyhemocyanin and oxytyrosinase, the dioxygen is bound as peroxide. OxyHcs from both arthropods and molluscs typically exhibit a resonance-enhanced feature at ~ 745 cm^{-1} when excited into either the 570 nm or the 345 nm absorption bands.[10,11] This Raman feature has been assigned to ν(O-O) of the bound dioxygen by its large isotopic shift (~ 40 cm^{-1}) with $^{18}O_2$.[4,10] The bound dioxygen was identified as a peroxide species on the basis of its low vibrational frequency. RR studies using $^{16}O^{18}O$ further suggested that the two oxygen atoms are essentially equivalent and, thus, bound to the two Cu(II)'s in a symmetric manner.[12]

Model Compounds. The unusual spectroscopic and magnetic properties of hemocyanin and tyrosinase have long been of interest to inorganic chemists, and a number of model complexes have been synthesized and reported.[13-16] However, only a few have been demonstrated to bind dioxygen reversibly (Table 1). A [$Cu(I)_2$(XYL-O^-)] (XYL = m-xylene connected to bis[2-(2-pyridyl)ethyl]amine ligands) complex was the first reported to bind dioxygen and form a peroxo dinuclear copper(II) complex.[17] The latter exhibits a quite different absorption spectrum from

oxyHc, with bands at 505 nm (ϵ = 6300 $M^{-1}cm^{-1}$) and 385 nm (ϵ = 3000 $M^{-1}cm^{-1}$). Detailed RR studies of the Cu(II)-peroxo complex revealed that the peroxide is terminally or unsymmetrically bound to one of the Cu(II) ions.[18] A Cu(I)(TEEN)(C_2H_4) complex, where TEEN = N,N,N',N'-tetramethylethylenediamine was also reported to bind O_2 to form a peroxide complex; the latter gives IR bands at 825 cm^{-1} with $^{16}O_2$ and 770 cm^{-1} with $^{18}O_2$.[19]

Karlin and co-workers also synthesized a series of Cu_2(NnPy$_2$) complexes where two Py (bis(2-(2-pyridyl)ethyl)amine) units are connected by alkyl chains of varying length (referred to as N3, N4, and N5 in Table 1). These complexes react reversibly with dioxygen, presumably giving rise to Cu(II)-peroxide products. To some extent, these Cu(II)-O_2 complexes exhibit absorption spectroscopic properties similar to oxyHc, with λ_{max} at ~360 nm (ϵ = 15000-21000 $M^{-1}cm^{-1}$), ~450 nm (ϵ = 3600-5300 $M^{-1}cm^{-1}$), and ~550 nm (ϵ = 1200 $M^{-1}cm^{-1}$).[20] EXAFS analysis suggested their coordination structure to be either cis μ-η^1:η^1 or μ-η^2:η^2.[21] A [Cu(I)(TPA)]$_2$ complex with TPA = Tris(2-pyridylmethyl)amine was also reported to bind dioxygen. The UV-Vis absorption spectrum of the dioxygen complex (Cu(TPA))$_2$(O_2) are quite different from those of oxyHc, with prominent features at 520 nm (ϵ = 11500 $M^{-1}cm^{-1}$) and 600 nm (ϵ = 7600 $M^{-1}cm^{-1}$). The X-ray crystal structure of the O_2 complex showed that the two oxygen atoms bridge the two Cu(II)'s in a trans μ-η^1:η^1 fashion.[22]

Recently, a series of [Cu(HB(R_2Pz)$_3$)]$_2$ complexes, where R = methyl, isopropyl, and phenyl, were also reported to be capable of binding dioxygen reversibly.[23] Although all above mentioned dinuclear LCu(II)$_2$(O_2) complexes are EPR silent, as are oxyHc and oxytyrosinase, the latter set of complexes, synthesized by Kitajima and co-workers, are so far the best models in mimicking the spectroscopic properties of oxyHc and oxytyrosinase (Table 1). For example, the [Cu_2(HB(3,5-i-Pr_2Pz)$_3$)]$_2$(O_2) exhibits absorption maxima at 349 (ϵ = 21000 $M^{-1}cm^{-1}$) and 551 nm (ϵ = 790 M^{-1} cm^{-1}), respectively, in the UV-Vis spectrum and a ν(O-O) at 741 cm^{-1} in the Raman spectrum. These match the known spectroscopic properties of oxyHc very closely.[24] The X-ray crystal structure of this dioxygen

complex shows that the dioxygen bridges the two Cu(II) in an η^2:η^2 fashion.[23]

X-ray Crystal Structures of Arthropod Hemocyanins. The structure of *Panulirus interruptus* (*P.i.*) lobster Hc at 3.2 Å resolution showed that the 450,000 dalton hexamer is composed of two trimers facing each other in a staggered arrangement.[25] Each 75,000 dalton subunit is folded into three domains, and the binuclear copper site is situated in the second domain. The crystals used for the structure determination lacked both 570 nm and 345 nm absorption bands and later UV, XAS, and EPR spectroscopic investigations using single crystals suggested that the protein was in its deoxy state.[26] Each of the Cu(I) ions is ligated to three histidines in domain 2: CuA to H194, H198 (both in helix 2.1) and H224 (helix 2.3); CuB to H344, H348 (both in helix 2.5) and H384 (helix 2.6).[25] The Cu···Cu separation is 3.7 $\pm$ 0.25 Å, and there is no bridging protein ligand present between the two copper atoms (Figure 1A). The two Cu(I) ions have the same copper-histidine ligation pattern: in each case, two of the three histidines come from a sequence -H-X-X-X-H- in one helix and the third histidine from the adjacent helix. Further investigations revealed a pseudo 2-fold axis appearing between the two copper binding sites suggesting that the dinuclear copper site of arthropodan Hc is the result of duplication and fusion of a gene for an ancestral mononuclear copper site.[27]

The X-ray crystal structures of the oxy and deoxy forms of hemocyanin subunit II from horseshoe crab, *Limulus polyphemus* (*L.p.*) are also emerging.[28] The structure of oxyHc shows that each Cu(II) is ligated to two equatorial His and one axial His, in addition to the bridging peroxide that is bound in a μ-η^2:η^2 geometry (Figure 1b). The four equatorial His, the two Cu(II) ions, and the dioxygen are in the same plane, whereas the two axial His are trans to each other. The structure of the deoxy form has also been solved. In this structure, as with *P.i.* Hc, each Cu(I) is also ligated to three histidines: CuA to His 173, 177, 204 and CuB to His 324, 328, 364. The Cu···Cu distances in the oxy and deoxyHc forms are 3.6 and 4.6 Å, respectively. As in *P.i.* Hc, there is no evidence for exogenous or endogenous

bridging ligands (other than peroxide) in either the oxy or the deoxy protein. The Cu-His ligation patterns of both the oxy and deoxy forms are the same as in *P.i.* Hc, i.e., both CuA and CuB are complexed to two His from a sequence -H-X-X-X-H- in one helix and the third from the adjacent helix.

Comparison of amino acid sequences of arthropodan Hc subunits reveals a considerable degree of homology.[29] Among the nine available sequences of ~625-660 amino acid residues each, 110 positions (~17%) are identical and this figure increases to ~29% if isofunctional residues are counted. Identities are often clustered in contiguous regions. The most strongly conserved regions are those near and including the six histidine residues that have been identified as copper ligands in *P.i.* and *L.p.* hemocyanins. Thus, it is likely that all arthropodan Hcs have a similar dinuclear copper site in which each Cu is ligated to three His with dioxygen bridging in an η^2:η^2 geometry.

Active Site in Molluscan Hemocyanins. There is no crystal structure available yet for any molluscan hemocyanin. Based on the similarity of the spectroscopic and magnetic properties of arthropodan and molluscan hemocyanins, it has been believed that they have similar dinuclear copper sites.[30] For example, EXAFS measurements of deoxyhemocyanins reveal that each copper is complexed by 2-3 His and that the Cu···Cu distance is 3.43-3.48 Å in proteins from both phyla.[31] Molluscan Hcs have very little sequence homology to arthropodan Hcs, except for a region that corresponds to the copper B binding site in *P. interruptus* and the *L. polyphemus* Hcs.[32] This region is also conserved in all tyrosinases.[33] It has been proposed that molluscan Hcs as well as tyrosinases have the same CuB site as arthropodan Hcs, with the copper atom complexed by three conserved histidines, two from an -H-X-X-X-H- segment in a single helix and the other from the adjacent helix.[32,33] Indeed, site-directed mutagenesis and photoinactivation experiments on tyrosinase have implicated CuB-site amino acids, His 174 and His 205, as copper ligands (using Hc numbering below).[34]

Molluscan Hcs have no sequence identity corresponding to the CuA site in arthropod Hcs. Comparisons among available sequences reveals considerable homology between molluscan functional units.[32] Among the six available sequences, 90 positions out of ~400 amino acid residues in each chain are occupied by identical residues and 44 by isofunctional residues. A total of six histidines are conserved in molluscan sequences. For Hc from *Octopus dofleini* (functional unit g),[32] His 174, 178, and 205 are suggested to be ligands of CuB by homology to *P.i.* and *L.p.* Hcs. His 204 positioned next to His 205 is conserved only in molluscan Hcs, not in arthropodan Hcs or tyrosinases, and thus is unlikely to be a Cu ligand. His 46 and 74 are conserved in all molluscan Hcs and tyrosinases, and thus could be ligands to copper A. The site-directed mutagenesis studies also suggested His 74 (Hc numbering) as a ligand to copper in *Streptomyces glaucescens* tyrosinase.[34,35] It seems likely that the CuA site in molluscan Hcs and tyrosinases has only 2 His ligands at most, with the third ligand position being either unfilled or occupied by a different amino acid. This difference in amino acid ligation is consistent with the electronic and CD spectra of oxyHcs from the two phyla which suggest that the Cu-peroxide entity is conserved but that the ligand fields of the Cu ions are different.[30]

Resonance Raman spectroscopy is a useful technique for providing more definitive information about the structure of the Cu_2O_2 moiety. Previous RR studies have detected similar O-O stretching vibrations at ~750 cm^{-1} in oxyHcs from both molluscs and arthropods.[4,11] We have now, for the first time, identified a $\nu_{as}(Cu_2O_2)$ mode and its first overtone $2\nu_{as}(Cu_2O_2)$ of the copper peroxo moiety at 542 and 1085 cm^{-1}, respectively, in the molluscan Hc from *Octopus dofleini (O.d.)*. Similar $\nu_{as}(Cu_2O_2)$ and $2\nu_{as}(Cu_2O_2)$ features have been observed for *Busycon canaliculatum* (*B.c.*, mollusc) and *L.p.* (arthropod) oxyHcs. These results suggest that oxyHcs from both phyla have the same structure for the $Cu_2(O_2)$ moiety, i.e., a μ-η^2:η^2 Cu_2-peroxo structure, as revealed by the X-ray crystal structure of *L.p.* oxyHc.[28] Furthermore, the Raman spectrum of *O.d.* oxyHc prepared from $^{16}O^{18}O$ reveals only a single $\nu_{as}(Cu_2{}^{16}O^{18}O)$ vibration, proving that the peroxide is bound to the copper ions in a

symmetric geometry. We have also corroborated the presence of Cu-N(His) vibrations in the RR spectrum of *B.c.* Hc on the basis of ^{65}Cu and deuterium isotopic shifts. While molluscan Hcs from different species show a very similar pattern of Cu-ligand vibrations, the arthropodan Hc pattern is somewhat different. This suggests that Hcs from the two phyla may have a slightly different set or coordination geometry of copper ligands.

Experimental Section

Protein Samples. *Octopus dofleini* (*O.d.*) hemolymph was generously provided by Dr. Karen Miller (Oregon State University). The hemocyanin was purified by ultracentrifugation for 2 hr at 55,000 rpm (Ti 65 rotor, Beckman). The pellet was dissolved in 0.1 M Tris-HCl, 50 mM $MgCl_2$, 10 mM $CaCl_2$ (pH 7.8) during a 48-hr incubation at 5°C. The concentration of the resultant protein was determined by its 345-nm absorption (ϵ = 10,000 $M^{-1}cm^{-1}$ per Cu).[36] Storage of this protein for several months at -80°C had little effect on the quality of either the electronic or the Raman spectra. *Busycon canaliculatum* (*B.c.*) hemocyanin was prepared from hemolymph of the mollusc designated *as Busycotypus* (Marine Biological Laboratory, Woods Hole, MA), as described previously.[4,11] After a brief centrifugation at 12,000×g, the protein was dialyzed versus 0.05 M sodium carbonate (pH 9.8) to cause dissociation into subunits. This lowered the turbidity and allowed the protein to be concentrated to ~5 mM in Cu by ultrafiltration in a Centricon 30 (Amicon) prior to storage at -15°C. The Hc concentration was determined from ϵ_{347} = 10,000 $M^{-1}cm^{-1}$ per Cu.[30] *Limulus polyphemus* (*L.p.*) hemocyanin was generously provided by Dr. Celia Bonaventura (Duke University Marine Laboratory, Beaufort, NC) and further purified[37] as follows. The hemocyanin was dissociated into subunits by dialysis versus 0.05 M Tris-HCl, 0.05 M glycine, 0.01 M EDTA, and 0.1 M NaCl (pH 8.9). 2 ml of Hc (0.8 mM in Cu) were applied to a DEAE Sepharose (CL-68, Pharmacia) column (1.5 × 25 cm) and eluted with a 500 ml linear gradient of

0.2-0.5 M NaCl. Subunit II, which eluted at 0.23 M NaCl, was concentrated using Centriprep and Centricon ultrafiltration devices. The Hc concentration was determined from ϵ_{340} = 12,000 $M^{-1}cm^{-1}$ per Cu.[37]

O_2 Isotope Exchange. OxyHc (*L.p.*, 4 mM in Cu) was flushed with carbon monoxide in a gas-delivery apparatus[38] until the blue color of the oxygenated protein disappeared. Excess CO was removed by evacuating the system. The protein was then reoxygenated by exposure to $^{18}O_2$ (99 atom %, ICON) or $^{16}O^{18}O$ (50% ^{18}O, Cambridge Isotope Laboratory) for 5 min., with reappearance of the characteristic blue color.

Deuterium Exchange. OxyHc from *B.c.* (5 ml, 1.4 mM in Cu) was centrifuged as described above for *O.d.* Hc and the pellet was dissolved in 5 ml 0.05 M carbonate buffer in D_2O (99.8 atom%, Aldrich) at a pH reading of 9.8. The protein was cycled through the deoxy state by flushing with buffer-equilibrated Ar for 6 hours. The sample was reconcentrated by centrifugation and dissolved in 100 μl D_2O buffer. A parallel sample was prepared in H_2O. Alternatively, the exchange was performed using several rounds of dilution in D_2O buffer and reconcentration by ultrafiltration. These two methods gave similar RR results.

$H_2{}^{18}O$ Exchange. OxyHc from *B.c.* in 0.05 mM carbonate (pH 9.8) was concentrated in a Centricon 30 to 8 mM in Cu, then diluted 5-fold with pH 9.8 buffer prepared in $H_2{}^{16}O$ or $H_2{}^{18}O$ (97 atom % ^{18}O, YEDA, Israel). This procedure was repeated for a second time. The oxyHc was then converted to deoxyHc by flushing 30 min with CO gas and incubated for 12 hours. Samples were then bubbled with O_2 gas for 10 min to allow reoxygenation and were reconcentrated by ultrafiltration. The filtrate of the $H_2{}^{18}O$ sample contained 80% ^{18}O according to a mass spectral analysis.

^{65}Cu Exchange. ApoHc from *B.c.* was prepared by dialysis against KCN and

reconstituted with ^{63}Cu (99.89%) or ^{65}Cu (99.7%, Oak Ridge National Laboratories) as described previously.[11]

Raman spectroscopy. Some of the Raman spectra were recorded on a Jarrell-Ash spectrophotometer at the Oregon Graduate Institute using an RCA C31034 photomultiplier and an ORTEC model 9302 amplifier-discriminator and interfaced with an Intel 310 computer. Excitation sources were Spectra-Physics 164-05 (Ar^+) and 2025-11 (Kr^+) lasers. Spectra were obtained on samples in capillaries in a Dewar maintained at either 278 K or 90 K or on samples frozen onto the cold head of a Displex (Air Products) at 15 K, all in a 150° backscattering geometry.[38] Other Raman spectra were recorded on a Spex 1401 spectrophotometer at Princeton University using an RCA C31034A photomultiplier and photo-counting electronics and interfaced to a DEC MINC computer. The excitation source was a Kr^+ laser (356.4 nm) and the spectra were obtained at 77 K as described previously.[39]

Results and Discussion

Peroxide O-O Stretch. Previous resonance Raman studies of oxyHc from many species of both arthropods and molluscs have revealed ν(O-O) at $\sim$750 cm^{-1} when excited within either the 570-nm or 345-nm absorption band.[4,10,11] The identity as a vibrational mode of a dioxygen moiety was confirmed by the large isotopic shift of $\sim$40 cm^{-1} when the protein was oxygenated with $^{18}O_2$. For example, in the RR spectra of *B.c.* Hc, ν(O-O) shifts from 749 cm^{-1} to 708 cm^{-1} with $^{18}O_2$.[4] The frequency ($\sim$750 cm^{-1}) of this vibrational mode has prompted identification of the dioxygen species as a peroxide ion.[10] Further RR experiments using the mixed isotope of $^{16}O^{18}O$ revealed only a single ν(O-O) at 728 cm^{-1}, suggesting that the two oxygen atoms are equivalent in the Cu_2-peroxo site.[12]

Oxyhemocyanin from *Octopus dofleini* gives similar results. Figure 2 shows the Raman spectra obtained using excitation within the 570-nm absorption band. The $^{16}O_2$ sample shows an intense peak at 749 cm^{-1} (Figure 2A). In the $^{18}O_2$ sample, the

intense peak has shifted to 709 cm^{-1} (Figure 1C). This 40-cm^{-1} isotopic shift in $^{18}O_2$ is consistent with those previously reported for *B.c.* and *Cancer magister* Hcs[10] and definitively identifies the 749-cm^{-1} feature of the *O.d.* Hc as the O-O stretch of peroxide. The broad feature centered at ~755 cm^{-1} in Figure 1C consists of two bands, one due to residual $^{16}O_2$ at 750 cm^{-1} and the other due to a protein band at ~760 cm^{-1}.[4] The latter is most likely a non-enhanced mode of tryptophan.[40]

The *O.d.* Hc was also oxygenated with a mixed isotope of O_2 containing ~50% $^{16}O^{18}O$. The Raman spectrum of this sample (Figure 1B) shows a peak at 709 cm^{-1} attributable to $\nu(^{18}O\text{-}^{18}O)$, while the broad feature at ~760 cm^{-1} has contributions from the $\nu(^{16}O\text{-}^{16}O)$ at 749 cm^{-1} and the protein peak at ~760 cm^{-1}. This protein peak is more prominent than it is in the $^{16}O_2$ and $^{18}O_2$ spectra, due to incomplete reoxygenation with mixed isotope O_2. The central 730-cm^{-1} peak is attributed to the $\nu(^{16}O\text{-}^{18}O)$. This frequency is very close to the 728- and 725-cm^{-1} values for Hc from *B.c.* and *L.p.*, respectively.[12,41] Its appearance halfway between $\nu(^{16}O\text{-}^{16}O)$ and $\nu(^{18}O\text{-}^{18}O)$ is also the same as with previous studies on *B.c.* and *L.p.* Hcs. There appears to be only a single $\nu(^{16}O\text{-}^{18}O)$, based on its having a similar band width to $\nu(^{18}O\text{-}^{18}O)$ as well as twice the intensity (in agreement with the isotope composition). This indicates that the oxygen atoms of the bound peroxide are equivalent in *O.d.* Hc, as was also observed for *B.c.* and *L.p.* hemocyanins.[12,41] However, even in the case of inequivalent oxygens, the splitting of $\nu(^{16}O\text{-}^{18}O)$ is small because the O-O stretch is a relatively pure mode and is not much affected by the atoms the peroxide is attached to. The observed splitting is only 5 cm^{-1} for the terminal peroxides in the $Cu_2(TMPA)(O_2)$ complex[18] and in oxyhemerythrin[42], and a splitting of 2-3 cm^{-1} (indicating some inequivalence) would not be detectable in the present RR spectrum. The mixed-isotope results for $\nu(Cu_2O_2)$ reported below provide considerably stronger evidence for equivalent oxygens in *O.d.* oxyHc..

DeoxyHc from *B.c.* was incubated in D_2O and then reoxygenated. The Raman spectrum of the resultant protein did not reveal any shift of the ν(O-O) peak at 750 cm^{-1} (Table 2). This suggests that the bound peroxide is not protonated or H-

bonded to solvent or to any other exchangeable proton.

Copper-Peroxo Vibrations. Excitation of hemocyanins (*O.d.*, *B.c.*, and *L.p.*) within their 345-nm absorption bands yields a broad and intense band at ~ 1090 cm^{-1} and a weak-to-medium band at ~ 545 cm^{-1} (Figure 3), in addition to a set of intense features in the 100-400-cm^{-1} region which have been attributed to copper-ligand vibrations (see below).[11,43] The unusually broad and intense feature at ~ 1090 cm^{-1} was originally suggested to be due to an electronic singlet → triplet transition associated with the antiferromagnetically coupled Cu^{2+} centers.[11] However, the newly detected RR mode at ~ 545 cm^{-1} is at exactly one-half the energy of the ~ 1090-cm^{-1} mode. When Hc from *O.d.* is oxygenated with $^{18}O_2$, the peaks at 542 and 1085 cm^{-1} shift to 519 and 1039 cm^{-1}, respectively, maintaining their 1:2 frequency relationship (Figures 3A and 4C). These two peaks can, therefore, be assigned to a copper-peroxide stretching vibration, $\nu(Cu_2{}^{18}O_2)$, and its first overtone $2\nu(Cu_2{}^{18}O_2)$. The fact that the overtone is considerably more intense than the fundamental indicates that the fundamental is an asymmetric stretch whose overtone is more symmetry allowed.[44] The observation of resonance-enhanced Cu-O vibrations with UV excitation provides strong supporting evidence for the assignment of the 345-nm absorption band to peroxide → Cu(II) CT.[5]

It is of interest that the same set of $\nu_{as}(Cu_2O_2)$ and $2\nu_{as}(Cu_2O_2)$ modes are present in mollusc *B.c.* Hc (Figure 3B, Table 3) as well as in arthropod *L.p.* Hc (Figure 3C). The latter spectra were obtained on subunit II, the same protein subunit shown to have a μ-η^2:η^2 side-on peroxide (Figure 1B) by X-ray crystallography.[28] The μ-η^2:η^2 model compound, $[Cu(HB(3,5\text{-}iPr_2pz)_3)]_2(O_2)$, similarly exhibits an intense and broad $2\nu_{as}(Cu_2O_2)$ mode at 1144 cm^{-1} that shifts 46 cm^{-1} to lower energy for the compound prepared with $^{18}O_2$.[6] The presence of the first overtone of $\nu_{as}(Cu_2O_2)$ in the RR spectrum appears to be diagnostic of a μ-η^2:η^2 peroxide since this feature has not been detected in the RR spectra of dimeric Cu(II) complexes with η^1 terminally bound peroxide.[18,24] Thus, it is likely that molluscan hemocyanins also bind dioxygen in a μ-η^2:η^2 fashion.

Further evidence in support of a μ-η^2:η^2 peroxide in molluscan Hc comes from the use of a mixed isotope of O_2 containing $\sim$50% $^{16}O^{18}O$ as in Figure 2B. Using UV excitation, the RR spectrum of *O.d.* hemocyanin in the $\nu_{as}(Cu_2O_2)$ region shows a broad feature around 530 cm^{-1} (Figures 4B and D) which is considerably broader than in either of the pure isotopes (Figures 4A and C). A curve fitting analysis of the band in Figure 4D indicates that this broad feature is actually composed of three peaks at 519, 529, and 542 cm^{-1} (Figure 4E). These peaks can be assigned as $\nu_{as}(Cu_2{}^{18}O_2)$, $\nu_{as}(Cu_2{}^{16}O^{18}O)$, and $\nu_{as}(Cu_2{}^{16}O_2)$, respectively. The fact that they are occurring in the approximate ratio of the O_2 gas is definitive evidence that the two oxygen atoms are equivalent in the oxyHc. If only one end of the peroxide were coordinated to Cu, as in a terminal configuration, then the different Cu-O stretching modes (Cu-$^{18}O^{16}O$ and Cu-$^{16}O^{18}O$) would have given rise to a spectrum as in Figure 4F. This type of spectrum has been observed for terminally coordinated peroxide in the $[Cu_2(XYL\text{-}O\text{-})(O_2)]^{2+}$ complex[18] and in the dinuclear iron center of oxyhemerythrin[42] with a splitting between ν(M-$^{18}O^{16}O$) and ν(M-$^{16}O^{18}O$) of 18 and 16 cm^{-1}, respectively. The absence of such a splitting for $\nu_{as}(Cu_2O_2)$ in oxyHc is conclusive proof of equivalent oxygens.

Copper-Ligand Vibrational Modes. Excitation of oxyHc within the 345-nm absorption band produces an additional set of 4-5 intense features between 200 and 400 cm^{-1} (Figure 3). These modes are distinguished from the higher energy modes between 540 and 1100 cm^{-1} by their lack of sensitivity to isotopes of O_2.[4,11] Earlier RR studies of *B.c.* Hc revealed that the bands at 227, 267, and 287 cm^{-1} were affected by Cu isotope substitution whereas the bands at 227 and 267 cm^{-1} were affected by exchange with D_2O.[11] The latter two bands were assigned to Cu-N(His) stretching since the NH of imidazole is capable of solvent exchange. The low energy of the Cu-N(His) stretch is due to the entire imidazole ring behaving as an oscillator with a point mass of 67. Whether other less intense peaks are also sensitive to isotope exchange was unclear due to the low resolution of spectra obtained at 298 K.

We have been able to obtain higher quality spectra by freezing samples at 77

or 15 K. The spectral improvement is due in part to peak sharpening at low temperature and in part to decreased sample deterioration during UV irradiation. Expanded and higher-resolution spectra of the low-frequency region are shown in Figure 5. The two molluscan hemocyanins from *O.d.* and *B.c.* exhibit almost identical frequencies and relative intensities, with the dominant feature at 270 cm^{-1}. The arthropod Hc from *L.p.* exhibits a somewhat different set of frequencies and intensities, with its dominant feature at 286 cm^{-1}.[43] The RR pattern for *L.p.* Hc appears to be characteristic of arthropod Hcs as a similar spectrum has been observed for Hc from the crab, *Cancer magister*.[11]

High resolution data have also been obtained for *B.c.* Hc that has undergone Cu substitution or D_2O exchange. Figure 6 shows a comparison between ^{65}Cu and ^{63}Cu Hcs. The four most intense peaks at 229, 270, 293, and 313 cm^{-1} each shifts by -2 cm^{-1} in the ^{65}Cu spectrum while the weaker peak at 345 cm^{-1} appears to shift by -1 cm^{-1} (Table 2). The isotopic shifts of the 229-, 270- and 293-cm^{-1} features are consistent with previous work.[11] The better resolution of the data shown here allows us to further identify the 313- and 345-cm^{-1} Raman bands as Cu-L stretching vibrations. The RR spectrum of *B.c.* Hc in D_2O shows that the four bands at 229, 270, 313, and 345 cm^{-1} shift to lower energy (Figure 7) by -1, -1, -2, and -1 cm^{-1}, respectively (Table 2). The D isotope shifts at 229 and 270 cm^{-1} were observed previously.[11] Each of these modes is likely to have significant Cu-N(His) stretching character.

To gain further information on the nature of the low frequency vibrations, the effects of $^{18}O_2$ and $H_2{}^{18}O$ were also examined. For *O.d.* Hc prepared with $^{18}O_2$, none of the well-resolved features between 174 and 345 cm^{-1} showed any indication of isotope dependence (Table 2). Similarly, no isotope shifts were observed for *B.c.* Hc in $H_2{}^{18}O$ (Table 2), even though it had been cycled through the deoxy state in $H_2{}^{18}O$. The total lack of any $H_2{}^{18}O$ dependence in either the Cu-N(His) or Cu_2O_2 vibrational regions suggests that there is no aqua ligand in molluscan oxyHc.

Normal Coordinate Analysis. Our discovery of the $\nu_{as}(Cu_2O_2)$ mode, improved resolution of low-frequency vibrational modes, and more accurate information on isotope dependence have made it feasible to use normal coordinate analysis (NCA) to aid in spectral assignments. The model for this analysis used a Cu-site geometry and bond distances from the crystal structure of *L.p.* oxyHc (Figure 1). It contained $Cu_2O_2(Im)_4$ in a planar array with 2 axial imidazoles at a longer distance. The equatorial and axial imidazoles, designated as N_e and N_a, respectively, were each treated as a point mass of 67. The model was constrained to have C_{2h} symmetry. Bond distances for the model and force constants from the calculation are listed in Table 3. These parameters are consistent with literature values for metal-ligand bonds where bending force constants can have up to 30% of the magnitude of stretching force constants.[45] The normal mode calculation was performed using the Wilson GF-matrix method and a Urey-Bradley force field.[46] Calculated frequencies and isotope shifts are compared with the observed quantities for molluscan Hc in Table 4. A simplified set of assignments based on the major contributor to each mixed mode is given in Table 2. Eigenvectors for the normal modes of the Cu_2O_2 core are shown in Figure 8.

Considering the complexity of the system and the uncertainties of metal coordination geometry in protein structures, the NCA gives a remarkably good fit with the observed frequencies and isotope shifts (Table 4). Every stretching mode predicted for the $Cu_2O_2(N_e)_4(N_a)_2$ structure can, in fact, be observed in the RR spectrum. Thus, in addition to the symmetry-allowed A_g and B_g modes, the symmetry-forbidden A_u and B_u modes all appear to have substantial Raman intensities. This type of enhancement of forbidden modes has been previously observed in RR spectra of other metalloproteins such as the $Fe_2S_2(Cys)_4$ cluster in ferredoxin.[47] A likely explanation is that asymmetry in the protein environment of the cluster causes a relaxation of the selection rules. This type of relaxation is not seen in the μ-η^2:η^2 model for oxyHc (Table 2) where mainly the A_g fundamentals are observed in the RR spectrum.[6]

In the high energy region, the calculated values for ν(O-O) at 750 cm^{-1}, the

$\nu_{as}(Cu_2O_2)$ B_g mode at 550 cm^{-1}, and the $\nu_{as}(Cu_2O_2)$ B_u mode at 610 cm^{-1} are close to the observed values for these fundamentals in oxyHc and their isotope shifts in $^{18}O_2$ (Table 4). The potential energy distribution (PED) shows them to be isolated and fairly pure vibrations. For this reason, an NCA calculation using only the Cu_2O_2 moiety in a μ-η_2:η_2 configuration produced a similar set of predicted frequencies for ν(O-O) and $\nu_{as}(Cu_2O_2)$.[6] These frequencies also agree well with the observed RR spectrum of the μ-η_2:η_2 model compound (Table 2), despite the fact that the nature and orientation of the other copper ligands are quite different from oxyHc. The unusually low energy of $\sim$750 cm^{-1} for ν(O-O) in oxyHc and the model compound compared to more typical values of 800-850 cm^{-1} for ν(O-O) in other peroxide complexes[10,24] has been ascribed to weakening of the O-O bond by back-bonding in μ-η^2:η^2 peroxide complexes.[6] A more likely explanation derives from our NCA which shows that the O-O stretch at 750 cm^{-1} is lowered in energy due to mixing with the symmetric Cu_2O_2 stretch (Table 4).

The $\nu_s(Cu_2O_2)$ A_g mode is predicted to occur at considerably lower energy, around 284 cm^{-1}, based on the NCA for a μ-η^2:η^2 Cu_2O_2 system.[6] Using the expanded ligand set of $Cu_2O_2(N_e)_4(N_a)_2$, we have found that the ν_s and ν_{as} motions of the Cu_2O_2 moiety undergo substantial mixing with ν_s and ν_{as} motions, respectively, of the $Cu(N_e)_4$ and $Cu(N_a)_2$ moieties (Table 4). Thus, all of the observed frequencies between 170 and 370 cm^{-1} in oxyHc appear to be coupled motions involving the Cu_2O_2 center and its equatorial and axial imidazole ligands. The majority of the vibrations in this region are predicted to have both Cu and H isotope dependence which is, on the whole, observed. The only surprising discrepancy is the apparent lack of a D-shift in the fairly well-resolved peak at 292 cm^{-1} in *B.c.* Hc. Comparison with the RR spectrum of the μ-η^2:η^2 model shows the sensitivity of this vibrational region to the orientation of the N ligands. While oxyHc has four imidazole N's in the Cu_2O_2 plane (Figure 1B), none of the pyrazole N's in the model compound are in the Cu_2O_2 plane. As a result, the RR spectrum of the model reveals a seemingly different set of Cu-L vibrations between 200 and 320 cm^{-1}.[6]

The A_g modes with $\nu_s(Cu_2O_2)$ character lack $^{18}O_2$ sensitivity because only the

Cu atoms move in this vibration (Figure 8).[6] The modes that are expected to have $^{18}O_2$ sensitivity are the A_u modes with $\nu_{as}(Cu_2O_2)$ character. These are calculated to occur at 233 and 311 cm^{-1} with $^{18}O_2$ shifts of -9 and -3 cm^{-1}, respectively. In the RR spectrum of *O.d.* Hc, the former is a poorly resolved shoulder at 237 cm^{-1} (Figure 5A) for which we have been unable to obtain definitive evidence regarding $^{18}O_2$ dependence. The other A_u mode at 314 cm^{-1} is better resolved, but no shift in $^{18}O_2$ is apparent (Table 2). Smaller $^{18}O_2$ isotope effects in the A_u modes would be expected if the O_2 molecule were not strictly coplanar with the two Cu atoms. This detail may be beyond the limit of resolution of the protein crystal structure. In the μ-η^2:η^2 model compound, which does have a coplanar Cu_2O_2 moiety, the IR-detectable $\nu_{as}(Cu_2O_2)$ mode at 331 cm^{-1} does undergo a -10 cm^{-1} shift in $^{18}O_2$.[6]

Arthropod hemocyanin from *L.p.* has strikingly similar RR frequencies to molluscan hemocyanins and also to the μ-η^2:η^2 model compound in the 550-770 cm^{-1} region (Table 2). It even exhibits a possible $\nu_{as}(Cu_2O_2)$ B_u mode at 570 cm^{-1} that has not yet been observed in the other species. These findings provide strong evidence that the same μ-η^2:η^2 binding of O_2 occurs in the proteins from both phyla. However, significant differences in the RR spectra can be noted in the low-frequency region, implying that there are differences in ligand identity or coordination geometry. Most striking are the intensity decreases at 224, 265, and 313 cm^{-1} and the intensity increase at 286 cm^{-1} in *L.p.* relative to *O.d.* and *B.c.* Hcs (Figure 5). Since RR intensities are responsive to changes in geometry in the electronic excited state and can be influenced by the protein environment, these intensity changes are difficult to interpret but do suggest a change in ligand field.

Molluscan Hc is believed to have only five His ligands, with the sixth coordination site being occupied by a water molecule or a different protein ligand or vacant.[32] The lack of any $H_2{}^{18}O$-sensitive modes in the low frequency region (Table 2) makes an aqua ligand less likely, but could also be due to the general lack of resonance enhancement of M-OH_2 modes. The presence of a different ligand would be expected to increase the number of vibrational modes in the low frequency region, but the RR spectrum of molluscan Hc shows no more peaks than in arthropod Hc

(Table 2, Figure 5). This points to the possibility of a vacant coordination site in molluscan Hc. Such a structure would also explain the observation that one of the two Cu atoms (presumably CuA) is more easily removed in molluscan hemocyanins.[30,32]

Conclusions

Oxygen Binding Site. In contrast to the iron-containing respiratory proteins hemoglobin and hemerythrin, the two oxygen atoms of the bound peroxide in the oxyhemocyanin are essentially equivalent. This was initially suggested by the observation of only a single $\nu(^{16}O\text{-}^{18}O)$ mode in mixed-isotope labeled *B.c.* Hc.[12] Cu-O stretching modes are more sensitive indicators of the peroxide environment. The present RR studies with UV excitation show only one $\nu_{as}(Cu_2\text{-}^{16}O^{18}O)$ mode in *O.d.* Hc. This proves that each of the oxygen atoms in molluscan Hc senses an equivalent copper environment and is, thus, consistent with a symmetric O_2^{2-} bridge between the two coppers.

The X-ray crystal structure of *Limulus* oxyhemocyanin revealed that the peroxide bridges the two Cu(II) ions in an $\eta^2:\eta^2$ geometry.[28] Considering the strikingly similar electronic[30] and RR spectroscopic properties exhibited by oxyhemocyanins from both arthropods and molluscs, it is very likely that they all have the same $\mu\text{-}\eta^2:\eta^2$ Cu_2-peroxo structure. Our observation of symmetric O_2 binding in molluscan Hc is consistent with a $\mu\text{-}\eta^2:\eta^2$ structure. The similar fundamental and overtone vibrational pattern for $\nu_{as}(Cu_2O_2)$ in molluscan and arthropodan Hc as well as the $\mu\text{-}\eta^2:\eta^2$ model compound strongly suggests that the molluscan Hc has the same $Cu(O_2)Cu$ geometry as arthropodan Hc.

Neither of the peroxide-related vibrational modes [i.e., ν(O-O) and $\nu_{as}(Cu_2O_2)$] is affected by D_2O exchange (Table 2). This observation suggests that the oxygen atoms of the bound peroxide are not hydrogen bonded either to the protein or to any other solvent-exchangeable groups in the oxygen binding pocket. These results are consistent with the X-ray crystal structure on hemocyanin from *P. interruptus* which

showed that the protein has mainly hydrophobic residues around its oxygen binding site.[25]

Histidine Ligands. The presence of His ligands in arthropod Hc has been well established by X-ray crystallographic studies.[25,28] In both deoxy and oxy states, each Cu atom is complexed by three conserved histidines in hemocyanin from *P. interruptus* and *L. polyphemus*. However, copper-histidine ligation in molluscan Hc and tyrosinase is less well understood. From the amino acid sequence identity among the CuB sites of arthropod Hc, molluscan Hc, and tyrosinase, it is almost certain that these three classes of proteins have the same CuB site involving three conserved histidine residues. On the other hand, molluscan Hc and tyrosinase lack the conserved CuA binding motif found in arthropodan Hc. Spectroscopic studies of the molluscan proteins suggest that each copper atom is ligated to two or three His. Comparisons of primary structures reveal two conserved His which could serve as ligands to CuA in both molluscan Hc and tyrosinase.[32-34] What, then, could be the third ligand to CuA? There are three possibilities: (i) a third His that is not conserved between molluscan Hc and tyrosinase, (ii) another residue that serves as the third ligand, or (iii) absence of a third ligand. Cysteinate and tyrosinate can be ruled out as ligands by the lack of any corresponding charge transfer bands in the absorption spectra. Other possible candidates include methionine, carboxylate, amide carbonyl, and H_2O.

As Figure 5 demonstrates, the molluscan Hcs from *Octopus* and *Busycon* exhibit almost identical Raman spectra in the Cu-His vibration region (100-400 cm^{-1}). Arthropod Hc from *Limulus* exhibits a similar set of vibrational modes, but with somewhat different frequencies and intensities. We are led to conclude that Hcs from the two phyla have different Cu-His ligation. Since CuB is almost certainly the same in both phyla, it is very likely that CuA in molluscan Hcs are complexed to only two His. Previously, it was found that, unlike arthropod Hc, one of the two coppers in molluscan Hc is removed much more easily than the second one.[30,48] This could be

rationalized if CuA is bound only by two His ligands while CuB has three.

The Raman peaks at 229, 270, and 314 cm^{-1} in *B.c.* Hc all appear to have significant Cu-N(His) stretching character (Table 2). The D_2O sensitivity (downshifts of 1 or 2 cm^{-1}) of these vibrations is attributed to the exchangeable protons of the coordinated imidazole rings. A terminal or bridging hydroxo ligand would also have a deuterium-sensitive ν(Cu-OH) vibration. However, in this case the frequency could be expected to be higher (>400 cm^{-1}) and the magnitude of the D_2O shift should be larger. Counting the (-OH) as a unit mass, a ν(Cu-OH) at 229, 270, or 314 cm^{-1} should downshift by 5, 6, and 7 cm^{-1}, respectively, in D_2O. Moreover, a ν(Cu-OH) should also show isotope dependence when the protein is prepared in $H_2{}^{18}O$, and that is clearly not the case (Table 2). In a hydroxo-bridged dinuclear copper complex, we identified ν_s(Cu-OH-Cu) at 462 cm^{-1} and observed -16 and -12 cm^{-1} shifts, respectively, in D_2O and $H_2{}^{18}O$ (Chapter 5). On the other hand, using the imidazole ring as a unit mass, ν[Cu-N(His)] vibrations at 229, 270, and 314 cm^{-1} are calculated to downshift -1 to -2 cm^{-1} (Table 4) which are fully consistent with the observed shifts.

Bridging Ligands in MetHc. The strongest evidence for a bridging ligand in metHc comes from the observation that metHc is EPR silent owing to antiferromagnetic coupling of the two Cu(II) ions.[5] X-ray studies of *P. interruptus* deoxyHc showed that there were no protein residues in the vicinity of the bridging position,[25] thus ruling out the earlier proposed tyrosinate bridge.[5] A smaller group such as an OH^- or a water molecule could still be a candidate. The putative bridge should have Cu-OX-Cu vibrational modes at about 200-600 cm^{-1}, and these modes should be sensitive to $H_2{}^{18}O$ exchange. In the present studies, we do not observe any Raman features in oxyHc which are sensitive to $H_2{}^{18}O$ exchange. It would be worthwhile to perform a similar $H_2{}^{18}O$ experiment with metHc to see if an exogenous bridging ligand may have been introduced during the oxidation process.

References

(1) (a) Oregon Graduate Institute of Science & Technology; (b) Princeton University; (c) College of the Holy Cross, Worcester, MA 01610; (d) University of Houston

(2) Van Holde, K.E., and Miller, K.I.(1982) *Q. Rev. Biophys.* **15**, 1-129

(3) Préaux, G., and Gielens, C. (1984) In *Copper Proteins and Copper Enzymes* (Lontie, R., Ed.), vol. II, pp. 160-198, CRC Press: Boca Raton, FL

(4) Freedman, T.B., Loehr, J.S., and Loehr, T.M.(1976) *J. Am. Chem. Soc.* **98**, 2809-2815

(5) Eickman, N.C., Himmelwright, R.S., and Solomon, E.I. (1979) *Proc. Natl. Acad. Sci. USA* **76,** 2094-2098

(6) Baldwin, M.J., Root, D.E., Pate, J.E., Fujisawa, K., Kitajima, N., and Solomon, E.I. (1992) *J. Am. Chem. Soc.* **114,** 10421-10431

(7) Ross, P.K., and Solomon, E.I. (1991) *J. Am. Chem. Soc.* **113**, 3246-3259

(8) Dooley, D.M., Scott, R.A., Ellinghaus, J., Solomon, E.I., and Gray, H.B. (1978) *Proc. Natl. Acad. Sci. USA.* **75,** 3019-3022

(9) Solomon, E.I. (1981) In *Copper Proteins* (Spiro, T.G., Ed.), pp. 41-108, Wiley, New York

(10) Loehr, T.M., and Shiemke, A.K. (1988) In *Biological Applications of Raman Spectroscopy* (Spiro, T.G., Ed.), vol. 3, pp. 439-490, Wiley: New York

(11) Larrabee, J.A., and Spiro, T.G. (1980) *J. Am. Chem. Soc.* **102,** 4217-4223

(12) Thamann, T.J., Loehr, J.S., and Loehr, T.M. (1977) *J. Am. Chem. Soc.* **99**, 4187-4189

(13) Tyeklár, Z., and Karlin, K.D. (1989) *Acc. Chem. Res.* **22,** 241-248

(14) Sorrell, T.N. (1989) *Tetrahedron* **45,** 3-70

(15) Kitajima, N. (1993) *Adv. Inorg. Chem.* **39,** 1-77

(16) Karlin, K.D., and Gultneh, Y. (1987) *Prog. Inorg. Chem.* **35**, 219-317

(17) (a) Karlin, K.D., Cruse, R.W., Gultneh, Y., Hayes, J.C., and Zubieta, J.

(1984) *J. Am. Chem. Soc.* **106,** 3372-3374; (b) Karlin, K.D., Cruse, R.W., Gultneh, Y., Farooq, A., Hayes, J.C., and Zubieta, J. (1987) *J. Am. Chem. Soc.* **109,** 2668-2679

(18) Pate, J.E., Cruse, R.W., Karlin, K.D., and Solomon, E.I. (1987) *J. Am. Chem. Soc.* **109,** 2624-2630

(19) Thompson, J.S. (1984) *J. Am. Chem. Soc.* **106,** 8308-8309

(20) (a) Karlin, K.D., Haka, M.S., Cruse, R.W., and Gultneh, Y. (1985) *J. Am. Chem. Soc.* **107**, 5828-5829; (b) Karlin, K.D., Haka, M.S., Cruse, R.W., Meyer, G.J., Farooq, A., Gultneh, Y., Hayes, J.C., and Zubieta, J. (1988) *J. Am. Chem. Soc.* **110**, 1196-1207

(21) Blackburn, N.J., Strange, R.W., Farooq, A., Haka, M.S., and Karlin, K.D. (1988) *J. Am. Chem. Soc.* **110**, 4263-4272

(22) Jacobson, R.R., Tyeklár, Z., Farooq, A., Karlin, K.D., Liu, S., and Zubieta, J. (1988) *J. Am. Chem. Soc.* **110**, 3690-3692

(23) (a) Kitajima, N., Fujisawa, K., Fujimoto, C., Moro-oka, Y., Hashimoto, S., Kitagawa, T., Toriumi, K., Tatsumi, K., and Nakamura, A. (1992) *J. Am. Chem. Soc.* **114,** 1277-1291; (b) Kitajima, N.; Fujisawa, K.; Moro-oka, Y.; Toriumi, K. (1989) *J. Am. Chem. Soc.* **111,** 8975-8976

(24) Baldwin, M.J., Ross, P.K., Pate, J.E., Tyeklar, Z., Karlin, K.D., and Solomon, E.I. (1991) *J. Am. Chem. Soc.* **113**, 8671-8679

(25) (a) Volbeda, A., and Hol, W.G.J. (1989) *J. Mol. Biol.* **209**, 249-279; (b) Gaykema, W.P.J., Volbeda, A., and Hol, W.G.J. (1986) *J. Mol. Biol.* **187**, 255-275; (c) Gaykema, W.P.J., Hol, W.G.J., Vereijken, J.M., Soeter, N.M., Bak, H.J., and Beintema, J.J. (1984) *Nature* **309,** 23-29

(26) Volbeda, A., Feiters, M.C., Vincent, M.G., Bouwman, E., Dobson, B., Kalk, K.H., Reedijk, J., and Hol, W.G.J. (1989) *Eur. J. Biochem.* **181,** 669-673

(27) Volbeda, A., and Hol, W.G.J. (1989) *J. Mol. Biol.* **206,** 531-546

(28) (a) Magnus, K.A., Ton-That, H., and Carpenter, J.E. (1993) in *Bioinorganic*

Chemistry of Copper (Karlin, K.D., and Tyeklár, Z., Eds.), pp143-150, Chapman and Hall, New York; (b) Magnus, K.A., personal communication

(29) (a) Linzen, B., Soeter, N.M., Riggs, A.F., Schneider, H.-J., Schartau, W., Moore, M.D., Yokota, E., Behrens, P.Q., Nakashima, H., Takagi, T., Nemoto, T., Vereijken, J.M., Bak, H.J., Beintema, J.J., Volbeda, A., Gaykema, W.P.J., and Hol, W.G.J. (1985) *Science* **229,** 519-524; (b) Bak, H.J., Neuteboom, B., Jeckel, P.A., Soeter, N.M., Vereijken, J.M., and Beintema, J.J. (1986) *FEBS Letters* **204,** 141-144

(30) Himmelwright, R.S., Eickman, N.C., LuBien, C.D., and Solomon, E.I. (1980) *J. Am. Chem. Soc.* **102,** 5378-5388

(31) (a) Brown, J.M., Powers, L., Kincaid, B., Larrabee, J.A., and Spiro, T.G. (1980) *J. Am. Chem. Soc.* **102,** 4210-4216; (b) Woolery, G.L., Powers, L., Winkler, M., Solomon, E.I., Spiro, T.G. (1984) *J. Am. Chem. Soc.* **106**, 86-92

(32) (a) Lang, W.H., and van Holde, K.E. (1991) *Proc. Natl. Acad. Sci. USA*, **88,** 244-248; (b) Lang, W.H. (1988) *Biochemistry* **27**, 7276-7282

(33) Lerch, K., Huber, M., Schneider, H.-J., Drexel, R., and Linzen, B. (1986) *J. Inorg. Biochem.* **26,** 213-217

(34) Huber, M., and Lerch, K. (1988) *Biochemistry* **27,** 5610-5615

(35) Jackman, M., Huber, M., and Lerch, K. (1989) *Highlights Mol. Biochem.* **1,** 281-290

(36) (a) Miller, K.I., and van Holde, K.E. (1982) *Comp. Biochem. Physiol.* **73B**, 1013-1018; (b) Miller, K.I., van Holde, K.E., Tourmadje, A., Johnson, W.C., Jr., and Larry, J. (1988) *Biochemistry* **27,** 7282-7288

(37) Brenowitz, M., Bonaventura, C., Bonaventura, J., and Gianazza, E. (1981) *Arch. Biochem. Biophys.* **210**, 748-761

(38) Loehr, T.M., and Sanders-Loehr, J. (1993) *Methods Enzymol.* **226**, 431-470

(39) Czernuszewicz, R.S., and Johnson, M.K. (1983) *Appl. Spectrosc.* **37**, 297-298

(40) Lord, R.C., and Yu, N.-T. (1970) *J. Mol. Biol.* **50**, 509-524

(41) Kurtz, D.M., Jr. (1977) *Ph.D. Dissertation*, Northwestern University

(42) Kurtz, D.M., Jr., Shriver, D.F., and Klotz, I.M. (1976) *J. Am. Chem. Soc.* **98**, 5033-5035

(43) Larrabee, J.A., Spiro, T.G., Ferris, N.S., Wooddruff, W.H., Maltese, W.A., and Kerr, M.S. (1977) *J. Am. Chem. Soc.* **99,** 1979-1980

(44) Clark, R.J.H., and Stewart, B. (1979) *Struct. Bonding (Berlin)*, **36,** 1-80

(45) Nakamoto, K. (1986) *Infrared and Raman Spectra of Inorganic and Coordination Compounds*, 4th Ed., Wiley, New York

(46) Fuhrer, H., Kartha, V.B., Kidd, K.G., Krueger, P.J., and Mantsch, H.H. (1976) *Computer Programs for Infrared Spectrophotometry* (National Research Council of Canada, Ottawa, ON), Vol. 5, Bull. No. 15

(47) Yachandra, V.K., Hare, J., Gewirth, A., Czernuszewicz, R.S., Kimura, T., Holm, R.H., and Spiro, T.G. (1983) *J. Am. Chem. Soc.* **105**, 6462-6468

(48) Himmelwright, R.S., Eickman, N.C., and Solomon, E.I. (1978) *Biochem. Biophys. Res. Commun.* **81,** 243-247

TABLE 1

Properties of μ-Peroxo Binuclear Cu(II) Complexes

Compound	UV-vis Spectrum[a]	ν(O-O) (cm^{-1})	Cu-Cu (Å)	Bridge Mode	Magnetism	Ref.
$\{[Cu(TEEN)]_2(O_2)(H_2O)\}^{2+}$	630(—)	825	—	—	EPR inactive	19
$[Cu_2(XYL\text{-}O\text{-})(O_2)]^{2+}$	385(2900), 505(6000), 610(sh)	803	3.3[b]	asymmetric η^1	—	17, 18
$[Cu_2(N_3)(O_2)]^{2+}$	365(15,000), 490(5250), 600(1200), >850(—)	—	3.2[b]	η^2:η^2 or η^1:η^1	EPR inactive	20
$[Cu_2(N_4)(O_2)]^{2+}$	360(15,000), 458(5000), 550(1200), 775(200)	—	3.4[b]	η^2:η^2 or η^1:η^1	Diamagnetic	20
$[Cu_2(N_5)(O_2)]^{2+}$	360(21,400), 423(3600), 520(1200), >600(—)	—	—	η^2:η^2 or η^1:η^1	EPR inactive	20
$[Cu_2(N_3OR)(O_2)]^{2+}$	350(20,000), 485(1400), 600(880), 875(sh)	—	3.3[b]	η^2:η^2 or η^1:η^1	Diamagnetic	15
$[Cu_2(TMPA)_2(O_2)]^{2+}$	435(1700), 524(11,300), 615(5800), 1035(160)	832	4.35	trans-η^1:η^1	Diamagnetic	22, 24
$[Cu(HB(3,5\text{-}Me_2pz)_3)]_2(O_2)$	338(20,800), 530(840)	731	—	—	Diamagnetic	23
$[Cu(HB(3,5\text{-}iPr_2pz)_3)]_2(O_2)$	349(21,000), 551(790)	741	3.56	η^2:η^2, coplanar	Diamagnetic	23
$[Cu(HB(3,5\text{-}Ph_2pz)_3)]_2(O_2)$	355(18,000), 542(1040)	759	—	—	Diamagnetic	23
Oxy-Hc	340(20,000), 580(1000)	744-752	3. 6	η^2:η^2, coplanar	Diamagnetic	15,28
Oxy-Tyr	345(18,000), 600(1200)	755	~3.6[b]	—	Diamagnetic	15

[a] λ_{max} in nm (ϵ in M^{-1} cm^{-1} per 2Cu).
[b] Estimated by EXAFS.

Table 2. Resonance Raman Spectra of Oxyhemocyanins and a Model Compound[a]

Octopus Hc[b]			*Busycon* Hc[c]					*Limulus* Hc[d]		μ-η^2:η^2 model[e]		Assignment[f]
ν	$\Delta^{18}O_2$	$\Delta^{16}O^{18}O$	ν	$\Delta^{18}O_2$	$\Delta^{65}Cu$	ΔD_2O	$\Delta H_2{}^{18}O$	ν	$\Delta^{18}O_2$	ν	$\Delta^{18}O_2$	
174	0		174		0	0	0	190				$\nu_s(Cu_2O_2)$
228	0		229		-2	-1	0	224				$\nu_{as}(Cu\text{-}N_a)$
237			240									$\nu_{as}(Cu_2O_2)$
270	0		270		-2	-1	0	265		284	0	$\nu_s(Cu\text{-}N_a)$
285			289					286				$\nu_{as}(Cu\text{-}N_e)$
294	0		293		-2	0	0	303				$\nu_{as}(Cu\text{-}N_e)$
314	0		314		-2	-2	0	313				$\nu_{as}(Cu\text{-}N_e)$
342	0		345		-1	-1	0	336				$\nu_s(Cu\text{-}N_e)$
								363				
542	-23	-13	547			0	0	543		572[g]	-23[g]	$\nu_{as}(Cu_2O_2)$
								570				$\nu_{as}(Cu_2O_2)$
749	-40	-19	749	-41		0	0	744	-39	763	-40	ν(O-O)
1085	-46		1093					1087		1144	-42	$2\nu_{as}(Cu_2O_2)$

(continued)

Table 2, continued:

[a]Frequency in cm^{-1}. Isotope shift (Δ) in presence of heavier isotope.

[b]*Octopus dofleini* Hc data were obtained on the Jarrell-Ash instrument at 15 K, except for the 750-cm^{-1} peak which was observed at 278 K. Isotope shifts relative to $^{16}O_2$ preparation.

[c]*Busycon canaliculatum* Hc. Data for $^{16}O_2/^{18}O_2$ at 298 K from Ref. 4. Data for $^{63}Cu/^{65}Cu$ obtained at 77 K (Spex). Data for H_2O/D_2O and $H_2O/H_2{}^{18}O$ obtained at 15 K (Jarrell-Ash) on samples cycled through the deoxy state.

[d]*Limulus polyphemus* Hc subunit II data obtained on Jarrell-Ash at 15 K, except for the 744-cm^{-1} peak at 278 K.

[e]Data for $[Cu(HB(3,5\text{-}Ph_2pz)_3)]_2(O_2)$ from Ref. 30.

[f]Major PED contributor to each mode from normal coordinate analysis. N_a = axial His; N_e = equatorial His.

[g]Calculated from $2\nu_{as}(Cu_2O_2)$.

Table 3. Data Used for Normal Mode Analysis

Bond[a]	Distance[b]	Force constant[c]
O-O	1.4	2.66
Cu-O	2.0	1.57
Cu-N_e	2.1	1.62
Cu-N_a	2.4	1.00
N_e-Cu-N_e		0.55
N_e-Cu-N_a		0.11
N_a-Cu-O		0.19
N_e-Cu-O		0.28
Cu-O_2-Cu		0.19

[a]N_e = equatorial His; N_a = axial His. Each His treated as an imidazole point mass of 67.

[b]Bond lengths in Å for *Limulus polyphemus* Hc at 2.4-Å resolution from Ref. 23.

[c]Stretching constants (k) for 2 atoms in mdyn/Å; bending constants (h) for 3 atoms in mdyn · Å/rad^2. (Data contributed by R. Fraczkiewicz and R. Czernuszewicz.)

Table 4. Calculated Frequencies and Isotope Shifts for Oxyhemocyanin[a]

Hc		$\Delta^{18}O_2$		$\Delta^{65}Cu$		ΔD		Potential energy distribution[b]	Assignment[c]
obs	calc	obs	calc	obs	calc	obs	calc		
174	163		0.0	0	0.3	0	2.0	Cu-O(37) + Cu-N_e(37) + Cu-N_a(15)	A_g
228	223	0	0.7	2	0.9	1	2.0	Cu-N_a(62) + Cu-N_e(21)	B_u
237	233		9.3		0.0		1.1	Cu-O(47) + Cu-N_e(34) + N_e-Cu-O(12)	A_u
270	267	0	0.0	2	2.2	1	1.0	Cu-N_a(60) + Cu-O(20)	A_g
285	283		0.7		1.6		1.9	Cu-N_e(107) + N_e-Cu-O(6)	B_g
294	293	0	0.6	2	2.0	0	1.5	Cu-N_e(72) + Cu-N_a(23) + N_e-Cu-N_e(6)	B_u
314	311	0	3.0	2	2.0	2	1.0	Cu-N_e(72) + Cu-O(30) + N_e-Cu-O(12)	A_u
342	355	0	0.0	1	3.0	1	0.9	Cu-N_e(60) + Cu-O(35)	A_g
542	550	23	29.8	0	0.3	0	0.0	Cu-O(99)	B_g
d	610		27.8		1.3		0.0	Cu-O(97)	B_u
749	750	39	42.7	0	0.0	0	0.0	O-O(100) + Cu-O(9)	A_g

(continued)

Table 4, continued:

[a]The NCA was performed by R. Fraczkiewicz and R. Czernuszewicz. Observed frequencies (in cm^{-1}) and isotope shifts from Table 2 (ν's and $^{16}O_2/^{18}O_2$ for *O.d.* Hc; $^{63}Cu/^{65}Cu$ and H_2O/D_2O for *B.c.* Hc). Calculated frequencies and isotope shifts based on normal coordinate analysis using data in Table 3. Input coordinates were from *L.p.* Hc, input frequencies from *O.d.* Hc.

[b]Calculated PED in %. 2-atom and 3-atom contributions are from stretching and bending vibrations, respectively. Cu-O, Cu-N_e, and Cu-N_a refer to motions of the Cu_2O_2, $Cu(N_e)_4$, and $(CuN_a)_2$ moieties, respectively.

[c]Based on C_{2h} point group symmetry.

[d]570 cm^{-1} in *L.p.* Hc.

Figure Legends

Figure 1. Active site structures for deoxy and oxy forms of arthropod hemocyanin. (A) DeoxyHc from *Panulirus interruptus* at 3.2-Å resolution, adapted from Ref. 24a. (B) OxyHc from *Limulus polyphemus* at 2.4-Å resolution, adapted from Ref. 23.

Figure 2. RR spectra of OxyHc from *Octopus dofleini*. (A) Hc in $^{16}O_2$. (B) Hc oxygenated with mixed isotope O_2 (0.4 $^{18}O_2$: 1.0 $^{16}O^{18}O$: 0.6 $^{16}O_2$ based on Raman spectrum of the gas). (C) Hc oxygenated with $^{18}O_2$ (99 atom %). Spectra were obtained with a Jarrell-Ash instrument on samples (4 mM in Cu) in sealed capillaries at 278 K using the following conditions for laser excitation (power), spectral resolution, scan rate, and repetitive scanning: (A) 530.9 nm (25 mW), 8 cm^{-1}, 1 $cm^{-1}s^{-1}$, 7 scans; (B) 514.5 nm (40 mW), 8 cm^{-1}, 0.5 $cm^{-1}s^{-1}$, 50 scans; (C) 514.5 nm (30 mW), 8 cm^{-1}, 1 $cm^{-1}s^{-1}$, 4 scans. Each spectrum was subjected to a 15-point Savitsky-Golay smoothing. Pr = protein mode.

Figure 3. RR spectra of oxyHc from *Octopus dofleini* (A), *Busycon canaliculatum* (B), and *Limulus polyphemus*, subunit II (C). Spectra were obtained with a Jarrell-Ash instrument using 350.7-nm excitation (30 mW) at 15 K and the following conditions for concentration (in Cu), spectral resolution, scan rate, and repetitive scanning: (A) 2.7 mM, 8 cm^{-1}, 0.5 $cm^{-1}s^{-1}$, 6 scans; (B) 5.3 mM, 8 cm^{-1}, 0.5 $cm^{-1}s^{-1}$, 8 scans; (C) 2 mM, 8 cm^{-1}, 0.5 $cm^{-1}s^{-1}$, 5 scans. The upper traces in (A) are for Hc oxygenated with $^{18}O_2$. All spectra were subjected to a 15-point Savitsky-Golay smoothing. P = plasma line, Pr = protein Phe ring mode at 1004 cm^{-1} and C-N bend at 1109 cm^{-1}.[38]

Figure 4. ν_{as} (Cu_2O_2) vibrations in Hc from *Octopus dofleini* with (A) $^{16}O_2$, (B) and (D) mixed isotope O_2 containing $^{18}O_2$, $^{16}O^{18}O$, and $^{16}O_2$ (0.4:1.0:0.6), and (C) $^{18}O_2$. Spectra were obtained with a Jarrell-Ash instrument using 350.7-nm excitation (18 mW) at 90 K with a spectral resolution of 12 cm^{-1} and scan rate of 0.5 $cm^{-1}s^{-1}$. Spectra (A), (B) and (D), and (C) are signal average of 8, 25, and 8 repetitive scans, respectively, and each was subjected to a 25-point smoothing. (E) Simulated RR spectrum with three components at 519, 529, and 542 cm^{-1} using a constant width at half-height of 17.5 cm^{-1} and an intensity ratio of 0.6:1.0:0.7. (F) Simulated RR spectrum for an asymmetric peroxide with four components at 520, 522, 540, and 542 cm^{-1} using a width at half-height of 17.5 cm^{-1} and an intensity ratio of 0.6:0.5:0.5:0.7.

Figure 5. Low-frequency RR spectra of oxyHc from (A) *O. dofleini*, (B) *B. canaliculatum*, and (C) *L. polyphenus*, subunit II. Spectral conditions and protein concentrations as in Figure 3 except that the spectral resolution and repetitive scanning in (A) are 6 cm^{-1}, 4 scans and in (C) are 5 cm^{-1}, 10 scans, respectively. Each spectrum was subjected to a 9-point Savitsky-Golay smoothing.

Figure 6. RR spectra of oxyHc from *B. canaliculatum* reconstituted with ^{63}Cu or ^{65}Cu. Hc samples (2-4 mM in Cu) were in 0.026 M sodium borate, 0.5 M sodium cacodylate (pH 8.5) at 77 K. Spectra were obtained on a Spex instrument using 356.4-nm excitation (50 mW), 10-cm^{-1} slit width, 2 seconds counting per 0.5-cm^{-1} increment, and 10 scans. (Data contributed by L. Nestor and T. G. Spiro.)

Figure 7. RR spectra of oxyHc from *B. canaliculatum* incubated in H_2O or D_2O. Hc samples (2-4 mM in Cu) were in 0.05 M sodium carbonate, 0.5 M

sodium cacodylate (pH 9.8) and 50% glycerol. Spectral conditions as in Figure 6, except for a 5-cm^{-1} slit width. (Data contributed by L. Nestor and T. G. Spiro.)

Figure 8. Eigenvectors for normal modes involving Cu-O stretching in a μ-η_2:η_2 Cu_2O_2 moiety. Calculated frequency for major contribution of each mode from Table 4.

A

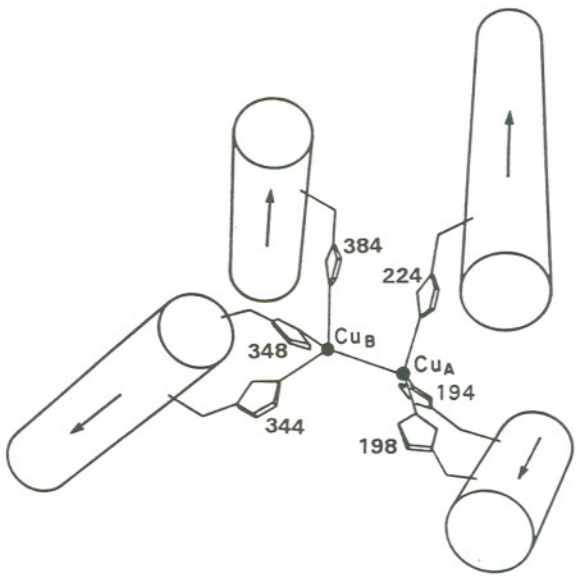
384
224
348
Cu B
Cu A
194
344
198

B

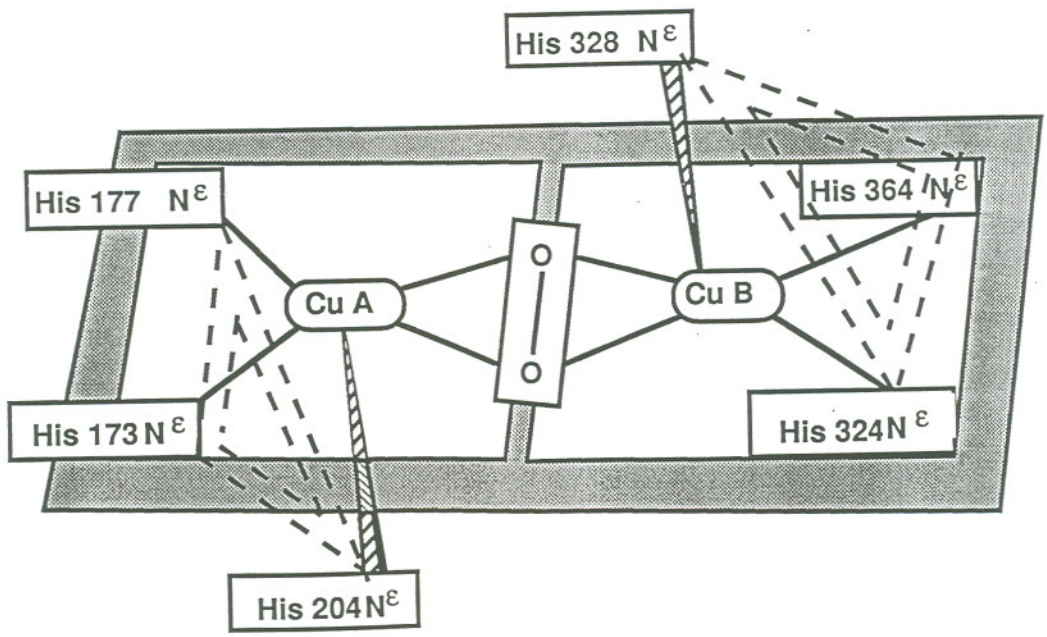
His 328 Nε
His 177 Nε
His 364 Nε
Cu A
Cu B
His 173 Nε
His 324 Nε
His 204 Nε

Figure 1

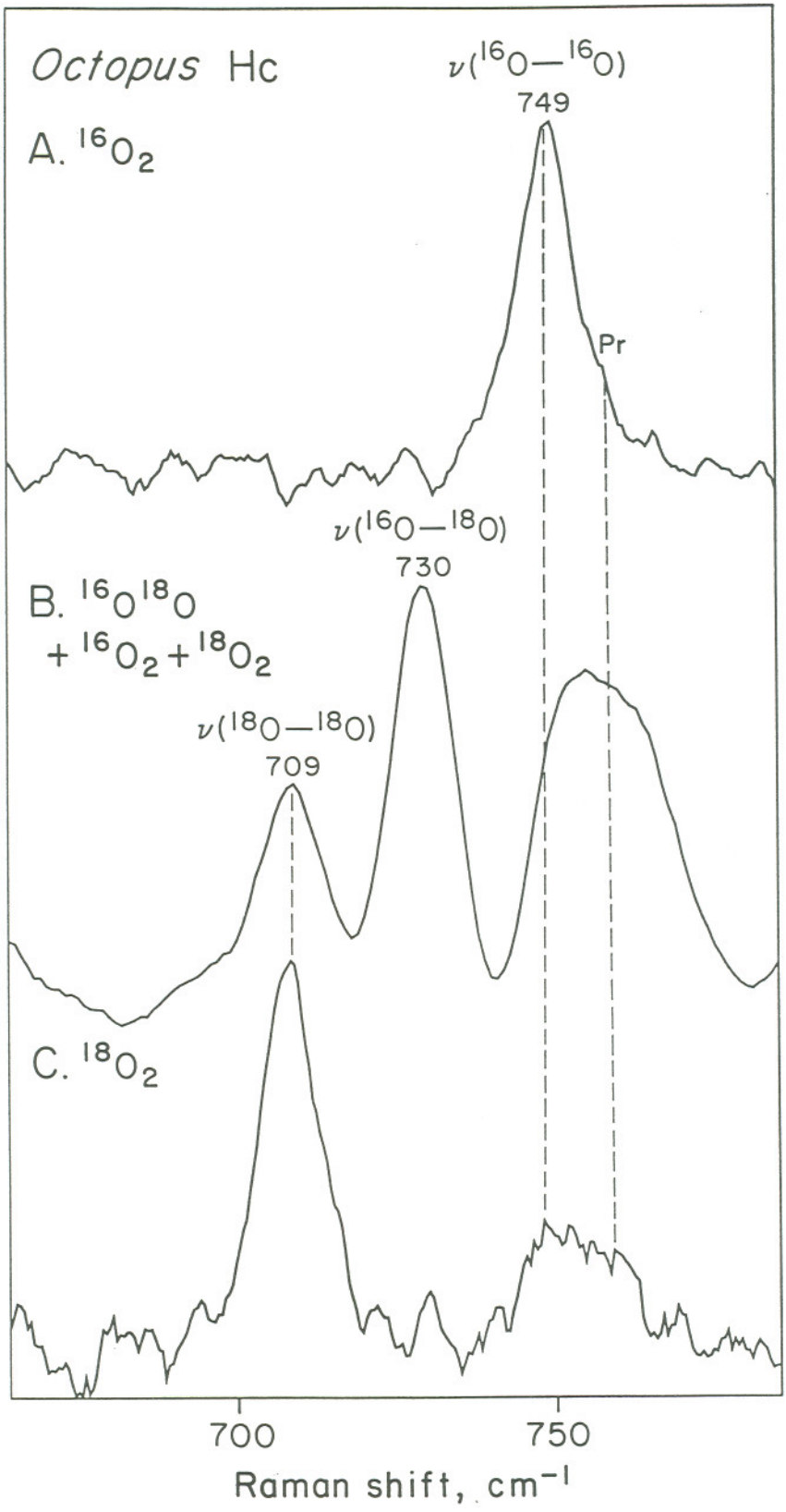
Octopus Hc
A. $^{16}O_2$
$\nu(^{16}O-^{16}O)$
749
Pr
$\nu(^{16}O-^{18}O)$
730
B. $^{16}O^{18}O$
$+ ^{16}O_2 + ^{18}O_2$
$\nu(^{18}O-^{18}O)$
709
C. $^{18}O_2$
700
750
Raman shift, cm^{-1}

Figure 2

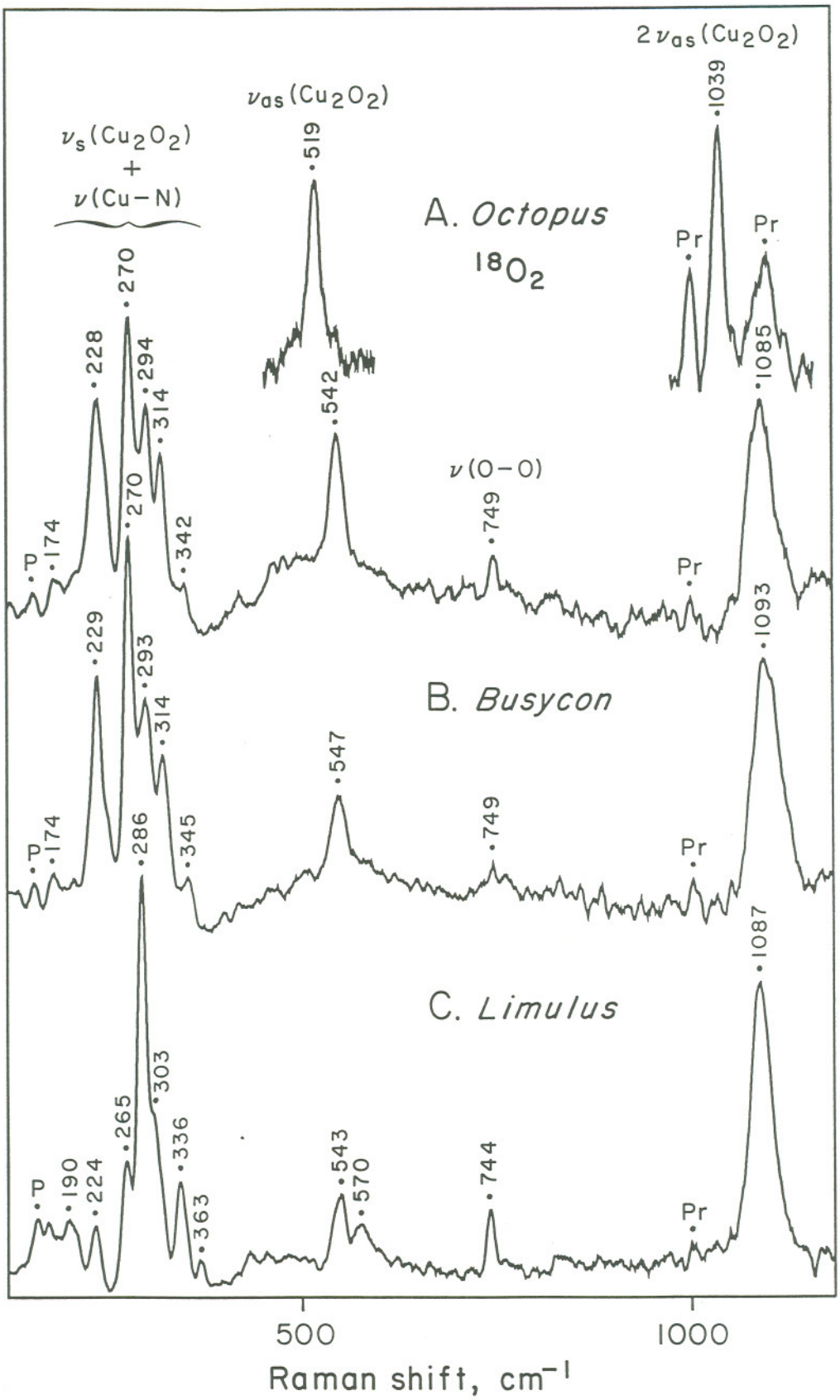
$2\nu_{as}(Cu_2O_2)$
1039
$\nu_{as}(Cu_2O_2)$
519
$\nu_s(Cu_2O_2)$ + $\nu(Cu-N)$
A. *Octopus*
$^{18}O_2$
Pr
Pr
228
270
294
314
542
1085
$\nu(O-O)$
749
P
174
270
342
Pr
1093
229
293
314
B. *Busycon*
547
P
174
286
345
749
Pr
1087
C. *Limulus*
303
265
336
543
570
744
P
190
224
363
Pr
500
1000
Raman shift, cm^{-1}

Figure 3

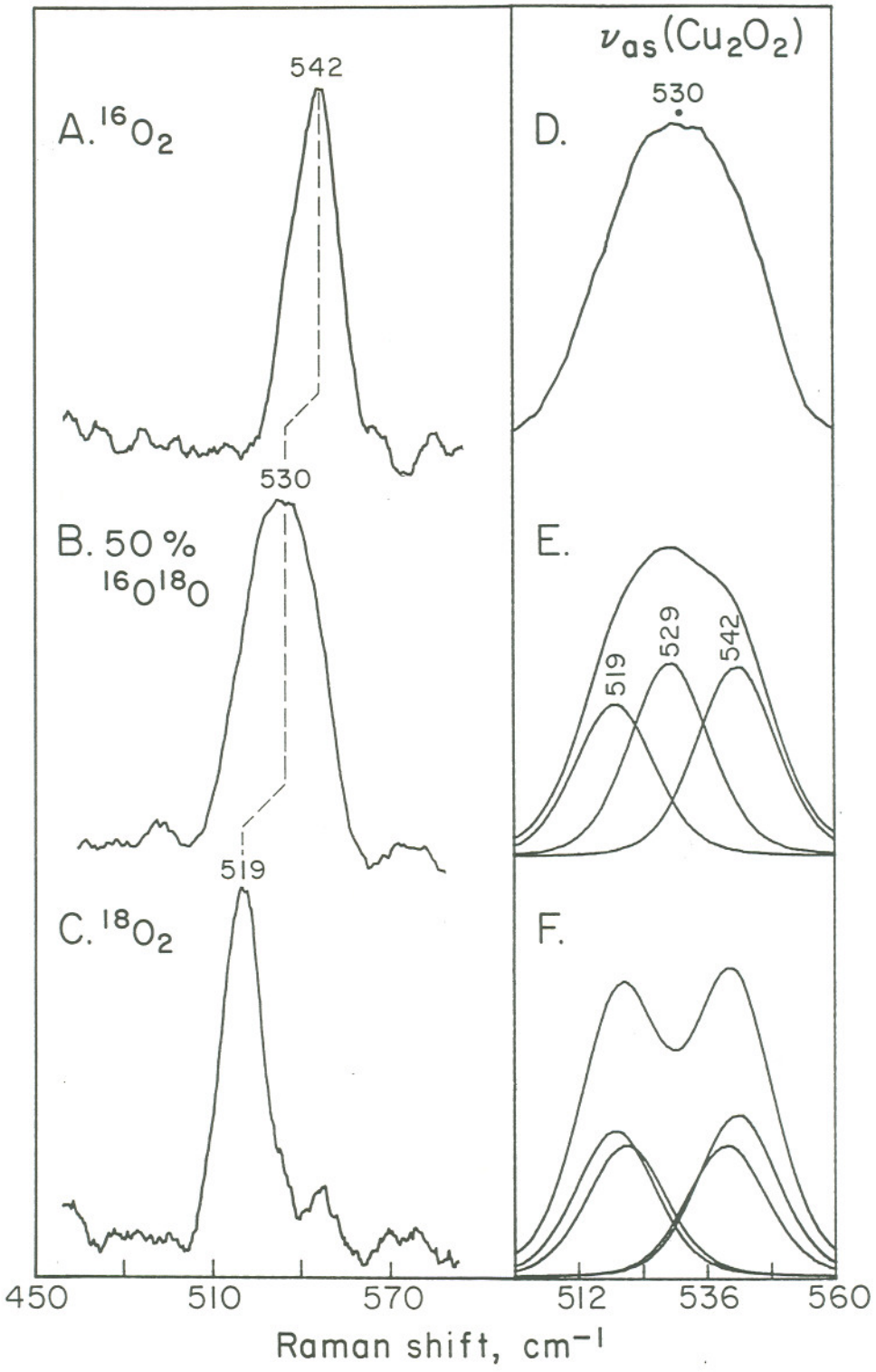
$\nu_{as}(Cu_2O_2)$
542
A. $^{16}O_2$
530
D.
530
B. 50 %
$^{16}O^{18}O$
E.
519
529
542
519
C. $^{18}O_2$
F.
450
510
570
512
536
560
Raman shift, cm^{-1}

Figure 4

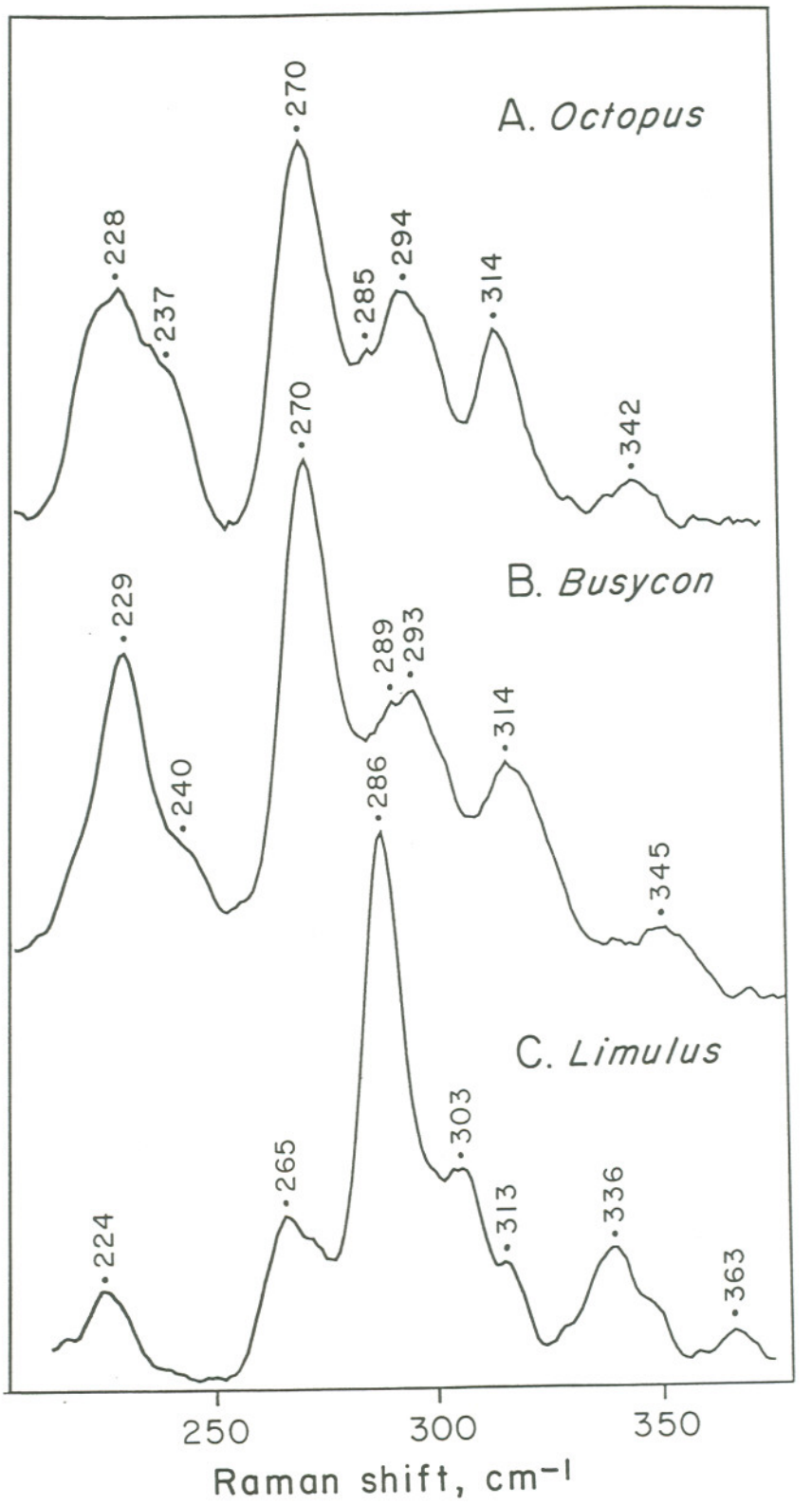
A. Octopus
228
237
270
285
294
314
342
B. Busycon
229
240
270
289
293
314
345
C. Limulus
224
265
286
303
313
336
363
250
300
350
Raman shift, cm⁻¹

Figure 5

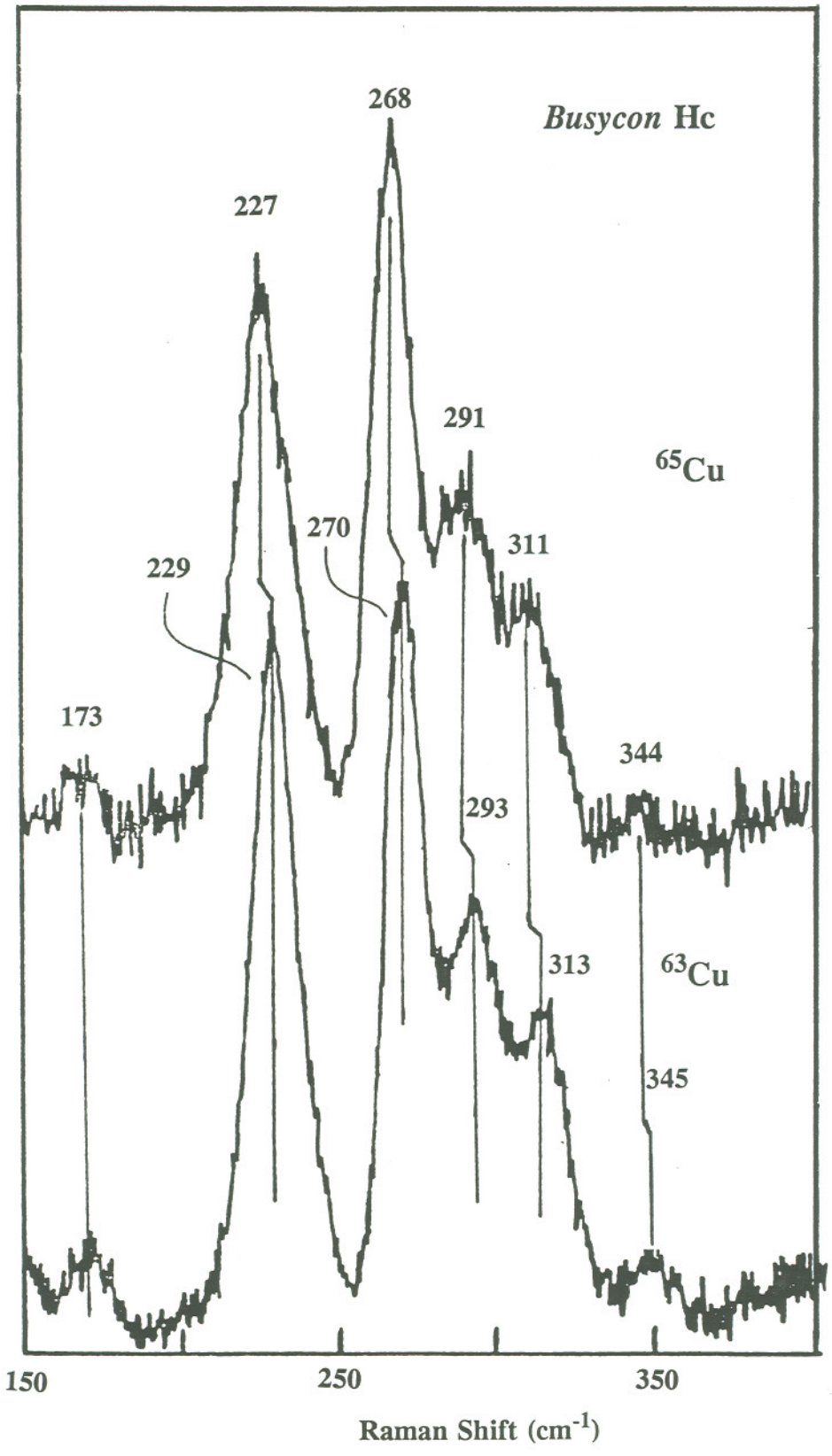
Busycon Hc
268
227
291
65Cu
270
311
229
173
344
293
313
63Cu
345
150
250
350
Raman Shift (cm-1)

Figure 6

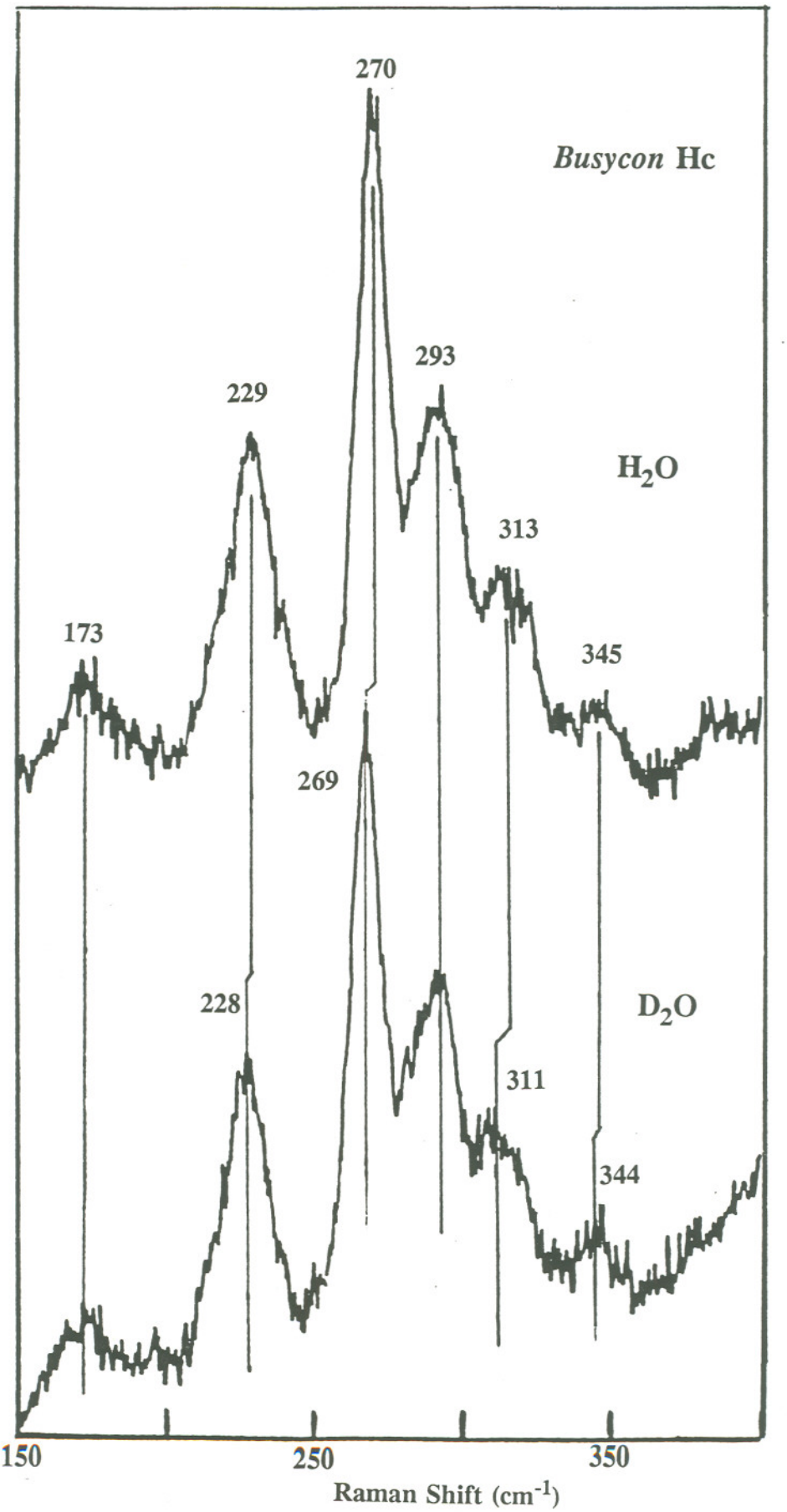
270
Busycon Hc
293
229
H2O
313
173
345
269
228
D2O
311
344
150
250
350
Raman Shift (cm-1)

Figure 7

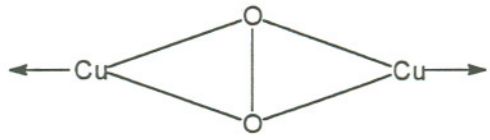

A_g (174 cm^{-1})

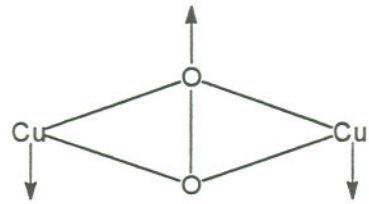

A_u (237 cm^{-1})

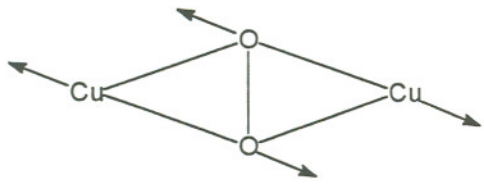

B_g (550 cm^{-1})

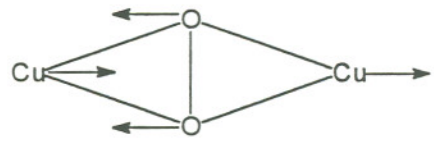

B_u (610 cm^{-1})

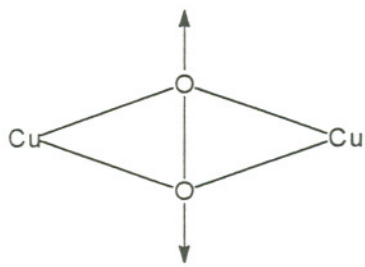

A_g (750 cm^{-1})

Figure 8

CHAPTER V

VIBRATIONAL SPECTROSCOPY STUDIES OF A HYDROXO-BRIDGED DINUCLEAR COPPER COMPLEX, A POTENTIAL MODEL FOR MULTI-COPPER PROTEINS

Jinshu Ling,[1a] Amjad Farooq,[1b] Kenneth D. Karlin,[1b]
Thomas M. Loehr,[1a] and Joann Sanders-Loehr[1a]

As published in *Inorganic Chemistry*, 1992, **31**, 2552-2556

Abstract

The copper complex $[Cu_2(XYL\text{-}O\text{-})(OH)]^{2+}$, XYL = *m*-xylene connected to two bis[2-(2-pyridyl)ethyl]amine ligands, serves as a potential model for the dinuclear copper sites in hemocyanin, tyrosinase, and the multi-copper oxidases. Resonance Raman (RR) and infrared spectra of the complex reveal a ν_s(Cu-OH-Cu) mode at 465 cm^{-1} and a ν_{as}(Cu-OR-Cu) mode at 603 cm^{-1}. These represent the first such modes to be definitively identified by isotopic shifts and polarization behavior. These two vibrational modes have RR enhancement maxima at 430 and 460 nm, respectively, indicating that they are associated with different phenolate → Cu charge transfer bands. Since no RR enhancement of ν_s(Cu-OH-Cu) was observed for the homologous μ-alkoxo, μ-OH complex, it appears that coupling to a chromophoric ligand such as phenolate may be important for the observation of M-OH vibrations in the RR spectra of such systems.

Introduction

A number of copper proteins contain EPR-silent, antiferromagnetically coupled Cu(II) ions.[2-4] These proteins include hemocyanin, the respiratory protein of mollusks and arthropods, and tyrosinase, a monooxygenase. Coupled copper sites are also found in multi-copper oxidases such as laccase, ceruloplasmin, and ascorbate oxidase. In all of these proteins, the dinuclear copper sites appear to be directly involved in reactions with O_2.

Extensive chemical and spectroscopic comparisons of the hemocyanins and tyrosinases indicate that these proteins have similar dinuclear copper sites.[4] In the X-ray crystal structure of *Panulirus interruptus* deoxyhemocyanin, each Cu(I) is ligated to three histidines.[5] Resonance Raman spectroscopy of oxyhemocyanin has revealed that the dioxygen is bound as a symmetrical peroxide bridging the two copper ions,[6] and a similar structure is likely for oxytyrosinase.[7] Although recent modelling studies demonstrate that a single bridging peroxide could be responsible for

the strong antiferromagnetic coupling of the oxy-proteins,[8,9] it is also possible that an additional bridging group is present at the Cu(II) sites in these proteins.[4] In particular, methemocyanin (which does not react with O_2) appears to have a pH-sensitive, ionizable group coupling the two Cu(II) ions.[10] The X-ray data on deoxyhemocyanin exclude tyrosinate or other amino acids as the bridge between the two Cu(I) atoms, but the existence of a solvent-derived bridging ligand such as hydroxo or aqua cannot be ruled out at the present resolution of 3.2 Å.[5]

In the X-ray crystal structure of ascorbate oxidase,[11] each subunit has a type 1 (blue) copper site well-separated from a trinuclear copper cluster. The trinuclear cluster is composed of a type 2 copper (normal EPR) with two His and one aqua ligand and a spin-paired dimer with three His coordinated to each Cu. The X-ray refinement suggests that the dimer has two bridging O^{2-} or OH^- groups, one of which is also coordinated to the third Cu of the cluster.[12] Laccase and ceruloplasmin also contain all three types of copper sites and have homologous primary structures to ascorbate oxidase in the C-terminal part which contains ligand binding sites for the three types of copper atoms.[12]

This paper reports vibrational spectroscopic studies of a model complex for the dinuclear coupled copper site. This dinuclear cupric compound contains hydroxo (μ-OH) and phenoxo (μ-OR) bridges between the two Cu(II) atoms, with the μ-OR group being part of a dinucleating ligand (Scheme 1). Both the hydroxo and phenoxo oxygen atoms were originally incorporated into the compound by reaction with molecular oxygen.[13] However, only the hydroxo oxygen is exchangeable with water. This makes it possible to investigate Raman and IR spectra of the complex with ^{18}O in either position. With isotope studies, we assign a ν(Cu-OH-Cu) mode at 465 cm^{-1} and a ν(Cu-OR-Cu) mode at 603 cm^{-1}. Raman polarization studies and IR absorption studies allow us to further assign them as symmetric and asymmetric vibrations, respectively.

Experimental Section

The μ-hydroxo, μ-phenoxo dinuclear-copper complex $[Cu_2(XYL\text{-}O\text{-})(OH)](PF_6)_2$ was synthesized by the addition of O_2 to the dicopper(I) complex $[Cu_2(XYL)](PF_6)_2$, as described previously[13] (Scheme 1).

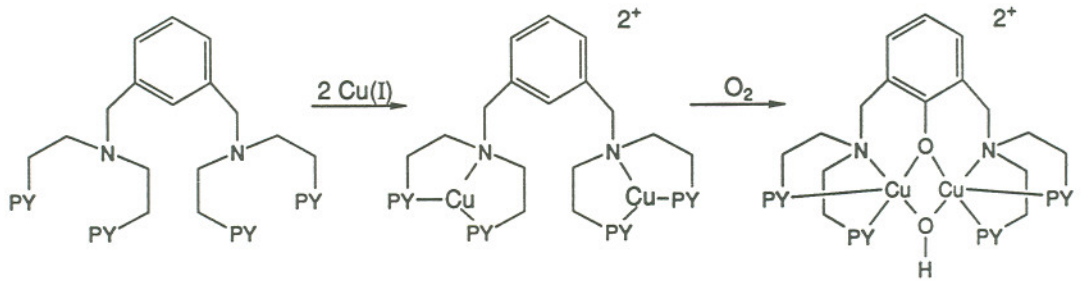

XYL ligand, PY = 2-pyridyl $[Cu_2(XYL)]^{2+}$ $[Cu_2(XYL\text{-}O)(OH)]^{2+}$

Scheme 1

After precipitation with dry diethyl ether, the compound was recrystallized twice from wet CH_2Cl_2:ether (1:3). A μ-^{18}OR complex $[Cu_2(XYL\text{-}^{18}O\text{-})(OH)]^{2+}$ was synthesized using $^{18}O_2$ instead of $^{16}O_2$ in the process. A μ-^{18}OH complex $[Cu_2(XYL\text{-}O\text{-})(^{18}OH)]^{2+}$ and a μ-OD complex $[Cu_2(XYL\text{-}O\text{-})(OD)]^{2+}$ were prepared by adding 1% $H_2{}^{18}O$ and 1% D_2O, respectively, to CH_3CN solutions of the μ-OR complex $[Cu_2(XYL\text{-}O\text{-})(OH)]^{2+}$, sealing in capillaries, and equilibrating for 1 to 2 h prior to measuring the Raman spectra. For IR spectra, these samples were evaporated to dryness on NaCl plates under argon and examined in an N_2-purged instrument.

Infrared spectra were recorded on a Perkin-Elmer 1800 FT-IR spectrophotometer connected to a Perkin-Elmer 7500 Professional Computer. Raman spectra were recorded either on a computerized Jarrell-Ash spectrophotometer equipped with a cooled RCA C31034 photomultiplier tube and an ORTEC model 9302 amplifier-discriminator or a Dilor Z-24 spectrophotometer having a cooled Hamamatsu 943-02

PMT. Excitation sources were Spectra-Physics 164-05 (Ar) and 2025-11 (Kr) lasers. Raman spectra of solutions were obtained in a 90°-scattering geometry, whereas those for solid samples in an $\sim$150°-backscattering geometry using a spinning disk. Peak frequencies were corrected using indene as a standard and are accurate to ± 1 cm^{-1}.

Depolarization ratios of Raman features were measured in a 90° scattering geometry with the scattered light passing through an analyzer and a polarization scrambler placed ahead of the entrance slit. For each sample, two spectra were obtained sequentially under the same conditions except that one was with the polarization analyzer in the parallel (0°) and the other with the polarization analyzer in the perpendicular position (90°). The ò value of a specific peak was determined by the ratio of $I_{\perp}/I_{\parallel}$.

Results

Raman studies of the $[Cu_2(XYL\text{-}O\text{-})(OH)]^{2+}$ complex in the 1100- to 1700-cm^{-1} region have been reported previously and show a number of resonance-enhanced phenolate vibrational modes.[14] A ν(C-O) vibration at 1307 cm^{-1} was identified from the shift of -8 cm^{-1} for the ^{18}OR-substituted complex. Our Raman studies in this high frequency region with ^{18}OR-substituted sample gave similar results (Table I). In order to observe Cu-O-Cu vibrations, we conducted resonance Raman and infrared studies in the region below 1100 cm^{-1}. Although such vibrations are expected to occur between 200 and 600 cm^{-1},[15,16] no specific vibrations of Cu-OH-Cu or Cu-OR-Cu have been definitively identified in the literature. The $[Cu(XYL\text{-}O\text{-})(OH)]^{2+}$ complex has a two-fold axis of symmetry perpendicular to the Cu$\cdots$Cu axis.[13] Since the OH^- and OR^- bridging groups have markedly different chemical character, four vibrational modes are expected arising from symmetric and asymmetric motions of the Cu(μ-O)$_2$Cu core: ν_s(Cu-OH-Cu), ν_s(Cu-OR-Cu), ν_{as}(Cu-OH-Cu), and ν_{as}(Cu-OR-Cu). The resonance Raman spectrum (Figure 1A) exhibits a large number of features in the low frequency region which can be assigned to Cu-O-Cu and/or phenolate modes through the use of isotopic substitution and excitation

profiles.

Cu-OH-Cu Vibration. The bridging hydroxo group was exchanged with solvent by dissolving $[Cu_2(XYL\text{-}O\text{-})(OH)](PF_6)_2$ in CH_3CN containing 1% water. This treatment did not result in any structural change other than bridge replacement as evidenced by the constancy of the electronic spectra (in $CH_3CN \pm H_2O$) and the RR spectra (solid vs. CH_3CN solution). As can be seen in Figure 1, the 465-cm^{-1} peak of the μ-OH complex shifts to 453 cm^{-1} with $H_2{}^{18}O$ exchange and to 449 cm^{-1} with D_2O exchange. This peak is attributed to a Cu-OH-Cu vibrational mode. Although Figure 1 shows spectra restricted to the 400- to 700-cm^{-1} region, we also collected Raman data from 100 to 1100 cm^{-1} on solids and in CH_2Cl_2 and CD_3CN solutions, which would have revealed any modes obscured by the CH_3CN solvent peaks. Only the feature at 465 cm^{-1} showed sensitivity to D_2O and $H_2{}^{18}O$ isotope exchange.

To establish the symmetry of the 465-cm^{-1} Cu-OH-Cu vibrational mode, we determined the depolarization ratio of the Raman feature, and investigated the low-frequency FT-IR spectra. The former established that the 465-cm^{-1} peak is polarized ($\rho = 0.5$; Table I), and no corresponding absorption was observable in the IR spectrum (Figure 2). Examination of the ν(O-H) stretching region in the IR did reveal isotopic exchange from the decreased intensity at 3625 cm^{-1} upon ^{18}O substitution. These results support the assignment of the 465-cm^{-1} peak as the symmetric vibration of the Cu-OH-Cu moiety.

Cu-OR-Cu Vibration. Two Raman peaks in the low energy region are sensitive to ^{18}O substitution of the XYL ligand (Figure 3). Comparing RR spectra of μ-^{18}OR and μ-^{16}OR complexes, it can be seen that the 603-cm^{-1} peak of μ-^{16}OR complex shifts to 592 cm^{-1} and the 623-cm^{-1} peak shifts to 620 cm^{-1}. We assign the 603-cm^{-1} peak to a Cu-OR-Cu vibration on the basis of its -11-cm^{-1} isotopic shift. Previous studies on ferric phenoxo complexes show the existence of a phenolate ring mode near 630 cm^{-1}.[17] It is likely, therefore, that the 623-cm^{-1} peak of the $[Cu(XYL\text{-}O\text{-})(OH)]^{2+}$ complex is predominantly due to a phenolate ring vibration and that its -

3-cm^{-1} isotope shift arises from motion of the phenolate oxygen in this mode.

The 603- and the 623-cm^{-1} peaks also appear in the IR spectrum (Figure 2). On ^{18}O substitution into the XYL-O bridge, these peaks exhibit the same isotopic shifts that were seen in the Raman spectrum. (The fact that the 639-cm^{-1} is unshifted in Figure 2 indicates that its decrease in intensity in Figure 3B is merely a consequence of RR intensity borrowing from the 623-cm^{-1} peak.) The appearance of the 603-cm^{-1} Cu-OR-Cu mode in both Raman and IR spectra, as well as its depolarization ratio of 0.7 (Table I), suggest that it be assigned as ν_{as}(Cu-OR-Cu). In contrast, the 623-cm^{-1} peak has a much smaller isotope shift and is strongly polarized ($\rho = 0.3$). These results indicate that this phenolate ring vibration is a symmetric mode. As a further probe of the assignment of the 603-cm^{-1} band as an asymmetric Cu-OR-Cu vibration, we looked for the presence of the overtone of this frequency. In oxo-bridged dinuclear metal complexes, weak ν_{as}(M-O-M) modes are often accompanied by quite intense $2\nu_{as}$ overtones.[18] However, in the present case, we observed no Raman feature near 1206 cm^{-1} ($2\nu_{as}$) or 930 cm^{-1} ($2\nu_s$). The absence of distinct overtones indicates that Cu-OX-Cu modes are less susceptible to overtone progressions than M-O-M systems.

Raman Enhancement Profiles. The electronic absorption spectrum of the $[Cu_2(XYL\text{-}O\text{-})(OH)]^{2+}$ complex has an intense maximum at 375 nm and a broad shoulder at ~430 nm (Figure 4A). A comparison of the RR spectra obtained with different excitation wavelengths (Figures 1 and 3) reveals that ν_s(Cu-OH-Cu) is more strongly enhanced with higher energy excitation relative to ν_{as}(Cu-OR-Cu). To further investigate the nature of the electronic absorption bands, intensity enhancement profiles of the 465-cm^{-1} [ν_s(Cu-OH-Cu)], 592-cm^{-1} [ν_{as}(Cu-^{18}OR-Cu)], 620-cm^{-1} [ν(phenol(^{18}O)ate)] and 1302-cm^{-1} [ν(C-^{18}O)phenolate] modes were obtained relative to $\nu_1(NO_3^-)$ of $NaNO_3$ used as an internal standard (Figure 4B). It is clear that the three Raman features at 592, 620, and 1302 cm^{-1} share a similar profile with an enhancement maximum at ~460 nm. In contrast, the ν_s(Cu-OH-Cu) mode at 465 cm^{-1} belongs to a different chromophore with an enhancement maximum near 430 nm.

Although the Raman enhancement profiles in Figure 4B were obtained on a solid sample, similar enhancement behavior was observed for a solution sample with intensities quantitated relative to an acetonitrile solvent peak.

Based on the Raman enhancement behavior of the three phenolate modes in the $[Cu_2(XYL\text{-}O\text{-})(OH)]^{2+}$ complex, the 460-nm component under the broad shoulder in the absorption spectrum can reasonably be assigned to a phenolate → Cu(II) charge transfer (CT) band. This assignment is in agreement with Raman studies on several other phenoxo-bridged dinuclear Cu(II) complexes which indicate that the phenolate vibrational modes are more enhanced with blue excitation (457.9 nm) than with green excitation (514.5 nm).[14,15] Electronic spectral comparisons between phenoxo-bridged and mononuclear complexes have also suggested the presence of phenolate → Cu(II) CT bands between 445 and 465 nm in the dinuclear complexes.[19,20] However, many other phenoxo-bridged Cu(II) complexes exhibit an intense absorption between 360 and 390 nm,[15,19,21] similar to the major 375-nm band in the XYL-O complex. Although these absorption bands also have been attributed to phenolate → Cu CT, the lack of Raman enhancement of phenolate modes for the XYL-O complex in the 350-400-nm spectral range (Figure 4) makes such an assignment problematic. In ferric-phenolate complexes, Raman enhancement maxima have been observed to be red-shifted by 40 to 70 nm relative to the position of the phenolate → Fe(III) CT bands.[22] This raises the possibility that 375- and 430-nm absorptions are both phenolate → Cu(II) CT bands, giving rise to the Raman enhancement maxima at 430 and 460 nm, respectively.

Since the Cu-OH-Cu stretch is selectively enhanced near 430 nm, an alternative assignment for this spectral region could be to a hydroxo → Cu(II) CT. Such a suggestion has been made for alkoxo-bridged dicopper(II) complexes where the dinucleating ligand N3OH is derived from 2-hydroxypropane connected to two bis[2-(2-pyridyl)ethyl]amine groups.[23] The $[Cu_2(N3\text{-}O\text{-})(OH)]^{2+}$ and the $[Cu_2(N3\text{-}O\text{-})(OCH_3)]^{2+}$ complexes have their respective absorption maxima at 418 and 375 nm (ϵ = ~800 $M^{-1}cm^{-1}$). However, the Raman spectrum of the $[Cu_2(N3\text{-}O\text{-})(OH)]^{2+}$ complex obtained with 413-nm excitation gives no indication of an ^{18}O-dependent Cu-

OH-Cu mode. Furthermore, no spectral feature has a molar scattering intensity greater than 2 relative to $\nu_1(NO_3^-)$, whereas the RR peaks in the homologous XYL-O complex are enhanced 15- to 40-fold relative to nitrate (Figure 4).

A similar lack of resonance enhancement occurs with the di-μ-OH complex, $Cu_2(L_2)(OH)_2$, where L = hydrotris(3,5-diisopropyl-1-pyrazolyl)borate.[24] This compound is altogether lacking in electronic spectral features in the 300-500 nm region and no Raman peaks with molar scattering greater than 1 relative to nitrate are observed. Similarly, the $Cu_2(L_2)(^{18}OH)_2$ complex shows no isotope-dependent Cu-OH-Cu modes between 350 and 650 cm^{-1}. These results suggest that the relatively strong enhancement of ν_s(Cu-OH-Cu) in the $[Cu_2(XYL\text{-}O\text{-})(OH)]^{2+}$ complex derives from its association with an additional phenolate → Cu(II) CT band at 430 or 375 nm. Other probable phenolate modes such as the peaks at 491 and 557 cm^{-1} also show maximal enhancement near 430 nm (Figures 1, 3).

Discussion

Vibrational Assignments. In this report, we present the first definitive identification of Cu-OH-Cu and Cu-OR-Cu vibrations in a dinuclear copper complex by oxygen-isotope substitutions. Analogous M-O-M vibrations are well-known for oxo-bridged metal clusters in both metalloproteins and inorganic model complexes. Examples include Fe-O-Fe,[25] Ru-O-Ru, Os-O-Os, Re-O-Re, W-O-W, Cr-O-Cr, Sn-O-Sn and V-O-V.[16,26] However, data for hydroxo-bridged systems are far less extensive. Previous IR and Raman studies on hydroxo-bridged Pt, Co, Cr, and Cu complexes placed symmetric M-OH-M vibrations at 290 to 370 cm^{-1} (Raman)[16,27] and asymmetric M-OH-M vibrations at 480 to 580 cm^{-1} (IR),[16,28] but these assignments were not based upon ^{18}O-isotope shifts, and, thus, have remained unsubstantiated.

For the $[Cu_2(XYL\text{-}O\text{-})(OH)]^{2+}$ complex, we have observed two 3-atom vibrational modes, ν_s(Cu-OH-Cu) and ν_{as}(Cu-OR-Cu). From ^{18}O- and D-isotope data, these are distinct, localized vibrations with no indication of any coupling between them. Moreover, these modes have different Raman enhancement profiles, indicating

that they are associated with different chromophores. Since the Cu-O-Cu angles are known,[13] the expected ^{18}O-isotope shift of each ν(Cu-OX-Cu) can be calculated using secular equations.[29] For a Cu-OH-Cu angle of 104°, ν_s(Cu-OH-Cu) at 465 cm^{-1} is predicted to shift -18 cm^{-1} with μ-^{18}OH and -10 cm^{-1} with μ-OD (assuming that the μ-OH group behaves as a point mass). The observed shifts are -12 and -16 cm^{-1}, respectively, with the Δ^{18}O being anomalously small and the ΔD value being anomalously large. For the known Cu-OR-Cu angle of 102°, a ν_{as}(Cu-OR-Cu) at 603 cm^{-1} is predicted to shift by -28 cm^{-1} (considering only the oxygen atom of the phenolate), whereas a shift of only -11 cm^{-1} is observed.

The fact that the ^{18}OH and ^{18}OR shifts are smaller than expected can be explained if ν_s(Cu-OH-Cu) and ν_{as}(Cu-OR-Cu) are not pure, but mixed, vibrational modes. It is likely that ν_{as}(Cu-OR-Cu) at 603 cm^{-1} undergoes *kinematic* coupling with another phenolate mode. Previously, smaller-than-expected ^{18}O-isotopic shifts for ν(Fe-O) of mononuclear phenoxo iron complexes have also been ascribed to the coupling of the ν(Fe-$O_{phenolate}$) mode with a benzene ring mode.[30] The ν(C-$O_{phenolate}$) stretch at 1310 cm^{-1} in the $[Cu_2(XYL\text{-}O\text{-})(OH)]^{2+}$ complex is similarly not a pure vibrational mode as it shifts by only -8 cm^{-1} in ^{18}O (Table I) compared to a predicted value of -26 cm^{-1} (considering only C-O). This finding is in agreement with a normal coordinate analysis for the 2,4,6-trichlorophenolate complex of Cu(II) where the vibrational mode at 1316 cm^{-1} was calculated to have only 43% C-O stretching character.[31] In addition to such kinematic coupling, *vibronic* coupling of Cu-OR-Cu motions with the electronically active phenolate moiety provides a mechanism for resonance enhancement[32] of ν_{as}(Cu-OR-Cu). The failure to observe the ν_s(Cu-OR-Cu) mode in the Raman spectrum underlines the importance of appropriate coupling with the phenolate chromophore in order to achieve resonance enhancement.

The ν_s(Cu-OH-Cu) mode at 465 cm^{-1} may undergo kinematic coupling with the δ(Cu-O-H) bend,[33] as suggested by the large shift of -16 cm^{-1} with deuterium. Alternatively, ν_s(Cu-OH-Cu) could be coupled with a pyridine ring deformation mode such as that observed at 440 cm^{-1} in mononuclear Cu(II) pyridine complexes.[34] The

pyridine ligands in $[Cu_2(XYL\text{-}O\text{-})(OH)]^{2+}$ may also contribute to electron delocalization in the electronic excited state, thereby explaining the rather large Raman enhancement of the Cu-OH-Cu symmetric stretch. In a previous RR study of phenoxo-, hydroxo-bridged Cu(II) complexes in which the dinucleating ligands lacked aromatic nitrogens such as pyridine, no such strongly enhanced ν(Cu-OH-Cu) modes were detected.[15]

Applicability to Metalloproteins. The RR scattering intensity of the ν_s(Cu-OH-Cu) mode of the $[Cu_2(XYL\text{-}O\text{-})(OH)]^{2+}$ complex reaches a maximum value of 40 relative to a nitrate internal standard (Figure 4). Given typically available protein concentrations of $\leq$5 mM, a vibration with a relative scattering intensity of 40 would be just at the limit of being detectable by RR spectroscopy and, thus, could potentially be observed in a dinuclear copper protein. However, the failure to observe resonance-enhanced Cu-OH-Cu modes in a number of other dinuclear copper complexes that lack phenolate or pyridine ligands[15,23,24] suggests that the presence of **both** types of ligands may be important. For the multi-copper proteins of known structure, hemocyanin and ascorbate oxidase, histidine ligands abound and are likely to have similar vibronic properties to pyridine. However, there is no evidence for phenolate ligation of copper in these proteins. Based on our studies of the μ-OH-bridged copper complexes, we feel that it will be difficult to use Raman spectroscopy to detect bridging OH groups in these proteins.

Hydroxo-bridged dinuclear metal clusters are also of relevance to dinuclear iron proteins where they have been implicated in the mixed valence forms of hemerythrin, purple acid phosphatase, and methane monooxygenase.[35] The μ-oxo bridge that is found in the fully oxidized forms of the dinuclear iron proteins is readily detected by RR spectroscopy.[25] The oxo $\rightarrow$ Fe(III) CT transition is a dominant chromophore in the near-uv region and leads to strong enhancement of the ν_s(Fe-O-Fe) mode. However, no such chromophoric character exists in the corresponding hydroxo-bridged complexes. We have been unable to detect ν_s(Fe-OH-Fe) in the RR spectra of hydroxo-bridged diiron(III) complexes containing pyrazole[36]

or benzimidazole[37] ligands. We have observed an Fe-OH vibration in the RR spectrum of the dinuclear iron protein, purple acid phosphatase, that may arise from a bridging OH group.[38] Interestingly, this Fe-OH mode is resonance-enhanced via a phenolate → Fe(III) CT band. Therefore, it is likely that an additional strong chromophore such as that provided by a phenolate ligand is required in order to obtain RR spectra from hydroxo-bridged metal systems.

Acknowledgment. We are grateful to Dr. Nobumasa Kitajima for providing samples of the $Cu_2(L_2)(OH)_2$ complex,[24a] and Dr. Roman Czernuszewicz for many helpful discussions. This work was supported by grants from the National Institutes of Health, GM 18865 (T.M.L. and J.S.-L.) and GM 28962 (K.D.K.).

References

(1) (a) Oregon Graduate Institute; (b) Johns Hopkins University

(2) Solomon, E. I. In *Copper Proteins*; Spiro, T. G., Ed.; Wiley: New York, 1981; Chapter 2.

(3) Ochiai, E.-I. *Bioinorganic Chemistry*; Allyn and Bacon: Boston, 1977, pp 218-262.

(4) Solomon, E. I.; Penfield, K. W.; Wilcox, D. E. *Struct. Bonding (Berlin)* **1983**, 53, 1-57.

(5) (a) Gaykema, W. P. J.; Volbeda, A.; Hol, W. G. J. *J. Mol. Biol.* **1986**, *187*, 255-275. (b) Volbeda, A.; Hol. W. G. J. *J. Mol. Biol.* **1989**, *209*, 249-279.

(6) Loehr, T. M.; Shiemke, A. K. In *Biological Application of Raman Spectroscopy*; Spiro, T. G., Ed.; Wiley: New York, 1988; Vol. III, pp 439-490.

(7) Eickman, N. C.; Solomon, E. I.; Larrabee, J. A.; Spiro, T. G.; Lerch, K. *J. Am. Chem. Soc.* **1978**, *100*, 6529-6531.

(8) (a) Kitajima, N.; Fujisawa, K.; Moro-oka, Y. *J. Am. Chem. Soc.* **1989**, *111*, 8975-8976. (b) Jacobson, R. R.; Tyeklár, Z.; Farooq, A.; Karlin, K. D.; Liu, S.; Zubieta, J. *J. Am. Chem. Soc.* **1988**, *110*, 3690-3692. (c) Karlin, K. D.; Tyeklár, Z.; Farooq, A.; Jacobson, R. R.; Sinn, E.; Lee, D. W.; Bradshaw, J. E.; Wilson, L. *J. Inorg. Chim. Acta*, **1991**, *182*, 1-3.

(9) Ross, P. K.; Solomon, E. I. *J. Am. Chem. Soc.* **1991**, *113*, 3246-3259.

(10) Wilcox, D. E.; Long, J. R.; Solomon, E. I. *J. Am. Chem. Soc.* **1984**, *106*, 2186-2194.

(11) Messerschmidt, A.; Rossi, A.; Ladenstein, R.; Huber, R.; Bolognesi, M.; Gatti, G.; Marchesini, A.; Petruzzelli, R.; Finazzi-Agro, A. *J. Mol. Biol.* **1989**, *206*, 513-529.

(12) Messerschmidt, A.; Huber, R. *Eur. J. Biochem.* **1990**, *187*, 341-352.

(13) Karlin, K. D.; Hayes, J. C.; Gultneh, Y.; Cruse, R. W.; McKown, J. W.; Hutchinson, J. P.; Zubieta, J. *J. Am. Chem. Soc.* **1984**, *106*, 2121-2128.

(14) Pyrz, J. W.; Karlin, K. D.; Sorrell, T. N.; Vogel, G. C.; Que, L., Jr. *Inorg. Chem.* **1984**, *23*, 4581-4584.

(15) Lorösch, J.; Haase, W.; Huong, P. V. J. *Inorg. Biochem.* **1986**, *27*, 53-63.

(16) (a) Hewkin, D. J.; Griffith, W. P. *J. Chem. Soc. A* **1966**, 472-475. (b) McWhinnie, W. R. *J. Inorg. Nucl. Chem.* **1965**, *27*, 1063-1070.

(17) Carrano, C. J.; Carrano, M. W.; Sharma, K.; Backes, G.; Sanders-Loehr, J. *Inorg. Chem.* **1990**, *29*, 1865-1870.

(18) (a) Czernuszewicz, R. S.; Sheats, J. E.; Spiro, T. G. *Inorg. Chem.* **1987**, *26*, 2063-2067. (b) Lincoln, S. E.; Loehr, T. M. *Inorg. Chem.* **1990**, *29*, 1907-1915.

(19) Sorrell, T. N.; O'Connor, C. J.; Anderson, O. P.; Reibenspies, J. H. *J. Am. Chem. Soc.* **1985**, *107*, 4199-4206 and references therein.

(20) Karlin, K. D.; Cohen, B. I.; Hayes, J. C.; Farooq, A.; Zubieta, J. *Inorg. Chem.* **1987**, *26*, 147-153.

(21) Karlin, K. D.; Farooq, A.; Hayes, J. C.; Cohen, B. I.; Rowe, T. M.; Sinn,

E.; Zubieta, J. *Inorg. Chem.* **1987**, *26*, 1271-1280.

(22) (a) Pyrz, J. W.; Roe, A. L.; Stern, L. J.; Que, L., Jr., *J. Am. Chem. Soc.* **1985**, *107*, 614-620. (b) Que, L., Jr.; Heistand, R. H., II; Mayer, R.; Roe, A. L., *Biochemistry* **1980**, *19*, 2588-2593. (c) Que, L., Jr.; Epstein, R. M., *Biochemistry* **1981**, *20*, 2545-2549.

(23) Karlin, K. D.; Sanyal, I.; Farooq, A.; Jacobson, R. R.; Shaikh, S. N.; Zubieta, J. *Inorg. Chim. Acta* **1990**, *174*, 13-15.

(24) (a) Kitajima, N.; Fujisawa, K.; Moro-oka, Y. *Inorg. Chem.* **1990**, *29*, 357-358. (b) Kitajima, N.; Ling, J.; Loehr, T. M.; Sanders-Loehr, J., unpublished results.

(25) Sanders-Loehr, J.; Wheeler, W. D.; Shiemke, A. K.; Averill, B. A.; Loehr, T. M. *J. Am. Chem. Soc.* **1989**, *111*, 8084-8093.

(26) San Filippo, J., Jr. ; Fagan, P. J., Di Salvo, F. J. *Inorg. Chem.* **1977**, *16*, 1016-1021.

(27) Bulliner, P. A.; Spiro, T. G. *Inorg. Chem.* **1969**, *8*, 1023-1025.

(28) (a) Blyholder, G.; Ford, N. J. Phys. Chem. **1964**, *68*, 1496-1500. (b) Ferraro, J. R.; Walker, W. R. *Inorg. Chem.* **1965**, *4*, 1382-1386.

(29) Wing, R. M.; Callahan, K. P. *Inorg. Chem.* **1969**, *8*, 871-874.

(30) Pyrz, J. W.; Roe, A. L.; Stern, L. J.; Que, L., Jr. *J. Am. Chem. Soc.* **1985**, *107*, 614-620.

(31) Tomimatsu, Y.; Kint, S.; Scherer, J. R. *Biochemistry* **1976**, *15*, 4918-4924.

(32) Spiro, T. G.; Stein, P. *Ann. Rev. Phys. Chem.* **1977**, *28*, 501-521.

(33) Nakamoto, K. *Infrared and Raman Spectra of Inorganic Coordination Compounds*, Wiley: New York, 1986; Fourth Edition, pp. 230-231.

(34) Clark, R. J. H.; Williams, C. S. *Inorg. Chem.* **1965**, *4*, 350-358.

(35) Sanders-Loehr, J. In *Iron Carriers and Iron Proteins*; Loehr, T. M., Ed; VCH Publishers: New York, 1989, pp 375-466.

(36) Armstrong, W. H.; Lippard, S. J. *J. Am. Chem. Soc.* **1984**, *106*, 4632-4633.

(37) Ben-Hussein, A.; Gomez-Romero, P.; Morris, N. L.; Zafarullah, O.;

Jameson, G. B.; personal communication.

(38) Backes, G.; Ling, J.; Loehr, T. M.; David, S.; Que, L., Jr.; Crowder, M. W.; Averill, B. A.; Sanders-Loehr, J., unpublished results.

Table 1. Vibrational Spectroscopic Properties of the $[Cu_2(XYL\text{-}O)(OH)]^{2+}$ Complex

frequency (cm^{-1})[a]	spectroscopic activity	isotope shift (cm^{-1})[b]			Raman depolarization ratio (ρ)	Raman enhancement maximum (nm)	assignment
		ΔOD	Δ^{18}OH	Δ^{18}OR			
465	RR	-16	-12	0	0.5	430	ν_s (Cu-OH-Cu)
603	RR, IR	0	0	-11	0.7	460	ν_{as}(Cu-OR-Cu)
623	RR, IR	0	0	-3	0.3	460	δ(phenolate)
1310	RR, IR	n.d.	n.d.	-8	n.d.	460	ν(C-O)phenolate

[a]Frequencies from RR spectra of samples in acetonitrile. Similar values were observed in the IR spectra of solid samples in KBr pellets.

[b]Average of values obtained by RR and IR spectroscopy.

Figure Legends

Figure 1. Resonance Raman spectrum of $[Cu_2(XYL\text{-}O\text{-})(OH)](PF_6)_2$ in CH_3CN (1 mg/ml) containing (A) 1% $H_2{}^{16}O$, (B) 1% $H_2{}^{18}O$, and (C) 1% D_2O. Spectra were obtained at 273 K (ice bath) with 413.1 nm excitation (20 mW) using a spectral resolution of 8 cm^{-1}, scan rate of 1 cm^{-1}/s, and an average of 6 scans.

Figure 2. Infrared spectra of $[Cu_2(XYL\text{-}^{16}O\text{-})(OH)](PF_6)_2$ and $[Cu_2(XYL\text{-}^{18}O\text{-})(OH)](PF_6)_2$ in KBr pellets. Each spectrum is an average of 20 scans.

Figure 3. Resonance Raman spectra of $[Cu_2(XYL\text{-}^{16}O\text{-})(OH)](PF_6)_2$ and $[Cu_2(XYL\text{-}^{18}O\text{-})(OH)](PF_6)_2$ in CH_3CN (0.02 M). Spectra were obtained at room temperature with 457.9-nm radiation (25 mW) using a spectral resolution of 7.2 cm^{-1}, scan rate of 1 cm^{-1}/s, 3 s integration per point, and an average of 4 scans.

Figure 4. Resonance Raman enhancement profiles for the $[Cu_2(XYL\text{-}^{18}O\text{-})(OH)]^{2+}$ complex. (A) Absorption spectrum in CH_3CN. (B) Relative molar Raman scattering intensities. A solid sample of the μ-^{18}OR complex, $[Cu_2(XYL\text{-}^{18}O\text{-})\text{-}(OH)](PF_6)_2$, was mixed with a 3× excess of $NaNO_3$ and its Raman spectrum was obtained at a series of excitation wavelengths. The intensities (areas) of the peaks at 465, 592, 620, and 1302 cm^{-1} were determined relative to $\nu_1(NO_3^-)$ at 1055 cm^{-1} and corrected for differences in molar concentrations.

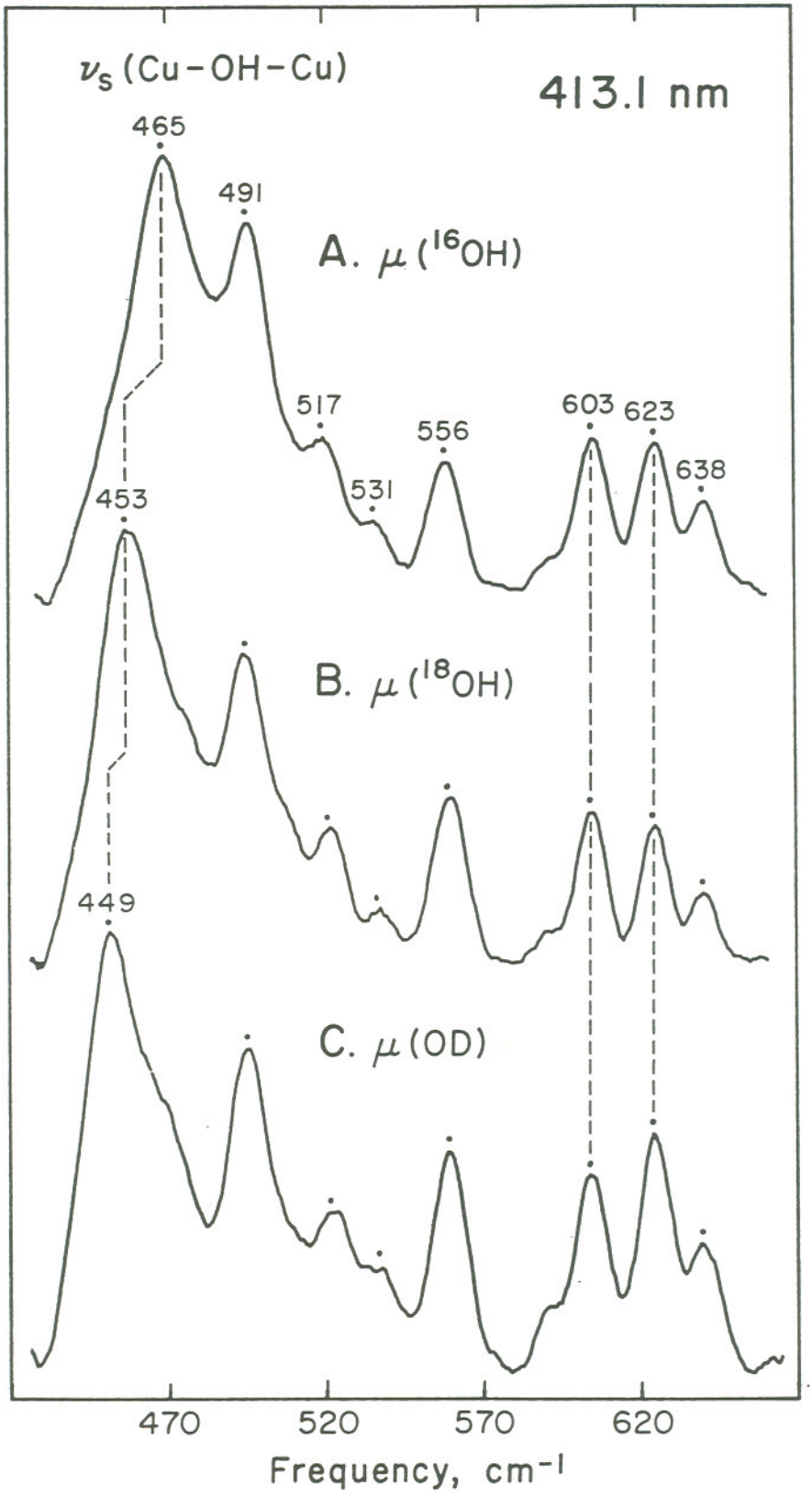
ν_s (Cu-OH-Cu)
413.1 nm
465
491
A. μ(^{16}OH)
517
603
623
556
638
531
453
B. μ(^{18}OH)
449
C. μ(OD)
470
520
570
620
Frequency, cm^{-1}

Figure 1

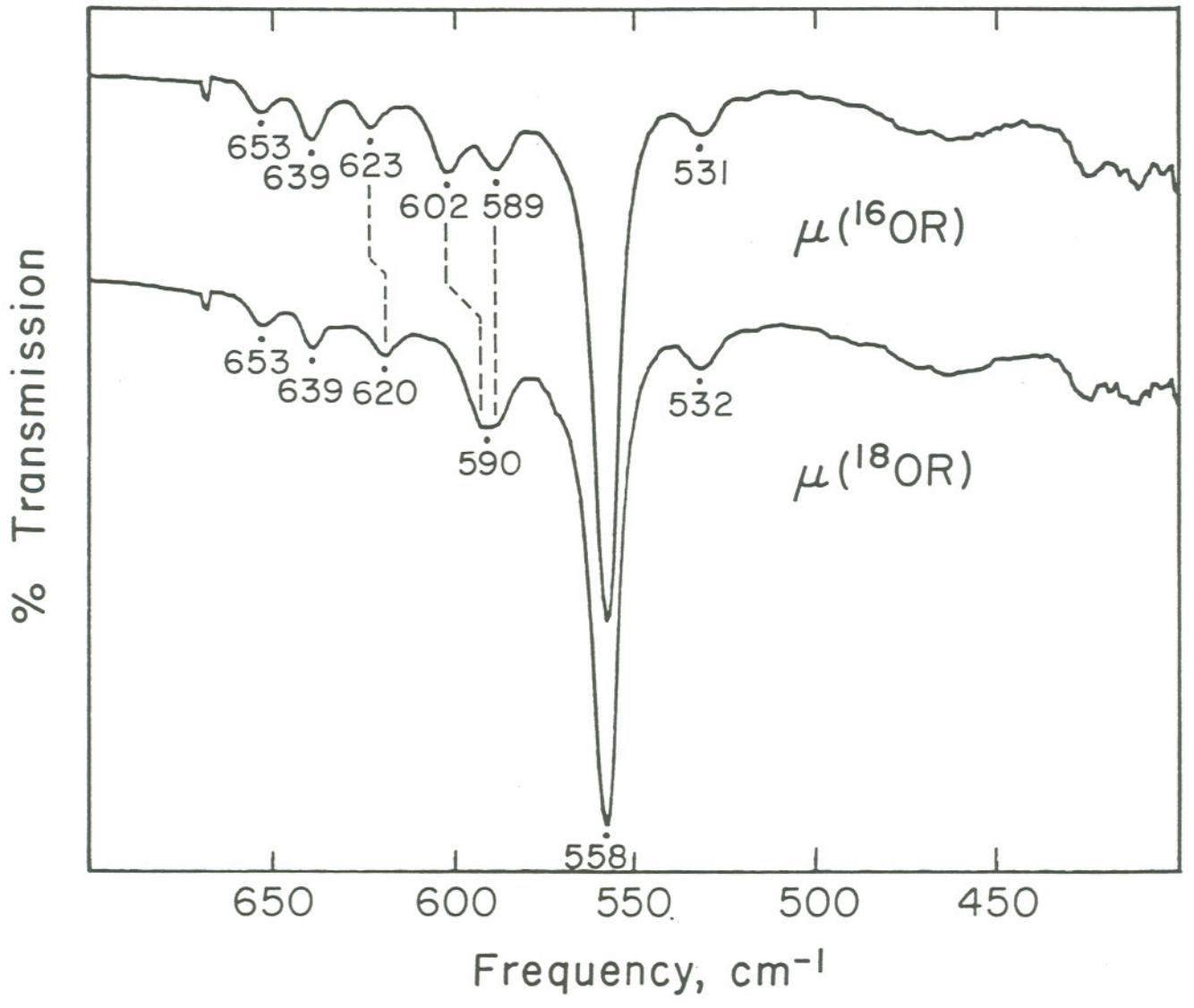
% Transmission
653
639
623
602
589
531
μ(16OR)
653
639
620
590
532
μ(18OR)
558
650
600
550
500
450
Frequency, cm-1

Figure 2

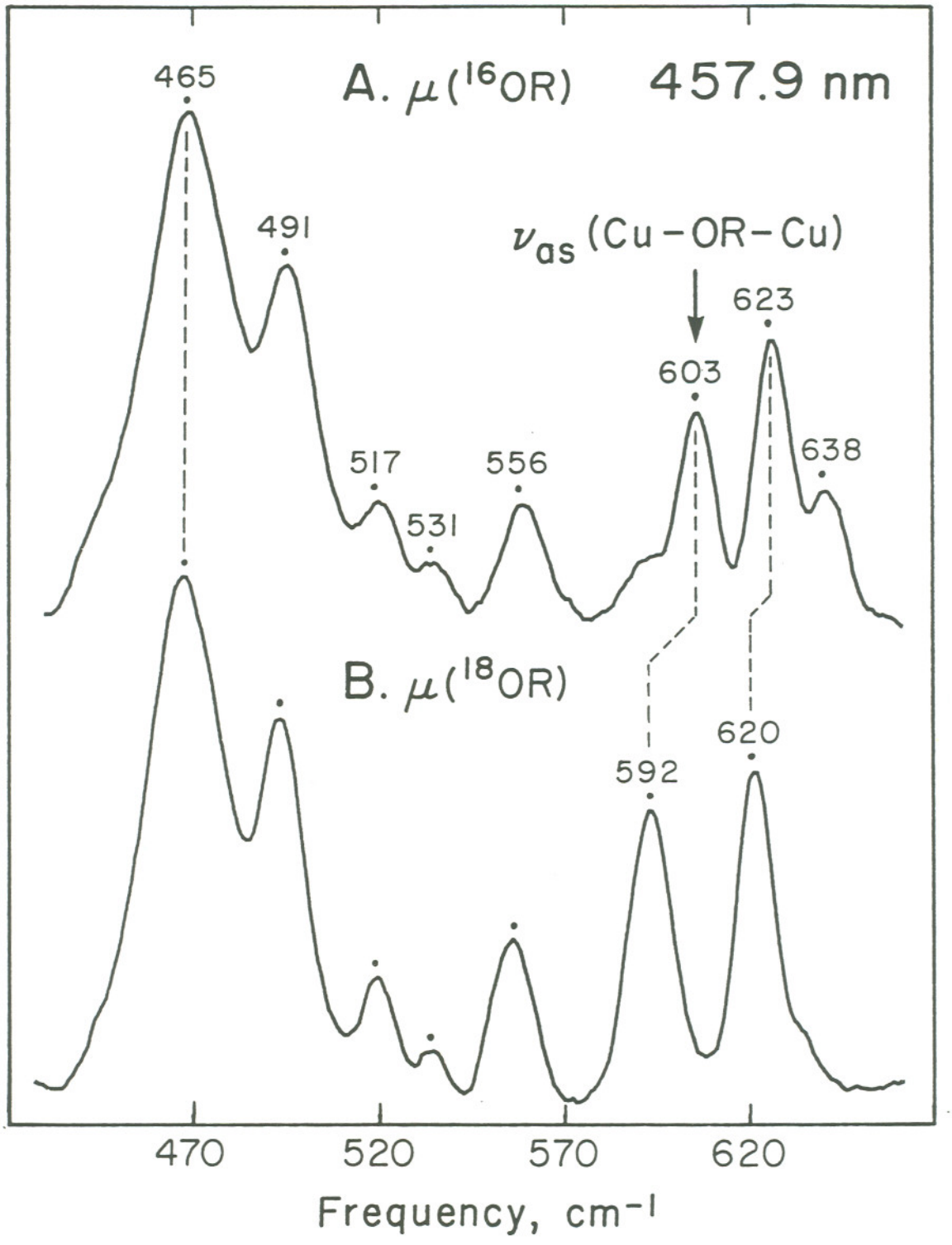
465
A. μ(16OR) 457.9 nm
491
νas (Cu-OR-Cu)
623
603
638
517
556
531
B. μ(18OR)
620
592
470
520
570
620
Frequency, cm-1

Figure 3

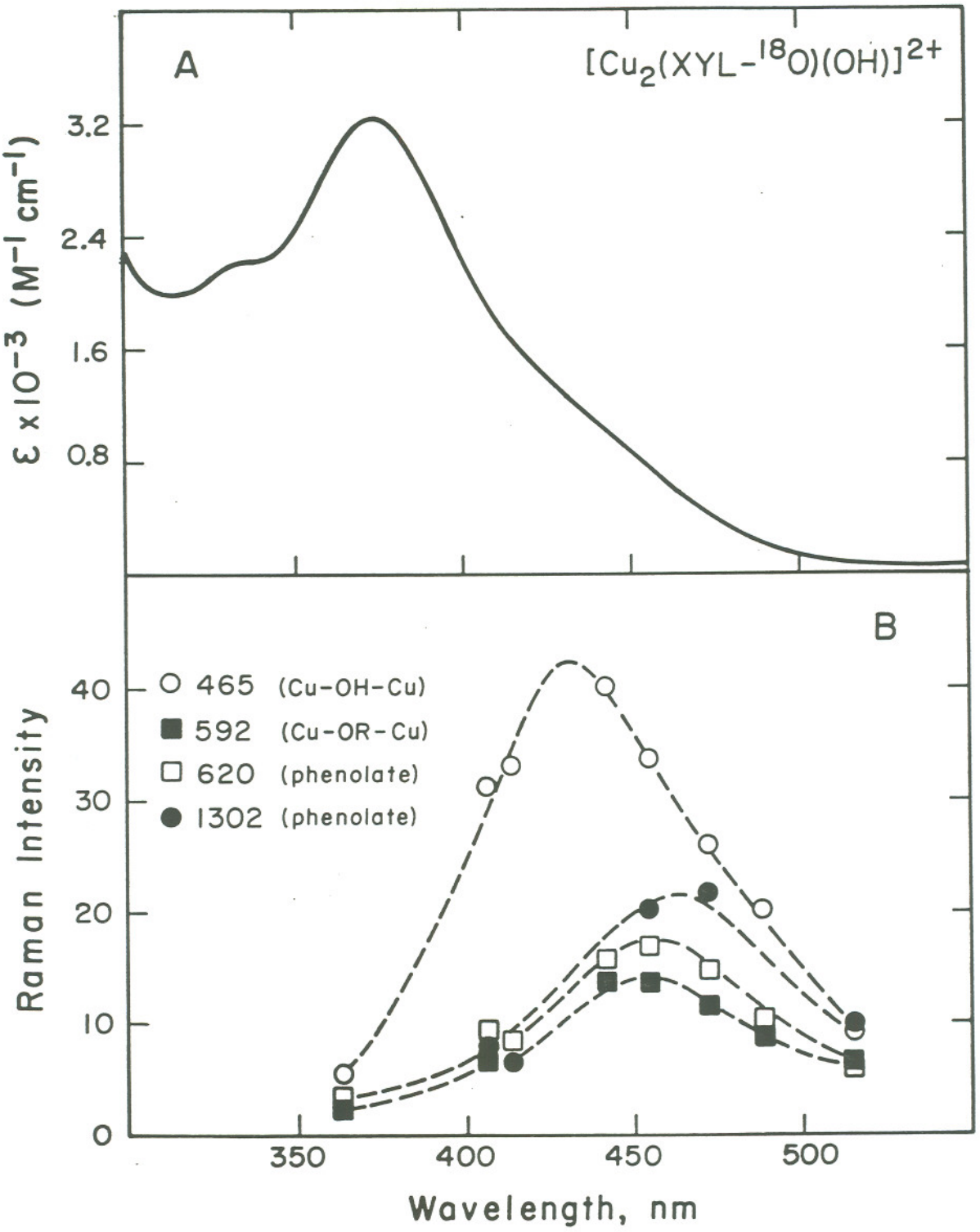
A
[Cu2(XYL-18O)(OH)]2+
ε x10−3 (M−1 cm−1)
3.2
2.4
1.6
0.8
B
Raman Intensity
40
30
20
10
0
465 (Cu-OH-Cu)
592 (Cu-OR-Cu)
620 (phenolate)
1302 (phenolate)
350
400
450
500
Wavelength, nm

Figure 4

CHAPTER VI
CONCLUSIONS AND FUTURE DIRECTIONS

Ribonucleotide Reductase R2

As described in Chapter 3, resonance Raman spectroscopy has been used to study oxygen activation by ribonucleotide reductase R2. This work was performed on the Y122F mutant instead of wild-type R2, because it has an identical dinuclear iron center to native R2 but lacks the Tyr radical, making it more stable to laser irradiation. By monitoring the ν_s(Fe-O-Fe) vibration, our Raman data clearly demonstrate that one oxygen atom of O_2 is incorporated into the Fe-O-Fe moiety. In the probable mechanism for this reaction (Figure 1), O_2 binds to the diferrous iron center and becomes reduced to peroxide. Since the μ-oxo bridge is produced quantitatively from O_2, the peroxide most likely bridges the two Fe(III) in a μ-η^1 fashion. This is followed by a heterolytic cleavage of the O-O bond, generating H_2O and a high valent iron-oxo species (ferryl). In the wild-type protein, the latter species provides the oxidizing power needed to generate a Tyr radical.

RR spectroscopy has also been used to investigate the reaction between the F208Y mutant of R2 and O_2, which results in formation of a dihydroxyphenylalanine (DOPA).[1] When the reduced protein was oxidized with $^{18}O_2$ in H_2O, the RR spectrum of the Fe(III) catecholate product was indistinguishable from that of the same protein oxidized with $^{16}O_2$ in H_2O. However, when the protein was oxidized with $^{16}O_2$ in $H_2{}^{18}O$, the Fe-O vibrational modes at 512 and 592 cm^{-1} shifted ~ 10 cm^{-1} to lower energy. This is good evidence for O incorporation from H_2O into Fe(III)-bound catecholate. We believe that the ferryl intermediate oxidizes Tyr 208 to a

radical which then recombines with a solvent-exchangeable OH^- associated with the dinuclear iron center (Figure 7, Chapter 3). Thus, the F208Y mutant behaves as an internal tyrosine oxidase, rather than a hydroxylase as previously proposed.[1]

The above mechanisms for the oxygen activation in R2 (Y122F and F208Y mutants) are indirectly deduced based on the Raman investigations of the products of the reaction (Fe-O-Fe and Fe-catecholate moieties) using $^{18}O_2$ and $H_2{}^{18}O$. In order to obtain direct evidence for the mechanisms, important reaction intermediates need to be characterized.

In recent work on the R2 protein it was demonstrated that if a ferryl intermediate exists in the R2 reaction, it is too short-lived to be detected spectroscopically, even using the rapid freeze quench technique.[2] However, using this technique, two other later intermediates in the tyrosyl radical formation were successfully characterized by EPR and Mössbauer spectroscopy. The first one (named intermediate U) exhibits a broad absorption band centered at 565 nm and was originally proposed to be a μ-peroxo-diferric complex.[2] However, more recently it has been shown to be a diferric, diradical species.[3] The second intermediate (named intermediate X) has a broad absorption band centered at 360 nm and a sharp, isotropic EPR signal at $g = 2.00$ that is broadened by ^{57}Fe. Intermediate X is believed to contain a single free radical which is coupled to the diferric center and may be one of the iron ligands.[2,4]

These two intermediates are susceptible to RR investigations, provided the spectra are not dominated by the isopentane solvent used for rapid freeze quenching. If the first intermediate were a ferric-peroxide, the 565 nm absorption would most likely be a peroxide $\rightarrow$ Fe(III) CT. Raman spectra with excitation into this absorption band should reveal a ν(O-O) at ~ 800 cm^{-1} that has large isotopic shift with $^{18}O_2$. If the first intermediate is rather already oxidized to the diradical state, it should exhibit an Fe(III)-O-Fe(III) vibration at ~ 500 cm^{-1} with a large isotopic shift when prepared with $^{18}O_2$. The second intermediate, X, should also exhibit an Fe-O-Fe vibration that is sensitive to $^{18}O_2$. It is possible that one of these radicals is localized on the oxo bridge. In this case, there should be a significant lengthening of the Fe-O bond,

shifting ν_s(Fe-O-Fe) to lower energy.

Other Dinuclear Iron-Oxo Enzymes

Two other oxygen utilizing enzymes, methane monooxygenase (MMO) and Δ^9 stearoyl-acyl protein desaturase (Δ^9D) from castor bean, also contain a dinuclear iron-oxo cluster.[5,6] An analysis of sequences of R2 and MMO hydroxylases from various sources suggests that the two proteins have the same set of protein ligands that is dominated by negatively charged carboxylate.[5] The sequence of Δ^9D reveals two sets of the Glu-X-X-His motif that is similar to those in R2 and MMO, and are likely to provide the ligands to the dinuclear iron center.[6] A unified mechanism for oxygen activation by R2, MMO, and Δ^9D is shown in Figure 1. All three reactions are proposed to involve a common ferryl intermediate that is stabilized by the oxygen dominated, negatively charged ligand environment.

The most interesting questions in studying oxygen activation by these nonheme iron enzymes are how the dioxygen is cleaved and how a ferryl intermediate might be involved in each reaction. Although a ferryl species in the R2 system may be too short-lived to be characterized spectroscopically, a high-valent Fe^{IV}/Fe^{IV} intermediate was recently identified in MMO using rapid freeze-quenching in combination with Mössbauer spectroscopy.[7] This intermediate presumably resulted from heterolytic scission of a diferric-peroxide intermediate, and it showed maximal accumulation $\sim$4 seconds after addition of O_2. It contains two indistinguishable Fe^{IV} and is suggested to have an Fe^{IV}-O-Fe^{IV} moiety.[7] Resonance Raman spectroscopy may be used to verify the ferryl species. This intermediate has absorption maxima at 330 and 430 nm, which are likely due to the high valent iron-oxo species. Excitation into these absorption bands should reveal resonance enhanced vibrations of the ferryl species [e.g., $\nu(Fe^{4+}\text{-O})$ at $\sim$600-800 cm^{-1}] that are sensitive to an $^{18}O_2$ reaction. It would be of particular interest to determine whether the oxygen derived from O_2 is bridging or terminal in the ferryl intermediate of MMO. A terminal $Fe^{IV}=O$ would be expected to have a higher frequency ($\sim$800 cm^{-1}) compared to a bridging Fe^{IV}-O-Fe^{IV}.

The Δ^9 desaturase catalyzes oxidative desaturation of long chain fatty acids. It is the second enzyme (after R2) that has been revealed by RR spectroscopy to have an Fe-O-Fe cluster.[6b] Like R2, it is an oxidase that utilizes O_2 as an electron acceptor, rather than being a monooxygenase that inserts one oxygen atom from O_2 into the substrate as in MMO. It is proposed that R2, MMO, and the desaturase all have an Fe^{IV}-O-Fe^{IV} ferryl intermediate with the bridging oxygen coming from O_2 (Figure 1). In MMO, this ferryl intermediate may abstract an electron from the substrate and then insert the bridging oxygen into the substrate. In R2 and Δ^9D desaturase, the ferryl intermediate functions only to provide the oxidizing power, thus the μ-oxo bridge is retained in the diferric cluster. In the F208Y mutant of R2 the ferryl intermediate may also abstract an electron from Y208 and insert an oxygen into the product, but in this case the oxygen is part of solvent-derived hydroxyl group and not the bridging oxo group.

To test the origin of the oxo bridge in Δ^9D, the same experiments as for the R2 Y122F mutant (Chapter 3) should be performed on this enzyme. The RR spectrum of the desaturase has revealed a ν_s(Fe-O-Fe) at $\sim$520 cm^{-1} that shifts to $\sim$500 cm^{-1} in $H_2{}^{18}O$.[6b] This promises RR spectroscopy to be a useful tool in studying the oxygen activation of this enzyme. However, in order to design successful new experiments, a few properties need to be established. First, the rate of the μ-oxo exchange with solvent needs to be checked.[8] If the exchange rate is too rapid, it will be difficult to determine the source of μ-oxo bridge. Second, the apoprotein needs to be isolated. Fox et al. have developed a gene expression system in *E. coli* for this enzyme.[6a] It should be possible to obtain the apoprotein by growing the cells in low-iron medium. Third, the conditions for oxygen activation (assembling the apoprotein with Fe^{2+} and O_2) needs to be developed and optimized. After the apodesaturase has been incubated with Fe^{2+} and reacted with $^{18}O_2$, the sample needs to be frozen quickly in a liquid nitrogen bath or in a rapid freeze-quench apparatus.[2,7] Detection of ν(Fe-^{18}O-Fe) in the RR spectra of the oxidized protein will be good evidence for O_2 as the source of the μ-oxo bridge in Δ^9D, supporting the mechanism proposed in Figure 1.

The reaction of reduced MMO with O_2 yields a relatively long-lived ferryl species.[7] There is a possibility that reaction of reduced desaturase with O_2 also produces a stable and long-lived ferryl intermediate. If that is the case, it will be interesting to study the two ferryl species comparatively to gain useful information of their different reactivity (hydroxylation vs. desaturation). For example, if a RR spectrum of the ferryl intermediate can be obtained, it can be determined whether the ferryl oxygen exchanges with solvent. Similarly, it is possible to determine if a ferryl species has H-bonds to surrounding residues by performing the reaction in D_2O buffer and observing a change in the $\nu(Fe^{IV}\text{-}O)$.

Hemocyanins and Tyrosinase

As described in Chapter 4, RR studies of oxyhemocyanin from *Octopus dofleini* have identified a Cu-O (peroxide) stretch, $\nu_{as}(Cu_2O_2)$, at 542 cm^{-1} (519 cm^{-1} in $^{18}O_2$) and its first overtone, $2\nu_{as}(Cu_2O_2)$ at 1085 cm^{-1} (1039 cm^{-1} in $^{18}O_2$). When the protein was oxygenated with $^{16}O^{18}O$, only a single $\nu_{as}(Cu_2{}^{16}O^{18}O)$ mode was observed at 529 cm^{-1}. These results provide definitive evidence that the peroxo group is symmetrically bound to the two Cu(II)'s. Oxyhemocyanins from both molluscs and arthropods exhibit similar $\nu_{as}(Cu_2O_2)$ and $2\nu_{as}(Cu_2O_2)$ Raman modes, suggesting that oxyHcs from both phyla have the same copper-peroxide structure. In both cases the Cu(II)'s would be bridged solely by a side-on peroxide in an $\eta^2{:}\eta^2$ geometry, as revealed by the X-ray crystal structure of *Limulus polyphemus* II oxyhemocyanin.[9]

In the low frequency region (100-400 cm^{-1}) oxyHc from *Busycon canaliculatum* exhibits eight distinct vibrational modes, most of which are sensitive to ^{65}Cu or D substitution, rather than $^{18}O_2$. These peaks are assigned to $\nu_s(Cu_2O_2)$ and $\nu_{as}(Cu_2O_2)$ modes coupled with Cu-N(His) stretching vibrations. Normal coordinate analysis yields an excellent match with the entire set of observed RR frequencies, thereby lending credibility to the spectral assignments. Comparisons of the low frequency RR spectra reveal that, whereas oxyHcs from molluscs (*B.c.* and *O.d.*)

have almost identical Cu-ligand vibrational patterns, oxyHc from arthropods (*L.p.* and *C.m.*) have a considerably different one. These findings are consistent with amino acid sequence comparisons which suggest that the dinuclear copper cluster in molluscan Hc does not have all six histidine ligands found in arthropod Hc.

Tyrosinase is another coupled dinuclear copper protein that catalyzes the oxidation of monophenols and plays an essential role in melanin biosynthesis. Tyrosinase binds O_2 to form a relatively stable dioxygen adduct. Oxytyrosinase has very similar spectroscopic and magnetic properties to oxyhemocyanins, and it is believed to have a similar copper site structure.[10] However, whereas hemocyanin binds oxygen reversibly, tyrosinase utilizes oxygen to hydroxylate monophenols. Thus, tyrosinase differs from hemocyanin in having an additional site where substrate binds and interacts with the copper peroxide complex. Whether oxytyrosinase has the same μ-η^2:η^2 geometry has been questioned because the corresponding model compound oxidizes, but does not oxygenate, organic substrates.[11]

Previous RR studies of oxytyrosinase revealed a ν(O-O) at 755 cm^{-1} that shifted to 714 cm^{-1} with $^{18}O_2$.[12] Surprisingly, no studies using mixed-isotope O_2 have been reported. Considering the uniqueness of this enzyme, it is definitely worthwhile to reinvestigate it thoroughly using mixed label O_2 oxytyrosinase. Studies on the ν(Cu-O) and ν(O-O) of the $^{16}O^{18}O$ should verify or disprove the speculation of the symmetric dicupric-peroxide structure, particularly if a $\nu_{as}(Cu_2O_2)$ mode near 550 cm^{-1} can be identified with UV excitation. Previous RR studies of oxytyrosinase also revealed several low-frequency (100-400 cm^{-1}) vibrations that are assignable to copper-ligand stretches.[12] These vibrations have a slightly different pattern from either molluscan or arthropodan Hcs (Figure 2), suggesting differences in copper ligation by the protein.

The difference between tyrosinase and hemocyanins is likely to be in the CuA site. As discussed in Chapter 4, sequence comparisons among arthropodan Hcs, molluscan Hcs, and tyrosinases have suggested that tyrosinases, like molluscan Hcs, have the same CuB binding site as arthropodan Hcs with three histidine ligands, but not the same CuA site.[13,14] Comparison of sequences of molluscan Hcs and

tyrosinases revealed two conserved histidines around the putative CuA binding site that are likely to be ligands to CuA. As in molluscan Hcs, the third ligand to CuA remains unknown and there are three possibilities: it could be another amino acid sidechain, perhaps carboxylate from an Asp or a Glu, an aqua group or it may be vacant. Considering that in tyrosinase the substrate needs to bind near the active site, and that very likely it binds to the copper cluster, as proposed earlier,[15,16] the first possibility seems unlikely. If the copper center has an aqua ligand, it may be possible to detect it using RR spectroscopy by incubating the enzyme in $H_2{}^{18}O$. Also it is worthwhile to obtain higher-resolution spectra of ^{65}Cu-substituted and D_2O-exchanged enzyme. These data, combined with normal coordinate analysis, should help assign the spectra and provide a better understanding of the copper ligation in tyrosinase.

References

(1) Ormö, M., deMare, F., Regnström, K., Åberg, A., Sahlin, M., Ling, J., Loehr, T.M., Sanders-Loehr, J., and Sjöberg, B.-M. (1992) *J. Biol. Chem.* **267**, 8711-8714

(2) Bollinger, J.M., Jr., Edmondson, D.E., Huynh, B.H., Filley, J., Norton, J.R., and Stubbe, J. (1991) *Science* **253**, 292-298

(3) Stubbe, J., personal communication.

(4) Bollinger, J.M., Jr., Stubbe, J., Huynh, B.H., and Edmondson, D.E. (1991) *J. Am. Chem. Soc.* **113,** 6289-6291

(5) Nordlund, P., Dalton, H., and Eklund, H. (1992), *FEBS*, **307**, 257-262

(6) (a) Fox, B.G., Shanklin, J., Somerville, C., and Münck, E. (1993) *Proc. Natl. Sci. USA* **90**, 2486-2490; (b) Fox, B.G., Ai, J., Loehr, T.M., and Sanders-Loehr, J., unpublished results.

(7) Lee, S.-K., Fox, B.G., Froland, W.A., Lipscomb, J.D., and Münck, E. (1993) *J. Am. Chem. Soc.*, in press

(8) Sjöberg, B.-M., Loehr, T.M., and Sanders-Loehr, J. (1982) *Biochemistry* **21,** 96-102

(9) Magnus, K.A.; Ton-That, H. (1992) *J. Inorg. Biochem.* **47**, 21

(10) Solomon, E.I. (1981) In *Copper Proteins* (Spiro, T.G., Ed.), pp 41-108, Wiley, New York

(11) Kitajima, N., Koda, T., Iwata, Y., and Moro-oka, Y. (1990) *J. Am. Chem. Soc.* **112,** 8833-8839

(12) Eickman, N.C., Solomon, E.I., Larrabee, J.A., Spiro, T.G., and Lerch, K. (1978) *J. Am. Chem. Soc.* **100,** 6529-6531

(13) Lerch, K.; Huber, M.; Schneider, H.-J.; Drexel, R.; Linzen, B. *J. Inorg. Biochem.* **1986** *26*, 213.

(14) (a) Lang, W.H., and van Holde, K.E. (1991) *Proc. Natl. Acad. Sci. USA* **88,** 244-248; (b) Lang, W.H. (1988) *Biochemistry* **27**, 7276-7282

(15) Wilcox, D.E., Porras, A.G., Hwang, Y.T., Lerch, K., Winkler, M.E., and Solomon, E.I. (1985) *J. Am. Chem. Soc.* **107,** 4015-4027

(16) Winkler, M.E., Lerch, K., and Solomon, E.I. (1985) *J. Am. Chem. Soc.* **103,** 7001-7003

Figure Legends

Figure 1 Proposed mechanism for oxygen activation by iron-oxo enzymes: methane monooxygenase (MMO), ribonucleotide reductase R2, and Δ^9 desaturase (Δ^9D).

Figure 2 UV-excitation RR spectra of oxyhemocyanins from mollusc *Busycon canaliculatum* (upper), arthropod *Limulus polyphemus* (Middle), and of tyrosinase from *Neurospora crassa* (Lower). Adapted from reference 10.

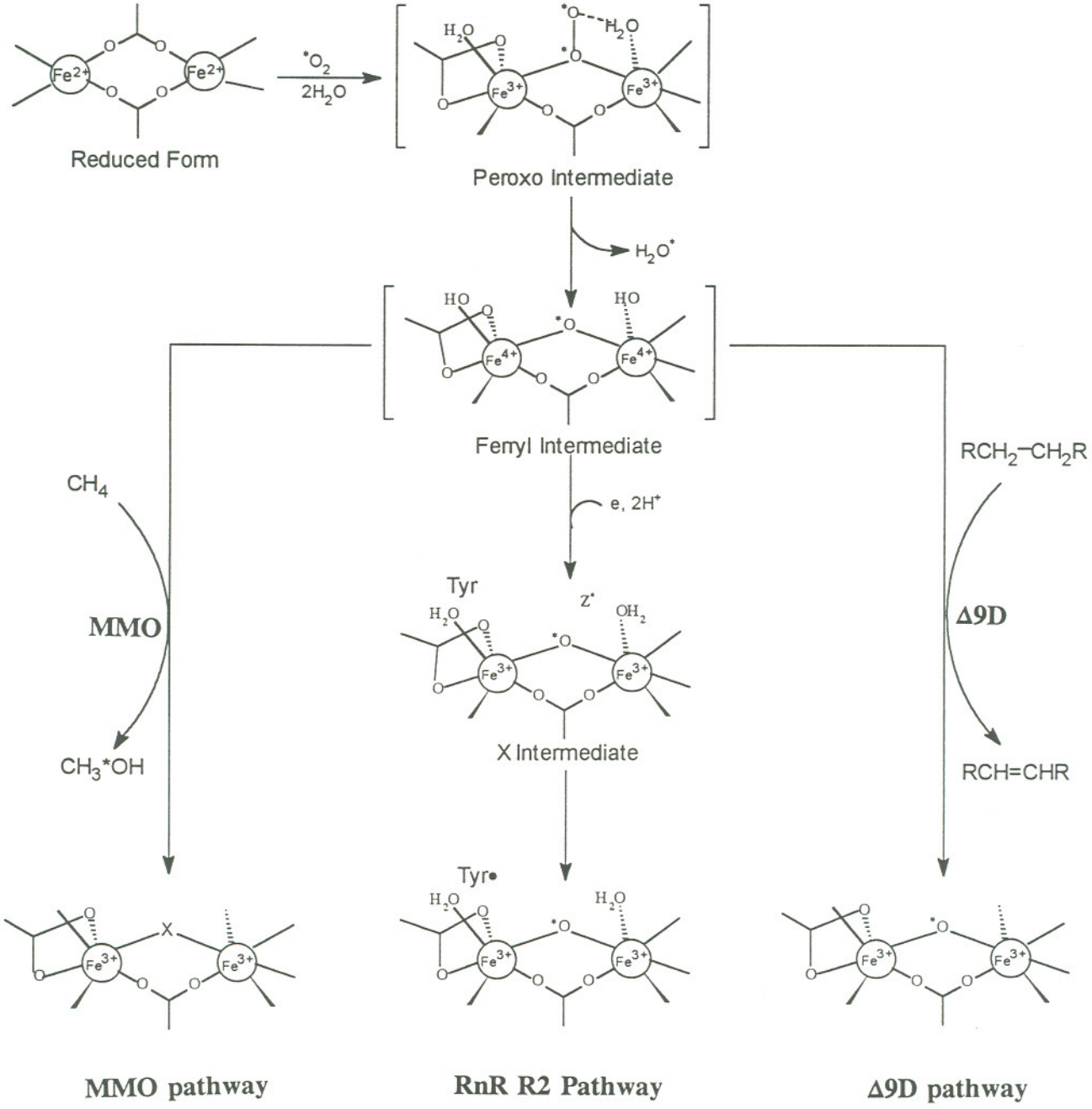
Reduced Form
Peroxo Intermediate
Ferryl Intermediate
X Intermediate
MMO
CH4
CH3*OH
Δ9D
RCH2–CH2R
RCH=CHR
Tyr
Tyr•
MMO pathway
RnR R2 Pathway
Δ9D pathway

Figure 1

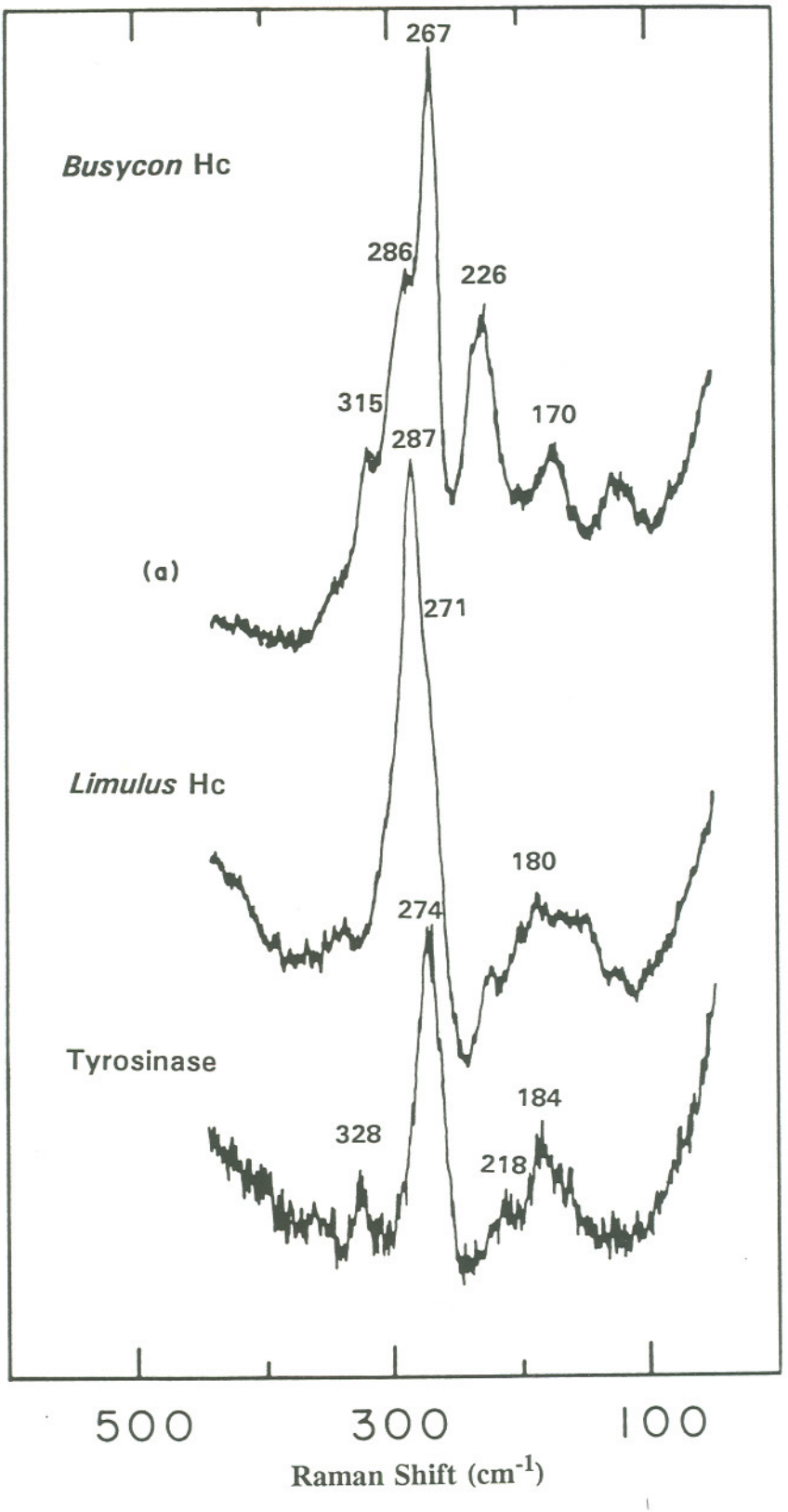
267
Busycon Hc
286
226
315
170
287
(a)
271
Limulus Hc
180
274
Tyrosinase
184
328
218
500
300
100
Raman Shift (cm-1)

Figure 2

BIOGRAPHICAL NOTE

The author was born in the Spring of 1963, in the village of Qilingxia, Guangdong, China. After nine years of schooling and one year of farming in his native land, he went to Nankai University (Tianjin, China) for his higher education in the Fall of 1979. In the Summer of 1983 he received his B.S. degree in Chemistry from Nankai University. Afterwards, he worked for China National Rice Research Institute (Hangzhou, China) for about 5 years. In the Summer of 1988, he came to Oregon and began his Ph.D. studies at the Oregon Graduate Institute with Professors Joann Sanders-Loehr and Thomas M. Loehr.